2013-12-19

A Computational Model of Aneurysmal Flow at the Abdominal Aorta

Nobakht, Samaneh

UNIVERSITY OF CALGARY

A Computational Model of Aneurysmal Flow at the Abdominal Aorta

by

Samaneh Nobakht

A THESIS

SUBMITTED TO THE FACULTY OF GRADUATE STUDIES

IN PARTIAL FULFILMENT OF THE REQUIREMENTS FOR THE

DEGREE OF MASTER OF SCIENCE

GRADUATE PROGRAM IN BIOMEDICAL ENGINEERING

CALGARY, ALBERTA

DECEMBER, 2013

Abstract

Abdominal Aortic Aneurysm is a dilatation of the aortic artery that occurs in response to degradation of the wall structure. The present research focused on developing a realistic hemodynamic model of the aneurysm using a new method to assign boundary conditions. A three element Windkessel model was coupled to the 3D geometry model of the disease in order to couple inlet flow with outlet pressure. This model resulted in more precise hemodynamic conditions for pulsatile flow: 1- in terms of realistic wall pressure values and pressure curves, 2- realistic geometry effect. Contours of wall shear stress, mean wall shear stress, static pressure, and velocity streamlines were calculated and results were compared for two patients and an ideal geometry of the aneurysm. Finally maps of mean wall shear stress were produced to investigate relationship between values of the mean wall shear stress and histological profiling of aneurysm specimens obtained during surgery.

Acknowledgements

I would like to appreciate my supervisor Dr. Di Martino for all her support and patience and great ideas throughout my research.

Thanks to Dr. Moor at Peter Lougheed hospital and Dr.Rinker's lab for providing samples of patient tissue and histology and histochemistry experiments.

Thanks to my supervisory committee, Dr. Tyberg, and Dr. Rival who have always been helpful in answering my questions.

Thanks to my love, Kamran, for supporting me emotionally through all my hard times.

Thanks to my lovely mom whose love and support is always a motivation in my life.

Thanks to the University of Calgary program of Biomedical Engineering for providing funding for my thesis (teaching assistantship, graduate research scholarship).

Table of Contents

Table of Figures

Table of Abbreviations

AAA	Abdominal Aortic Aneurysm
CFD	Computational Fluid Dynamics
HAEC	Human Aortic Endothelial Cells
VEC	Vascular Endothelial Cells
SMC	Smooth Muscle Cells
ILT	Intra Luminal Thrombus
FVM	Finite Volume Method
GA	Genetic Algorithm
WSS	Wall Shear Stress
PWS	Peak Wall Stress
UDF	User Defined Function
MDCT	Multi-detector Computed Tomography

1. INTRODUCTION

Abdominal Aortic Aneurysm (AAA) is a dilatation of the abdominal aorta below the renal arteries and above the iliac bifurcation[1]. There are different categories of researches on the pathology and progression of this disease. AAA studies investigate the cause and progression of the disease and aim at improving diagnostic tools so that individualized and patient specific indications for surgery can identify the aneurysms at greater risk for rupture, thereby decreasing the mortality rate due to the rupture of the vessel, without increasing the number of surgeries performed. Surgeries themselves, in fact, carry a significant risk of complication and should be reserved for cases that are at risk for rupture. It is thought that the interplay between biological factors and hemodynamics is the cause of the disease [2]. In order to understand the process some researches have focused on the clinical aspects and on screening the elder population who have the disease, to monitor the enlargement and rate of expansion of the bulge to prevent rupture. Another category of studies are on cell biology and the behaviour of smooth muscle cells and endothelial cells and possible alterations in the mechanotransduction process of these cells [3]. The third category studies the wall structure and mechanical testing of the wall and seeks to define rupture indices based on mechanical behaviour of the wall and stress analysis[4]. A fourth category are the computational flow studies of aneurysm models in order to find the wall shear stress patterns and its variations across the diseased wall compared to normal wall [5] [6]. The complex pattern of shear stress can be correlated with the activity and degeneration of the endothelial cells that are shear sensitive, as well as with signs of structural degeneration of the wall. The present research belongs to the last category. CFD analyses of an idealized model of an aneurysm as well as of real aneurysms from

patient subjects were developed. A realistic boundary conditions together with patient specific geometries were introduced to provide an overall realistic model of aneurysm. For one of the aneurysms analyzed, maps of mean wall shear stress in 12 right lateral and 12 left lateral regions of the aneurysm area were correlated with histological and mechanical tensile tests of sample tissues obtained during surgical repair of the aneurysm of the patient.

1.1 OBJECTIVE

The primary objective of this research was to make a realistic hemodynamic model of AAA to calculate regional maps of wall shear stress values and wall pressure. Understanding these factors is of important value in understanding the process of degeneration of the wall, aneurysm progression and finally its rupture. A good hemodynamic model requires realistic boundary conditions. Much of the literature work on AAA does not consider the effect of ventricular pulse wave in producing an extra pressure to the reservoir pressure in the aorta. The majority of these papers use wave velocity at the inlet and zero pressure at the outlet[7] [8] [9] [10]. We applied a wave velocity at the inlet, and we implemented a 0D 3-element Windkessel model of the downstream vasculature to couple the velocity at the inlet to the aortic wave pressure at the outlet. Using this methodology we can see that the pressure produced inside the whole vessel is not only due to lumen inflow and outflow difference, but it also includes the pulse wave effect; therefore, the pressure seen on the wall becomes very close to what a transducer measures. These results can be appreciated in the results chapter: pressure is about 8800 Pascal on the walls in early systole, 13000 Pascal in mid systole, 16000 Pascal in peak systole and 13000 Pascal in end systole, which are between 67 mmHg and 120 mmHg. Moreover the lag between pressure wave and flow wave

is noticeable in the results panels, which shows that the model is able to capture the phase shift of the pressure and velocity waves.

The objective of the overall research project is to correlate the wall shear stress values to the biochemical signalling happening at the wall to blood interface, which may have a role in the progression of the aneurysms. Average shear stress and flow waveforms are known to correlate with vascular diseases. In particular high shear stress and unidirectional flow appear to protect against vascular degeneration while low shear stress and oscillatory flow appear to promote diseased tissues. Our collaborators (Dr. Rinker's laboratory) have recently discovered a novel flow dependent signalling pathway that appears to influence gene expression in cultured human aortic endothelial cells (HAEC)[11] This pathway may provide novel targets for intervention in vascular diseases. To verify and evaluate this pathway's relevance to intact human tissue it was planed to utilize samples from aortic aneurysm repair. My role in this portion of the research is to demonstrate the feasibility of simulating the hemodynamics of patients scheduled for AAA repair and who underwent a CT scan examination up to two weeks prior to the operation. The results from the fluid dynamics analysis (see Objective 1) will help identify specific sections of the aneurysm to be biopsied during the surgical repair based on the prevailing flow conditions in different areas. One clinical case was completed where samples were collected corresponding to areas of high and low shear stress and the fluid dynamics variables were compared with mechanical tests on the specimens (to probe the weakening of the wall) and with histological results on the same specimens. The lab is currently performing a molecular profiling of the specimen to investigate any correlation between the fluid dynamic variables and specific molecular markers for inflammation. This portion of the project, while integral to the research goals as a whole, was not part of my own research project.

2 BACKGROUND

The wall of arteries is composed of three layers. Figure 2-1 shows these layers in a medium size artery. The most inner layer or tunica intima is made of endothelial cells, which are called vascular endothelial cells (VECs). The median layer or tunica media is made of smooth muscle cells (SMC) and bundles of collagen and elastin fibres. And the outer layer or tunica adventitia also made of collagen bundles[2][12], fibroblasts cells, blood vessels and nerves. The median layer is the load-bearing portion of the wall [13]. The cells present in the arterial wall sense the mechanical environment through a mechanism called mechanotransduction. There are some mechanosensors on the surface of the VECs that are sensitive to shear stresses. Change in shear stress can affect the release of vasodilatory chemicals from the surface of the VECs and also reduce adhesion of platelets and leukocytes. This mechanism is thought to also contribute to control the contractile tone of the vessel.[2]

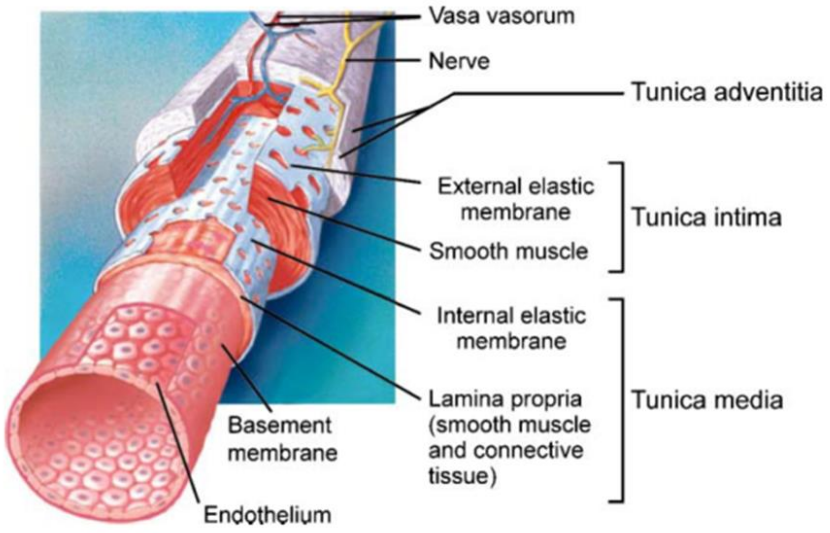

Figure 2-1. Three main layers of a medium sized artery[2]

2.1.1 Abdominal Aortic Aneurysm

An AAA is a degenerative process resulting in the local dilation of the abdominal aortic wall. This results from a loss of structural integrity of the aortic wall, causing a segment of the aorta to "balloon" outwards, as seen in Figure 2-2 [14]. A risk associated with aneurysms is formation of intraluminal thrombus, which causes hypoxia of the wall tissue. Another risk is the rupture of the AAA wall, which is life-threatening [15]. Thus, it is extremely important that diagnostic techniques are able to predict the likelihood of rupture based on a given metric and allow for suitable case-specific treatment.[16][14]

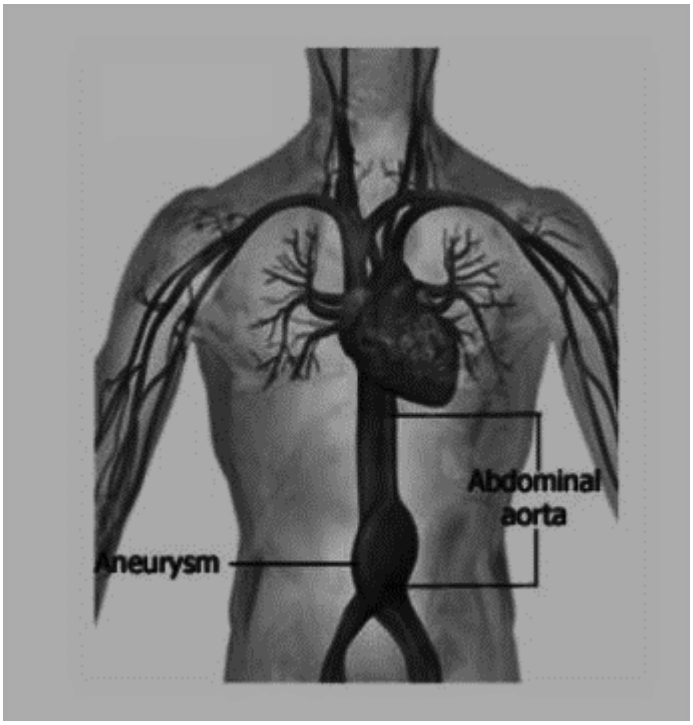

Figure 2-2. Abdominal Aortic Aneurysm[17]

Currently, the metric used to predict rupture potential is the maximum transverse diameter of the aneurysm. In some cases, despite the fact that the maximal diameter is higher than the threshold value of 5.5 cm, rupture doesn't occur. Conversely, there are aneurysms that may rupture even with a diameter less than the defined threshold[18]. Taking repeated computed tomography (CT) and ultrasound images can be useful in order to monitor the enlargement rate of the aneurysm[14][19] An enlargement rate greater than 1 cm/year is considered to be a risk and surgery is performed [20]. However, due to the radiation involved in CT imaging, the imprecisions of ultrasound measurements, and especially due to the great variability of rates of growth [21], monitoring enlargement rate is not an ideal solution. A recent study reported that 15 000 people die each year as a result of aneurysm rupture in the United States [22]. Clearly there remains a distinct need to develop more reliable indicators, such as: peak wall stress (PWS), intraluminal thrombus thickness (ILT) and wall shear stress pattern coupled with release of specific biochemicals.

2.1.2 Formation and Progression of AAA

AAA is a multifactorial degenerative process, in which both biological degradation and distorted hemodynamic pattern cause formation and progression of the disease. [2] It is thought that any changes in hemodynamics of the blood can cause calcification, thrombus formation and loss of integrity of the wall, and inflammation[15]. In the disease process the texture of the wall loses its strength and can no longer tolerate the stresses coming from the blood pressure and so finally it ruptures. [2] The elastic tone of the aorta changes based on the body demand of nutrients and oxygen. The thickness of muscle layer and the organization of collagen and elastin fibres can be regulated to either dilate it or constrict it, however in the case of an aneurysm a permanent dilation

(growth) happens and the mechanism of thickness adjustment becomes interrupted. It appears that loss of elasticity of the wall and collagen turnover along with loss of smooth muscle cells and disorganized elastic sheets weakens the wall and eventually causes the vessel to dilate further and rupture[23].

Because the exact causes of aneurysm formation and progression are not known, a large amount of research is done to understand the cause and the process of their progression. One category of such studies has focused on the effect of hemodynamic stimuli and changes in its normal pattern on the formation and progression of the disease[2]**.**

The content of elastin and collagen fibres in the abdominal aorta is less than in the thoracic aorta. The factors that contribute to altering these fibres are genetic such as any hereditary defects in connective tissue that may contribute in future aneurysm [1], aging, hypertension, disorders in collagen metabolism, and life style such as obesity, smoking. All of this factors can trigger the release of biochemicals from VECs that, in combination with hemodynamic and mechanical stimuli, may result in malformation and dysfunction of structural proteins and cause irreversible changes in the wall [2]. Specific hemodynamic conditions such as lower extremity amputation, chronic spinal cord injury or peripheral vascular diseases are other known risk factors of AAA [24]. From a geometrical viewpoint, most aneurysms form below major branches and above bifurcations. AAAs form above the iliac bifurcation and below the renal arteries. Dua et al. [25] showed that the shear stress in the normal aorta around bifurcations and branches is lower compared to other areas. [25] The infra-renal aorta also experiences reversed flow causing oscillatory shear stress patterns, which make this part of the aorta more prone to AAA formation [23]. Furthermore in the areas of the aorta above bifurcations the amplitude of pressure wave will increase due to reflected wave from the bifurcation and that can in itself be a reason for formation

of aneurysm in elder people. This happens because in elderly people the cross section of the bifurcated vessels to the parent vessel is increased, which can be worsened if atherosclerosis is also present. This causes the pulse wave to have a higher speed and be reflected in a stronger manner, which in turns increases the systolic pressure in the abdominal aorta causing higher wall stresses. In combination with geometrical factors, different regions of the aorta have different mechanical characteristics, for example the aorta below the renal arteries has less content of elastic lamellae than other parts and so it is stiffer compared to other regions of the aorta [23] [2]. The exposure of the wall to higher tension, due to higher wall stresses and greater stiffness, gradually causes disorganization of elastic sheets and reduces their tolerance for pressure loads, so that they become permanently dilated.[2]

2.2 INTRALUMINAL THROMBUS

Thrombus can cause hypoxia of the wall tissue, further destroying the vascular endothelial cells and the mechanisms of vasodilation and vasoconstriction. Moreover, it contributes to producing an inflammatory response due to captured leukocytes in the thrombus area [2]. Smooth muscle cells and VECs are sensitive to mechanical stimuli and thrombus acts like a barrier that prevents them from being exposed to physiologic wall shear stresses that are required for their normal function [23][26]. From another point of view, the intraluminal thrombus acts like a cushion in front of the weak wall preventing it from excessive exposure to normal stresses and so delaying the wall rupture. Therefore, thrombus has a dual effect, initially protecting the underlying wall from excessive wall stresses, but eventually contributing significantly to wall degeneration and to weakening of the tissue.

Treatment

Open elective aneurysm surgeries have 5.6% rate of mortality and ruptured aneurysms going for surgery have 45.7% risk of death[24]. There are two ways of treatments: endovascular stents and open surgery. Since 1991 endovascular stent grafts, are available as non-invasive treatment for AAA. These grafts open radially in the section of the aneurysm and prevent the wall from bearing stresses due to hemodynamics. Currently the first recommendation for treatment is using these grafts rather than conventional open surgery. Nonetheless there are some limitations related to them. According to morphology of patient's aneurysm, presence of ILT, location of the bulge, diameter of the iliac bifurcation and proximity of the dilation to bifurcation not all patients can be treated with these grafts. In cases when endovascular stents cannot be used open surgery is the only treatment. Surgical operation has its own risk of complications; besides the current clinical index used to determine the rupture risk is the maximum diameter or the rate of bulge expansion and as it was mentioned before, it is not a 100% reliable indicator[27].

2.3 PULSE WAVE

The pressure measured in aorta is not only the result of Windkessel or reservoir pressure, but the pressure in the aorta is the result of the instantaneous sum of the ventricular pulse wave pressure and the reservoir pressure. The pulse wave pressure is also called excess pressure. Figure 2-3 shows that subtracting reservoir pressure from aortic pressure can show the excess or wave pressure and using wave intensity analysis it can be shown whether the excess wave increase at systole is forward moving or backward moving, and either a compressive or a decompressive wave [28].

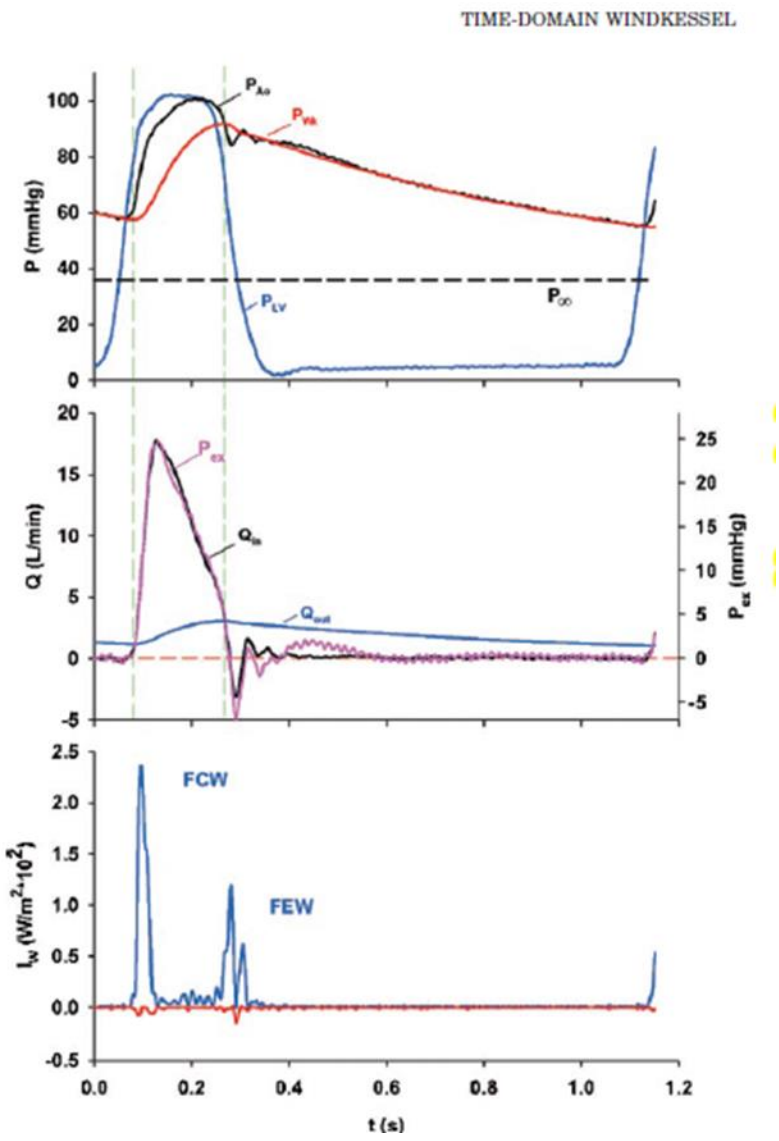

Figure 2-3 top: Aortic pressure in black, reservoir pressure in red and ventricular pressure in blue. Middle: excess pressure in purple and aortic inflow in black and outflow in blue bottom: forward compression and expansion waves in blue[29]

2.4 WINDKESSEL MODEL

The Windkessel model is a lump-parameters model of the aorta. Figure 2-4 shows the concept of the Windkessel model.

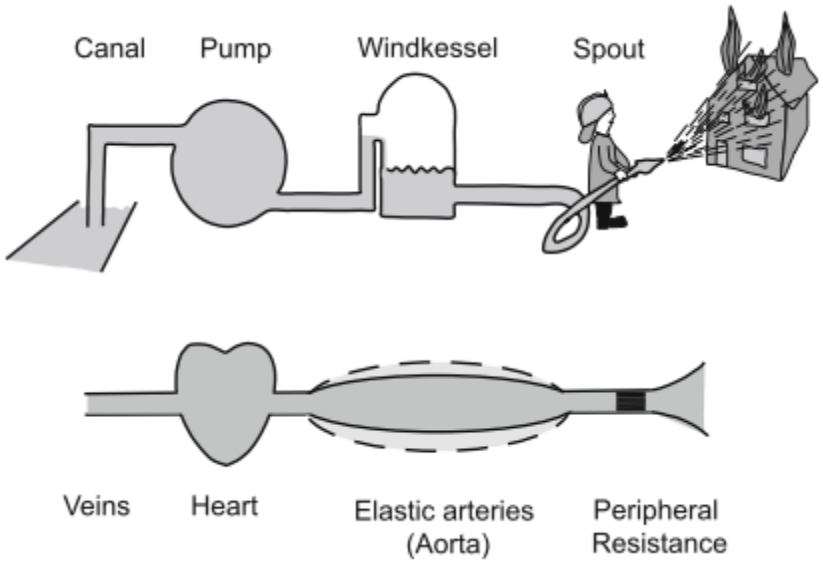

Figure 2-4 Top is a concept of Windkessel model, in which the reservoir acts like Windkessel, when changing in capacitance. Bottom: aortic Windkessel ensures that the compliance of the vessel along with the pumping action of the heart produces a continuous blood supply although the heart works intermittently [30]

The compliant wall works as a capacitor and because there is a decay in diastolic pressure after the aortic valve is closed, Frank [30] recognised that there should be a resistance component that together with the compliance of the wall causes this effect. So he introduced a two element Windkessel model composed of a capacitance and resistance.

He recognized that pressure in diastole decays exponentially with a characteristic decay time equal to RC. Equation 1 shows this relationship where Pdias is the diastolic pressure and Pes is the end systolic aorta pressure.

Equation 1 $$\boldsymbol{P_{dias}(t) = P_{es} \times e^{\frac{-t}{RC}}}$$

This model proved to be valuable in the smaller arteries and arterioles because of dissipating pulse wave. While in terms of the aorta it was only able to explain the diastolic decay satisfactorily but was unable to describe the augmentation in systolic pressure. Using this model Frank was able to

measure mean flow or cardiac output. He measured pressure and using the RC value and at the same time calculating the peripheral compliance he was able to calculate the peripheral resistance and mean flow. In 1930 and 1940 electromagnetic flowmeters became available to measure aortic flow and pressure. Scientists realized that the pattern of pressure described by the two-element Windkessel model subtracted from the measured pressure gives an excess pressure that is similar to the aortic flow in shape. Therefore, although the two element model predicts the decay in diastole, it is not capable to explain systolic pressure. Consequently, a third element was added to the Windkessel model [30]. The third element is the speed of flow times density divided by aortic cross sectional area and it was included as a measure of the resistance that could explain the increase in systolic pressure. In other words the measured pressure from 3 element windkessel model matches the aortic pressure while the measured pressure from 2 element windkessel model matches reservoir pressure. Figure 2-5.

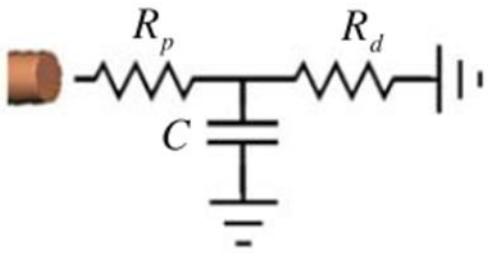

Figure 2-5 3-element Windkessel model Where Rp stands for characteristic impedance, Rd is resistance of downstream vessels and C is capacitance of downstream vessels. [32]

2.5 BIOMECHANICAL ANALYSIS OF AAA

A vast amount of studies have been done to understand the pathophysiology, formation and progression of AAA. Some of these studies focused on the biological factors that influence formation and progression of the disease and some on the effect of abnormal hemodynamics.

Finol et al [3] did a study on two aneurysm aortic models; they described a non-Newtonian flow with rigid wall and a pulsatile velocity at the inlet with a zero pressure at the outlet. The goal was to study pulsatile hemodynamics of blood on the wall of the aneurysm. They measured wall shear stresses, wall shear stress gradients and wall pressure and used a spectral element method. Their results showed that the patterns of wall pressure were similar to flow temporally and spatially; when the flow decelerated pressure increased, and inversely. Moreover the vortices in small and large aneurysms became smaller when flow accelerated. Also they found that wall shear stress resembles the temporal pattern of flow and its value is smallest at the center of aneurysm; however, the value is high at the distal ends of both small and large aneurysms. [5] In another paper with the same study protocol Finol et al concluded that there are secondary and primary vortices in the distal end of aneurysms, which occur together with high negative values of wall shear stresses. Moreover they showed that the pattern of blood pressure and shear stress is related to the frequency of the flow and not to the formation of the vortices. [3]

A study by Dalman et al showed that compromised hemodynamic conditions can lead to the formation of AAA. They studied the abdominal aorta and the iliac arteries of patients with spinal cord injury. The diameter of the abdominal aorta was increased and the iliac bifurcation had a diminished diameter, which could be happening because of remodelling of the vessel due to low blood flow. However the reason of the expansion of the abdominal aorta was not explained. This group also studied the effect of lower extremity exercise on improvement of AAA disease: surprisingly MR data after exercise showed an improved wall shear stress on all stages of cardiac cycle. As mentioned in the paper, exercise can be a good therapy for patient with smaller aneurysm and for those whose aneurysms' risk of rupture does not exceed the risk of surgery. [24]

Raghavan et al in 1996 did tensile tests on aneurysmal and non-aneurysmal tissues. They measured both yield and ultimate strength of tissues. Results showed a significant difference between the two types of specimens: the strength of aneurysmal tissues was noticeably lower than that of non-aneurysmal ones [33]. This could be due to the hypoxia in the wall of tissues of aneurysmal patients [34]and it shows the importance of taking into account the effect of changes in the strength of the wall due to hypoxia and other degenerative events [18].

Some of the studies have correlated the thickness of intraluminal thrombus with the rupture of the aneurysm finding that intraluminal thrombus reduces the strength of the wall due to it being a barrier for diffusion of nutrients and oxygen to the wall. It is also reported that at areas covered by thrombus wall has less elastin and smooth muscle cells [23]. Intraluminal thrombus prevents the leukocytes, platelets and endothelial cells from being exposed to natural wall shear stress which is a stimulus for normal performance of these cells, leading to altered behaviour of the cells[23].

Some of the biomechanical studies on aneurysm are based on fluid structure interaction studies, however most cases consider simplified boundary conditions ignoring the effect of propagating pulse pressure. In addition, due to low spatial resolution of the CT images the wall is considered uniform thickness and isotropic [23].

One study suggested that rupture index can be calculated by combining different factors, such as the history of AAA in family, gender, diameter and thickness of intraluminal thrombus. They introduced the value of Von Mises stress calculated via FEM analysis on the wall of the aneurysm, and divided it by the ultimate stress (or strength of the aneurysm), which can be calculated by Equation 2, to compute a rupture potential index:

Equation 2

$$\sigma_{ULT}(kPa) = 719 - 379\left(\sqrt{}ILT - 0.81\right) - 156(NORD - 2.46) - 213(HIST) + 193(SEX)$$

Where ILT is intraluminal thrombus thickness at the range of 0 and 3.6 cm. NORD is between 1.06 and 3.9 and is a normalized diameter. For having AAA in first degree relative HIST is 0.5 and -0.5 otherwise. SEX is 0.5 for male and -0.5 for female gender [23][35] [36].

2.6 BACKGROUND ON COMPUTATIONAL ANALYSIS

2.6.1 Computational Fluid Dynamics

Fluid dynamics is the study of fluids in motion. Studying fluids such as blood can help scientists comprehend the behaviour of flow before taking action and doing designs. Usually equations governing these fluids are partial differential equations which do not have an analytical solutions and so computational fluid dynamics (CFD) is a useful method to solve these equations[37]. CFD is a strong tool in analysing and is useful to comprehend the behaviour of fluids. CFD can be used to solve complex problems and offers solutions in terms of design and optimization to increase efficiency of engineering devices. In the area of cardiovascular science, CFD is also vastly used; however, due to tremendous complexity of body fluids, it is still progressing. In this area CFD is used for understanding the pathophysiology of diseases and their progression [37]. Although CFD is a strong tool for this purpose and can help in developing treatments for the diseases it can be

very challenging in terms of obtaining precise results. It is a useful tool because not all aspects of cardiovascular system and blood can be studied in a laboratory, such as remote areas, invasive techniques and costly experiments. However CFD results may not be as precise as experimental results. So collaboration between engineers and medical scientists to validate the results is essential. Every problem solved by CFD has to pass 3 components: Preprocessor, solver and post processor.

Preprocessing is when the geometry is defined and the appropriate grid is generated and is imported in the CFD code. Then the properties of the fluid are defined and the boundary conditions are described.

Solving the partial differential equations governing the fluid under analysis is done by means of a solver that uses different methods: finite volume method (FVM) or finite element method or other methods. In our research the FVM was used by implementing an appropriate discretization of partial differential equations to algebraic equations and solving them for discrete control volumes.

At the level of post processing, the results are visualized and are ready for interpretation. They come in forms of contour plots, vector plots, and streamlines among other. Results can show the wall shear stress values, contour plots of velocity , pressure and flow profiles[38].

2.6.2 FVM

In the area of fluid mechanics and heat transfer FVM is a numerical method for discretizing the governing equations in the described field. This method is valuable because it uses the balances of fluxes over small elements that are called control volumes; then the equations are integrated over boundaries of the control volume. So it fulfills the conservation laws for each discretized cell. This is used to gain the value of unknowns on the center of each cell or control volume and also on the

edges of the control volumes. It is applicable to both structured and unstructured meshes. In the present research, the mesh is unstructured and tetrahedrals are the control volumes [39] [40].

2.6.3 Grid Generation

Every CFD problem needs discretization of the geometry, which is called grid generation. Grid has a noticeable impact on the accuracy of the solution and on the convergence of the equations [41] . So it is important to make a high quality grid. However, a very dense grid may be very time and CPU consuming. So there should be an optimized grid which has a good density and also has high quality cells, characterized by low skewness, high orthogonal quality, small adjacent cell length ratios, and is cost effective in terms of time and computer memory. Other aspects of the mesh that are important are the characteristic of boundary layers in order to correctly capture all variations at the boundaries. Using this concept, elements at the boundaries are smaller than the cells at the center of the geometry. Using structured or unstructured mesh can also make a difference in results. For regular geometries structured meshes are recommended because they give more accurate results, especially if the grid lines are aligned with the flow direction. However, in case of complex geometries, having structured meshes is not possible so an unstructured mesh is constructed instead where cells are organized arbitrarily [41] [42].

2.6.4 Genetics Algorithm

Genetics algorithm is a search algorithm or an optimization method. It is inspired by evolutionary biology, which is based on natural selection and randomness. Based on the algorithm, the best individuals who are adapted better to the environment will survive to produce children, and their children will survive if they are best adapted to produce their own children and so on. Thus, the best or optimized population will be generated through several generations. Or in other words,

genes will be filtered generation by generation to produce the strongest genes adapted to conditions. In the computational environment, a fitness function will be defined; it is a function that shows the fitness of an individual to the environment. For example (x1, x2) is an individual and each one of x1, x2 is called a gene. First, a population is generated from the parameter space. Then each individual will be evaluated by fitness function and then the higher fitted individuals will have higher odds to get into the next generation. This process is repeated over and over until the stop criteria are met. The stop criteria can be the number of generations or a specified error, etc. The way the new generation is created is by crossover, mutation and re-attempt methods. In the cross over two individuals will make children; for example children of individual (x1,x2) and individual (x3,x4) can be (x1,x3) or (x1,x4) or (x2,x3) or (x2,x4). In re-attempt the same individual will be transferred to the next generation. And in the mutation scenario the genes of the chosen individual will be modified and be transferred to the next generation, for example the mutated version of the (x1,x2) can be (x1+$\delta, x2 + \varepsilon$) [43].

3 MATERIALS AND METHODS

One idealized aneurysm geometry and two aneurysm models from patient specific CT images were reconstructed and CFD analysis was performed. Mechanical tests and histology was performed on tissues explanted from one of the patients during surgical repair of their aneurysm. The results of the fluid dynamic analysis on the patient specific model were used to guide selection of surgical specimens corresponding to regions at different levels of shear stress.

The detailed explanation of the different steps of method will be in the following sections.

3.1 PATIENT SPECIFIC AAA MODEL

Many researches have been done on AAA by using an ideal geometry. Although overall results can be applied on different patients, every patient has a different geometry and pressure conditions. Ideal geometries are not capable of capturing all the complex features of an aneurysm, such as sudden changes in curvature which can effect distribution of stresses [44]. In order to provide individualized analysis, patient specific geometries should be used. For the purpose of gaining patient specific geometry of AAA, different transverse slices from the abdominal aorta in Dicom format are provided with computed tomography. Segmentation of the tomographic images was performed using the image processing software Scanip, which is based on region growing method (Simpleware). It is noteworthy to mention that for a better resolution and to avoid respiratory artefacts images should be captured with breath holding, or using a contrast agent for a less noisy

background. Moreover, they can be pre-processed to diminish the background noise and to increase the overall resolution. To extract the lumen from each image, the software uses the pixel intensity algorithm, in which the user defines some seed points in a certain pixel intensity threshold. Then the program compares every neighbouring pixel with these points. Every time a change in pixel intensity is detected region growing stops and the detected pixels are masked as a separate area. This is called segmentation. After masking 2D images Figure 3-1, the point cloud algorithm is used to associate an x, y and z spatial components to the masked areas of each slices. Therefore two-dimensional segmented images are converted to 3D structure. Because of some inevitable artefacts, external boundaries are not smooth Figure 3-1, thus a smoothing algorithm called Gaussian filter is applied on the surface to remove all non-real edges based on low pass filter method that removes the curvatures with radiuses higher than a defined value shown in Figure 3-1 [14][20][45].

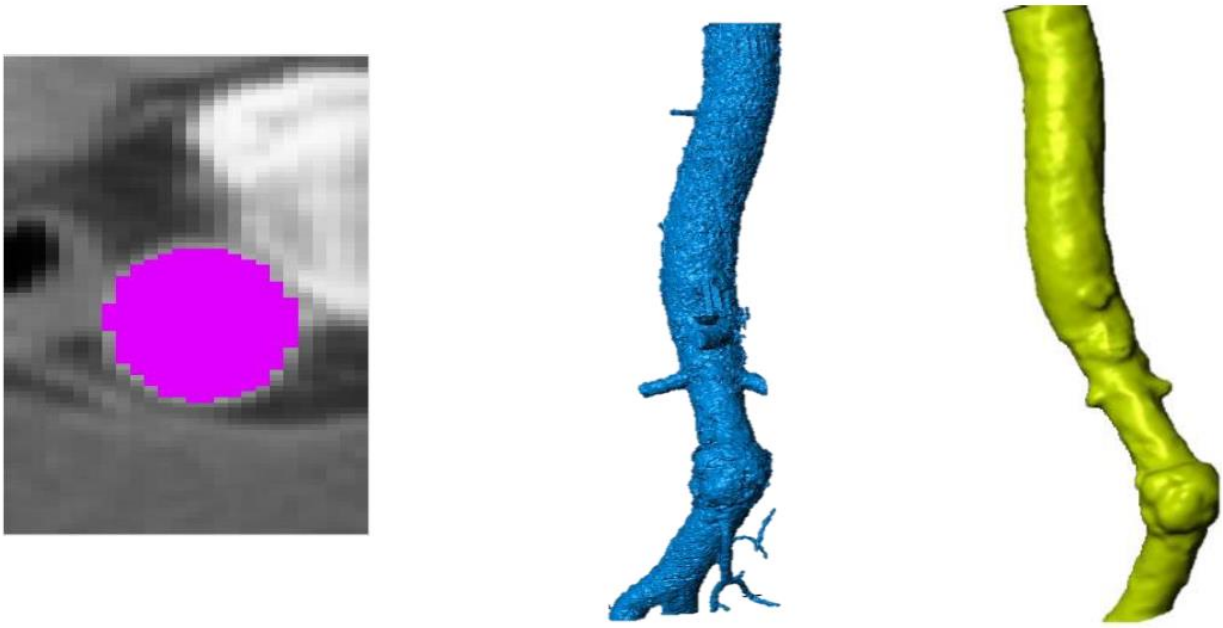

Figure 3-1. Lumen has been masked by region growing method, Middle: Small sharp edges on surface which requires filter, Right: Sharp edges have been smoothed by low pass filter

3.2 GRID GENERATION

First the surface of the geometry was imported in Hypermesh Altair software using the iges standard format. Then on the surface of the geometry, 2D triangles with the average edge sizes of 0.9mm were created. The boundaries were generated next. Before moving to volume meshing the quality of the boundary mesh was checked. Finally, a volume mesh was generated. The quality of the volume mesh was checked and the low quality cells, or cells with high skewness, shown in Figure 3-2 were removed. Orthogonal quality and aspect ratio were checked as a measurement of mesh quality. Values of minimum Orthogonal Quality is 0.16 and maximum Aspect Ratio is 28.

Figure 3-3 shows the cross section of the lumen with smaller elements at the boundary and larger inside, following the boundary layer paradigm. This way, regions of the geometry where flow variations are critical can be captured without the need for a very dense homogeneous mesh. Surface elements were divided into three domains, inlet, outlets and wall as boundary surfaces. Figure 3-4 shows this division. Finally data were exported in Nastran format compatible with ANSYS FLUENT software.

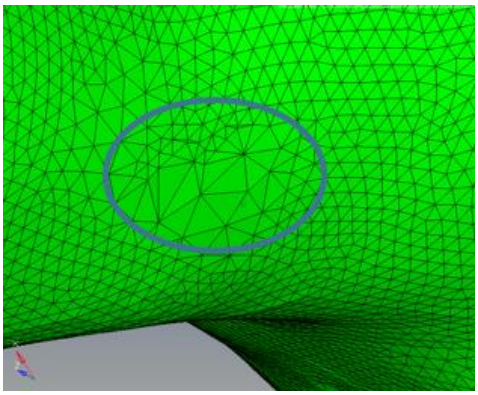

Figure 3-2. Cells with high skewness

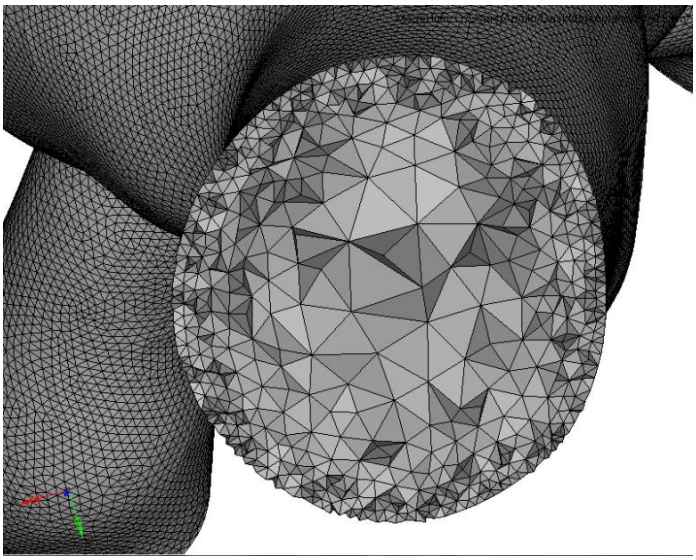

Figure 3-3. Cross section of the generated mesh

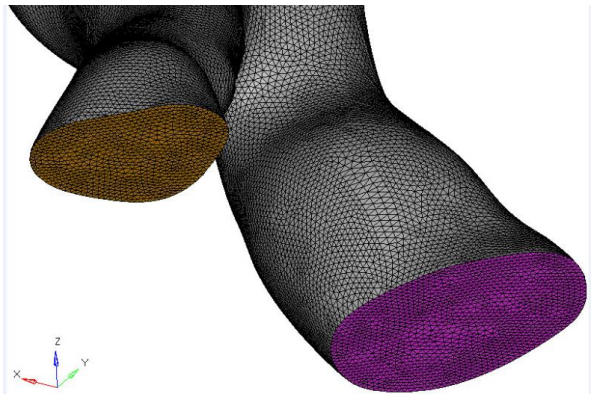

Figure 3-4 Detecting boundary surfaces purple and orange colors represents the outlets of the model

3.3 BOUNDARY CONDITIONS

.

The desired mesh was imported in the commercial ANSYS FLUENT 14 software for CFD simulation (Ansys, Canonsburg, PA, USA). Simulation was performed for 4 cardiac cycles. Figure 3-7 shows the velocity in the descending aorta that was applied to the inlet. The wave pressure, shown in Figure 3-6 was applied to the outlet. It should be noted that the outlet pressure was computed using a coupled 3-element Windkessel 0D model of the downstream vasculature described below. Flow was considered Newtonian and laminar.

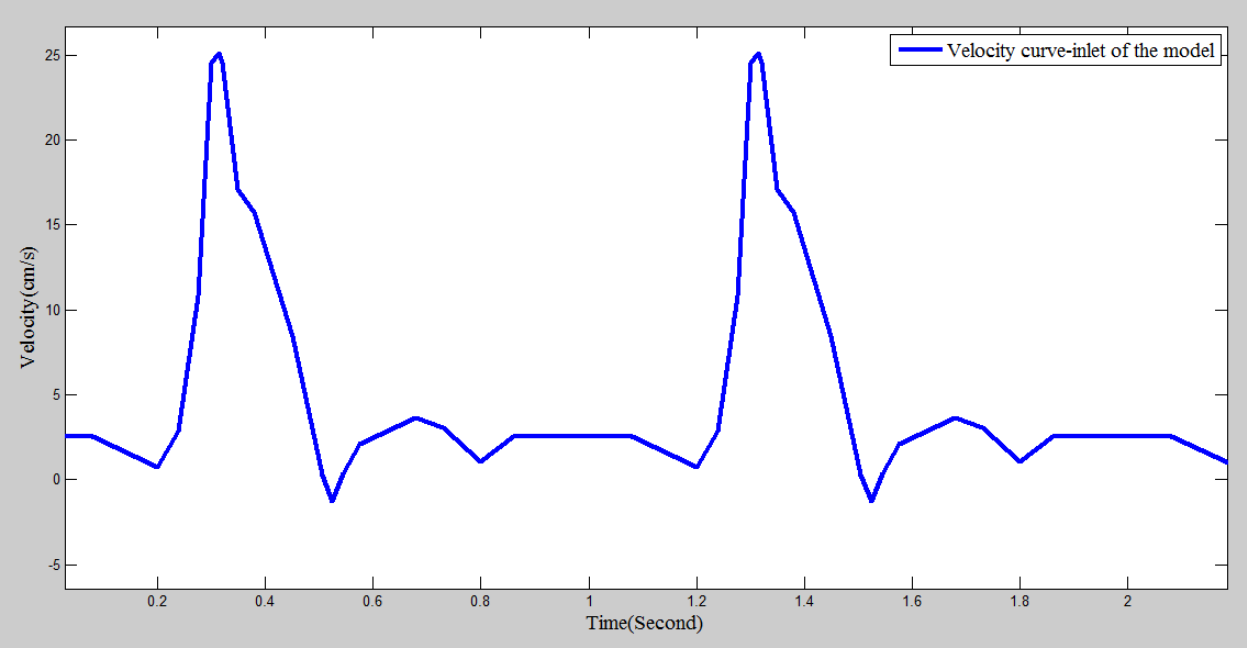

Figure 3-5 Wave velocity applied as inlet boundary condition

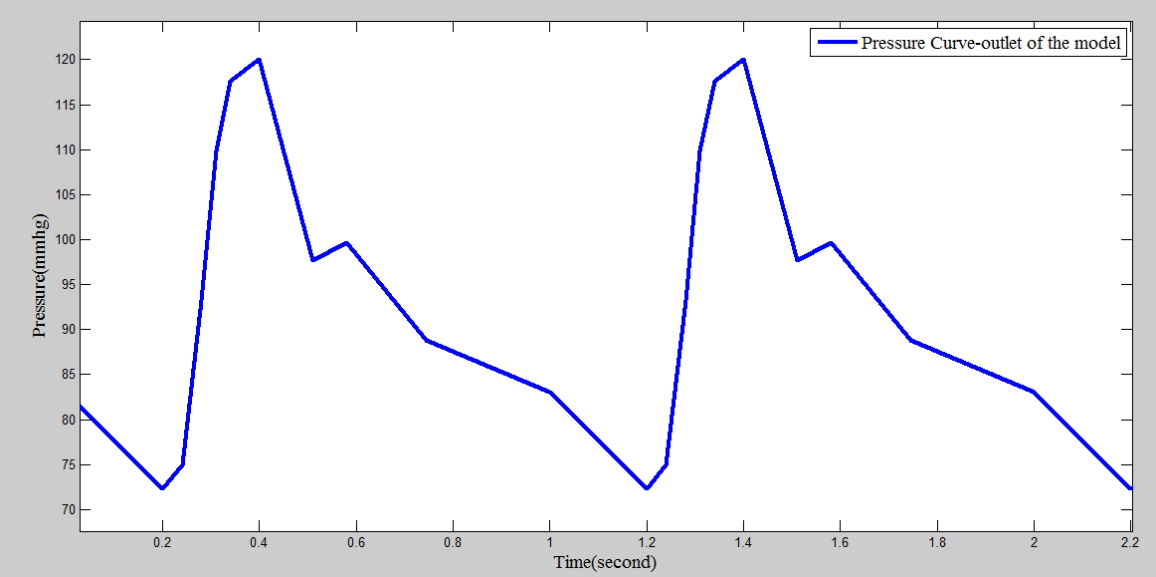

Figure 3-6. Pressure Curve produced at the outlet of the model

Patterns of velocity, static pressure and wall shear stress during one cardiac cycle were determined.

The model was evaluated at 4 times during the cycle; early systole, systolic midpoint, peak systole

and end systolic pressure. Figure 3-9 shows these points.

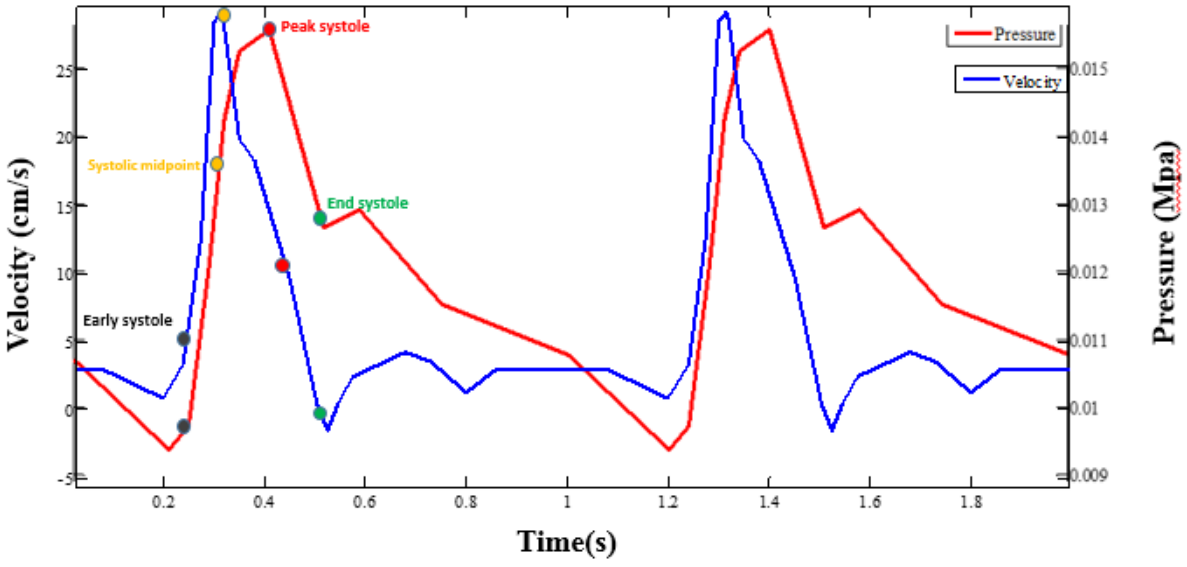

Figure 3-7. Four instances of cardiac cycle: early systole, mid systole, peak systole, end systole that results are shown in these instances

3.4 0D MODEL

A three-element Windkessel model was coupled to the 3D model of the AAA to serve as downstream vasculature. Figure 3-8, Figure 3-9 and Figure 3-10 show the models. Pulse wave, as stated in [46], travels faster than the blood and reflects back and forth: in order to capture backward traveling wave effect on the pressure, downstream vasculature impedance has to be taken into account.

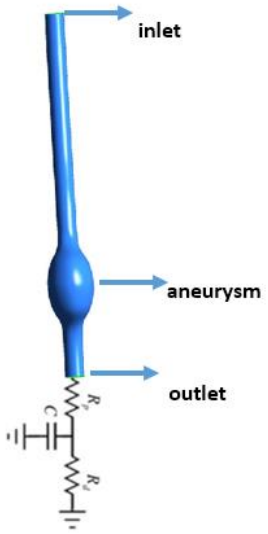

Figure 3-8. Ideal geometry aneurysm model, coupled 0D model of Windkessel and 3D model of aneurysm

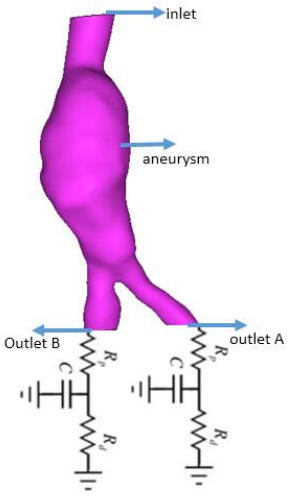

Figure 3-9. Patient A coupled 0D model of Windkessel and 3D model of aneurysm

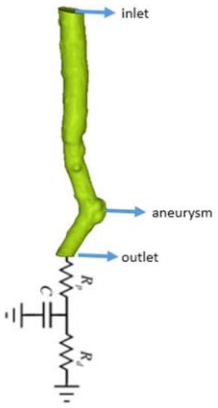

Figure 3-10. PatientB coupling 0D model of Windkesel with 3D model of aneurysm

There is a time delay between flow and pressure curves. Figure 3-11 shows this time delay. Not considering the Windkessel model would disregard the mentioned time delay or phase difference. Compliance of the wall plays a role in augmenting the reservoir pressure, because pulse wave velocity is affected by compliance of the downstream vessels. In aneurysmal cases, which usually occur in the elderly (populations over 55 years old), aging diminishes the compliance and formation of aneurysm makes the wall even stiffer. Despite this hardening of the wall still some compliance exists. We are using a completely rigid walls, however coupling the 3-element Windkessel model downstream of the 3D model will have two benefits, one is that it gives more realistic values of pressure at the outlet than if it was not used. The second benefit is that considering a 3 element Windkessel model models the effect of the downstream vessels. The downstream vasculature affects the speed of the pulse wave which is reflected back and augments the systolic pressures. Therefore having a 3-element Windkessel model allows coupling of the velocity and pressure curves and produces a dependency between them to fulfill the phase lag while producing a correct pressure wave at the inlet and eventually on the entire length of the model. Referring to Figure 3-12, the flow at point A is the flow produced by the heart at the

descending aorta level. Applying zero pressure at the outlet of 3D model or Point A in Figure 3-12will result in having non-realistic pressure contours on the body of vessel. To avoid this, Figure 3-6 curve is applied at point A in Figure 3-12. And the governing differential equations of Figure 3-12 will be solved. The goal is to find Rp, Rd and C in a way that for a particular amount of flow a specific value of pressure is produced at point A. So the differential equations in section 3.5 had to be solved in a way that the mentioned goal is reached.

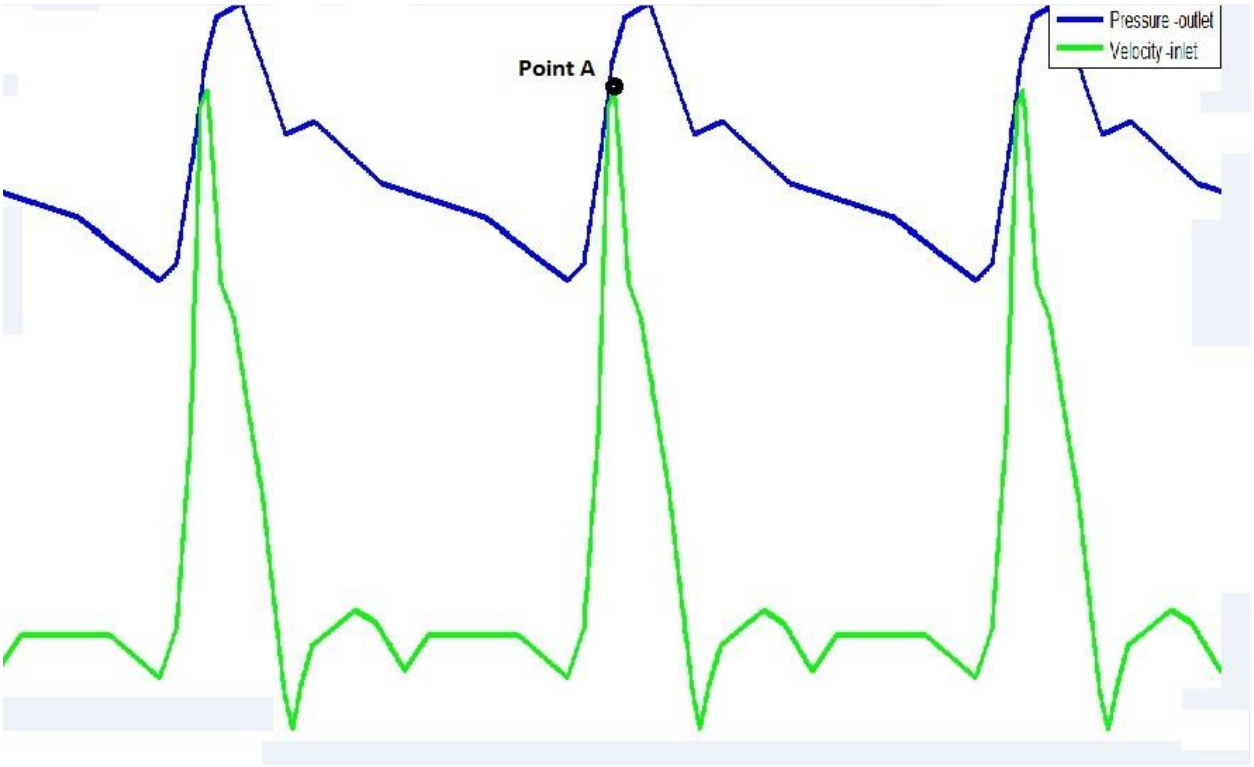

Figure 3-11. Phase delay between pressure and velocity curves, point A shows that max velocity does not correspond to max pressure

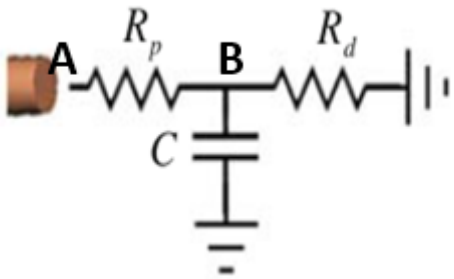

Figure 3-12. 3 element Windkessel model, Point A and B are exposed to the same amount of flow

3.5 NUMERICAL METHOD OF GENERATING BOUNDARY CONDITIONS

The differential equations Equation 3, Equation 4 and Equation 5 first are solved using a Simulink model shown in Figure 3-13, which uses ode45 (dormand prince) solver. Where Rp is the proximal resistance or characteristic impedance shown in Figure 3-12 and Rd is the distal resistance in 2element Windkesel model and C is the capacitance representing compliancy of the vessels. **V2** is the pressure at point B and **V** is pressure at point A in Figure 3-12. **I** is the flow of blood entering the circuit from point A in Figure 3-12.

Equation 3

$$V = I \times R_p + V_2$$

Equation 4

$$I = C \times \frac{dV_2}{dt} + \frac{V_2}{R_d}$$

Equation 5

$$\frac{dV_2}{dt} = \frac{1}{C} \times \left(I - \frac{V_2}{R_d} \right)$$

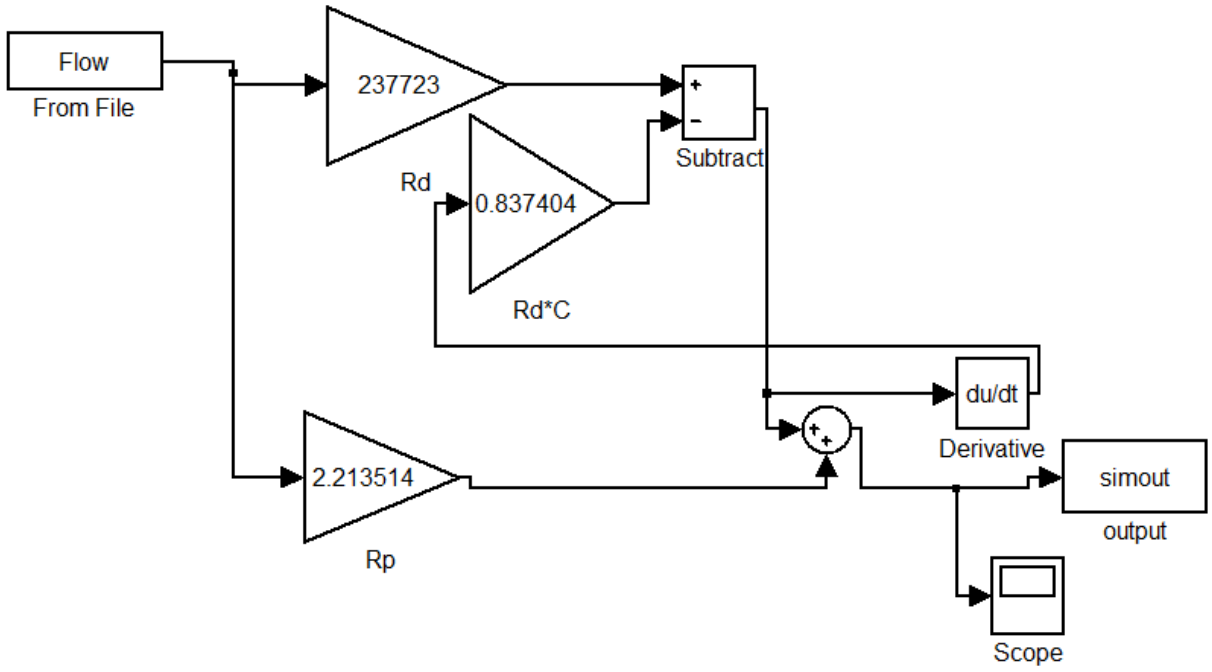

Figure 3-13. Simulink model of differential equations of Windkessel model

Then the result of the Simulink model was imported in a fitness function produced in MATLAB. The fitness function is equal to: fitness= sum ((y-optimalCurve). ^2), where y is the pressure graph in Figure 3-6 and the optimal curve is the result from the Simulink model. The developed Genetic algorithm code creates a population of 200 individuals in the format of (Rp, Rd, and C) from positive numbers. The program has been set to stop after 50 generations. The population of triple

gene individuals is entered in Simulink model and the result is checked with the fitness function. After each generation, the best fitted individuals (Rp,Rd,C) is transferred to the next generation and after 50 generations the program stops. The block diagram of the process is shown in Figure 3-14.

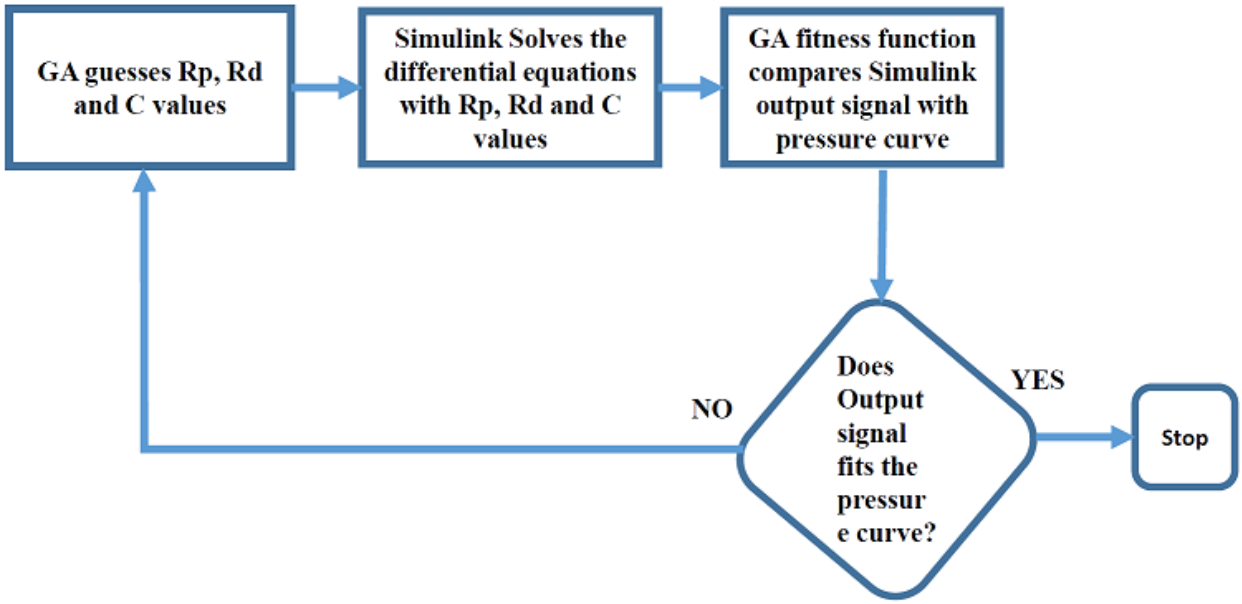

Figure 3-14. Block diagram of the algorithm used to find the values of the Windkessel model by Simulink model and genetic algorithm

The fitted curve is shown in Figure 3-15 . The red graph is the curve found by GA, and the blue graph is the pressure curve. The red graph is close enough to the blue for our purpose.

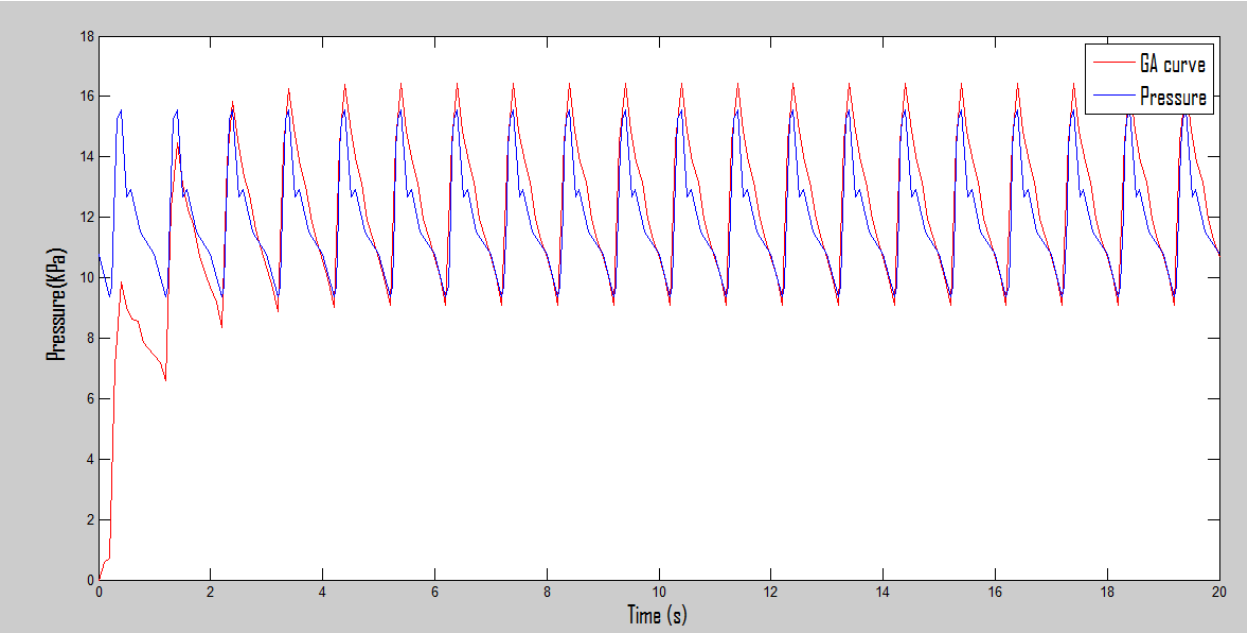

Figure 3-15. Fitted curve to pressure found by genetic algorithm

3.5.1 Euler numerical method of solving ordinary differential equations

The Euler numerical method was used to solve Equation 3, Equation 4, and Equation 5.

$$V = I \times R_p + V_2$$

$$I = C \times \frac{dV_2}{dt} + \frac{V_2}{R_d}$$

$$\frac{dV_2}{dt} = \frac{1}{C} \times \left(I - \frac{V_2}{R_d} \right)$$

Equation 6

$$V_2[n+1] = V_2[n] + \left(\frac{I[n]}{C} - \frac{V_2[n]}{C \times R_d}\right) \times \Delta t$$

Equation 7

$$V[n] = I[n] \times R_p + V_2[n]$$

$$\Delta t = 0.001$$

$$R_p = 2.213514$$

$$C = 3.9278e - 6$$

$$R_d = 237723.272583$$

Equation 8

$$I = M_0 + \sum_{k=1,n=1}^{k=5,n=N} (M_i \times \cos(2\pi k \times n \times \Delta t) + M_j \times \sin(2\pi k \times n \times \Delta t)$$

Where V is the pressure at point A at Figure 3-12, and V2 is pressure at point B, Rp and Rd and C are the components of windkessel model and I is the flow entering to the circuit of Figure 3-12 from point A. n is an integer number from 0 to number of time steps. Δt Is the time step. Equation 8 is the Fourier series form of velocity wave.

For the model Figure 3-9 that includes the iliac bifurcation the values of Rp and Rd becomes twice and the value of C becomes half.

A user-defined function (UDF) has been coded in ANSYS FLUENT to apply the outlet boundary conditions based on Equation 6, Equation 7 and Equation 8.

The inlet boundary condition is graphed in Figure 3-5 and was converted to Equation 8 using a Fourier series. A UDF was used to assign it to the ANSYS FLUENT aneurysm models.

3.6 ASSUMPTIONS

3.6.1 Elasticity of the vessel wall

The aortic wall contains collagen and elastin fibres that provide the elastic behaviour; however, in case of AAA elasticity of the wall is reduced. In the present model the wall was assumed to be rigid although some of the features of the elastic wall were captured by coupling the Windkessel model to the 3D model. One of these features is the lag between the flow and pressure curves. Another one is the shape and values of the pressure curve as will be seen in the results section. Finally, elasticity of the aorta is linked to changes in the pressure, moving from the aortic root to downstream areas. The pulse wave traveling from the heart is reflected at downstream branches and it contributes to augmenting the upstream pressure in amplitude as well as to sharpening the profile, while the dicrotic notch slowly is lost. A limitation of our model is the presence of the same pressure profile throughout the simulated portion of the aorta.

3.6.2 Newtonian flow

Blood is a suspension of red blood cells, other cells, and platelets and is categorised as non-Newtonian fluid. We assumes a Newtonian flow because first of all the non- Newtonian assumption is supported for vessels with diameters less than 1 mm[15] second of all the non-

Newtonian behaviour is more obvious at the core regions of the vessel where the values of the shear stress are considered low while in our model the wall shear stress values are important which still are enough high to rely on Newtonian assumption [15]. Most of the current literature utilized a Newtonian blood model. Further refinement of the model should investigate the use of non-Newtonian models.

3.6.3 Incompressible flow

Blood has been assumed to be incompressible with a constant density of 1050 kg/m^3.

3.6.4 Laminar viscous flow

Flow in an AAA is considered laminar because of the velocity values produced by heart, and because of flow properties. The Reynolds number at the inlet ranges between 100 and 1700 (refer to Figure 3-16). Viscosity was assumed 0.00319 Pascal.S

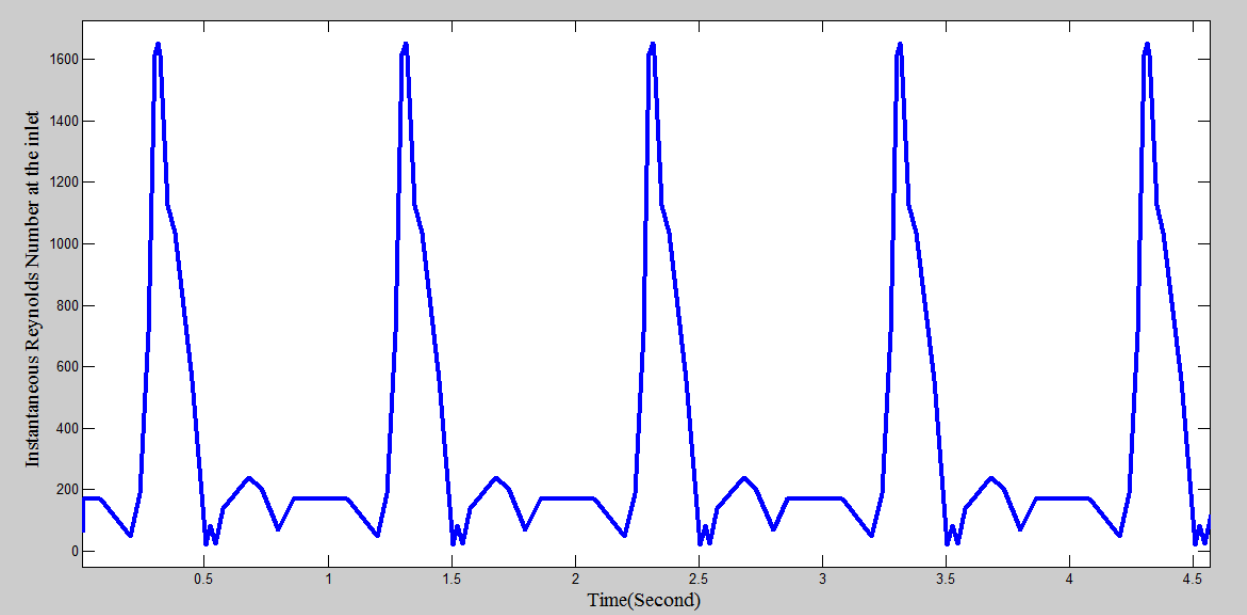

Figure 3-16. Reynolds number in the model

3.7 GOVERNING EQUATIONS

Conservation laws are the key components to solving fluid flow problems: namely, conservation of momentum, of mass and of energy. Continuity equation and conservation of momentum are the governing equations; because we consider the body to be at a constant temperature, temperature changes can be neglected and therefore conservation of energy does not need to be imposed. According to Newton's second law, balance of body forces and normal and tangential forces will result in 3 equations of momentum. When one considers the blood to be Newtonian and incompressible flow density and viscosity, the result is 3 equations of Navier stokes (Equation 9). Adding the continuity equation (Equation 10), we have four equations and four unknowns, 3 velocity and one pressure. Navier stokes equations are nonlinear second order partial differential equations and there are no analytical solutions for them, so the general approach for solving them is a computational approach. FVM is the computational approach used in solving these equations in the present research.

Equation 9

$$\frac{\partial V}{\partial t} + (V.\nabla)V = \frac{-\nabla P}{\rho} + \upsilon\nabla^2 V$$

$$V = (u, v, w)$$

Equation 10

$$\nabla.V = 0$$

Where V is the velocity vector composed of three components u, v, w.

ρ Is the density, P is the pressure and υ is the kinematic viscosity.

3.8 CFD ANALYSIS

Computational Approach

In this section the method used to solve the differential equations will be summarized. The mesh was imported in ANSYS FLUENT. Since the flow is incompressible, the pressure based segregated solver with the PISO scheme is used to solve the differential equations: PISO is similar to SIMPLE algorithm. SIMPLE algorithm is a pressure velocity coupling algorithm. When the momentum equation is solved by guessing the pressure for the first iteration, the face fluxes do not satisfy conservation of mass. So a correction is done to the fluxes in order to satisfy continuity equation, this correction is applied by SIMPLE algorithm. PISO is more accurate because it uses higher orders of approximation for velocity and pressure calculations.

In a simple way the idea of pressure based solver is that velocities will be gained by solving momentum equations. The velocity field is obtained by solving the momentum equation and using pressure at the previous iteration in order to satisfy continuity equation; the velocity field is updated until convergence of all equations. The segregated solver was chosen to minimize the memory usage. This solver solves the momentum and continuity equations sequentially resulting in a memory effective process. The FVM was implemented to discretize the governing equations, which implies that the variables are computed at the center of each cell or control volume. In order to interpolate cell center values for the faces of each cell, a second order upwind scheme was used, which gives higher accuracy while requiring more time to converge. The gradients of variables at cell centers were calculated by a green gauss cell based scheme. These gradients are required in

order to use upwind schemes. These gradients will be gained by taking the average of cell face area multiplied by average of two neighbor cell center values. Second order upwind scheme, finds the face values by adding the cell center value at upstream cell to multiplication of gradient at upstream cell and displacement vector from upstream cell center to face center.

3.8.1 Verification of CFD results

To verify the results of the CFD analysis four steps were done as follows.

1- Spatial convergence of the simulation

2- Temporal convergence of the simulation

3- Convergence of governing equations for each time step

4- Validation of CFD simulations with experimental data

To test whether the mesh resolution is satisfactory mesh sensitivity analysis was performed. Three meshes were created with edge sizes of 0.5, 0.7 and 0.9 millimetre. At time 3.9 of cardiac cycle at a specific line on the neck of the model the velocity was plotted for each mesh. Figure 3-17 shows these plots: from the plots it is noticeable that mesh 0.7 and 0.5 coincide and increasing mesh elements would not result in further improvements.

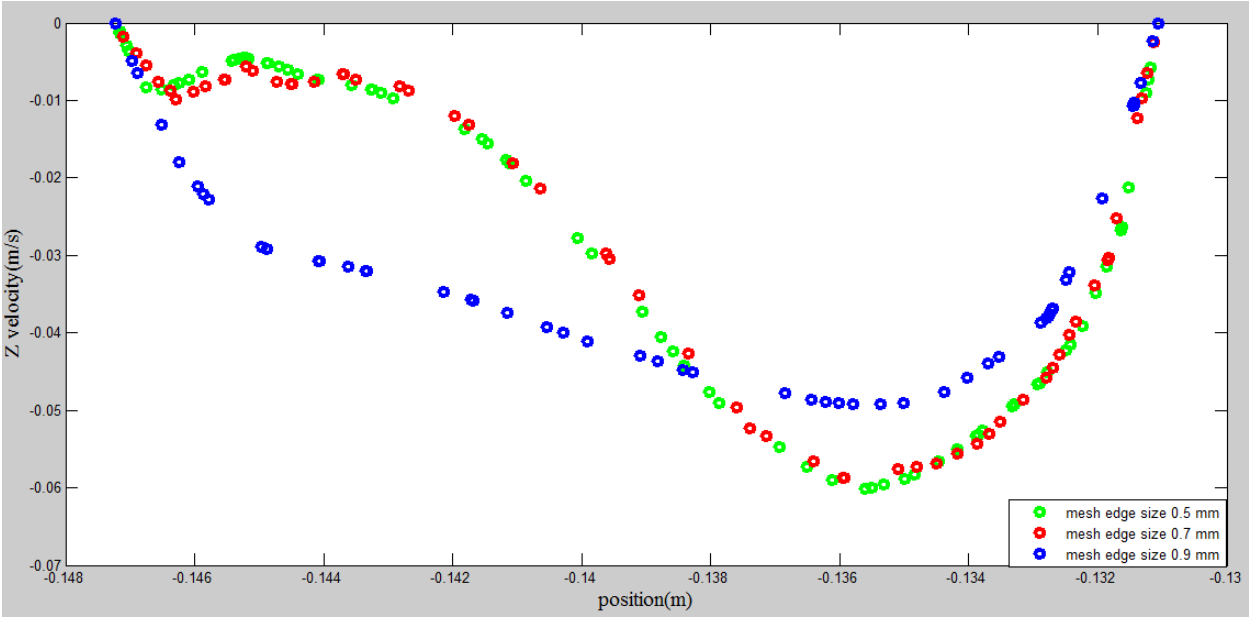

Figure 3-17. Mesh sensitivity analysis of patient A, it is seen that the results of mesh edge size 0.5 corresponds to mesh edge size 0.7 and so the mesh has converged.

For mesh with edge size 0.7, the temporal resolution was tested. A simulation was run for two time steps of 0.01 and 0.001 s and the velocity monitored for a specific line at time 3.5 s for both time steps Figure 3-18 shows no difference between the results; therefore it was concluded that the solution has enough temporal resolution.

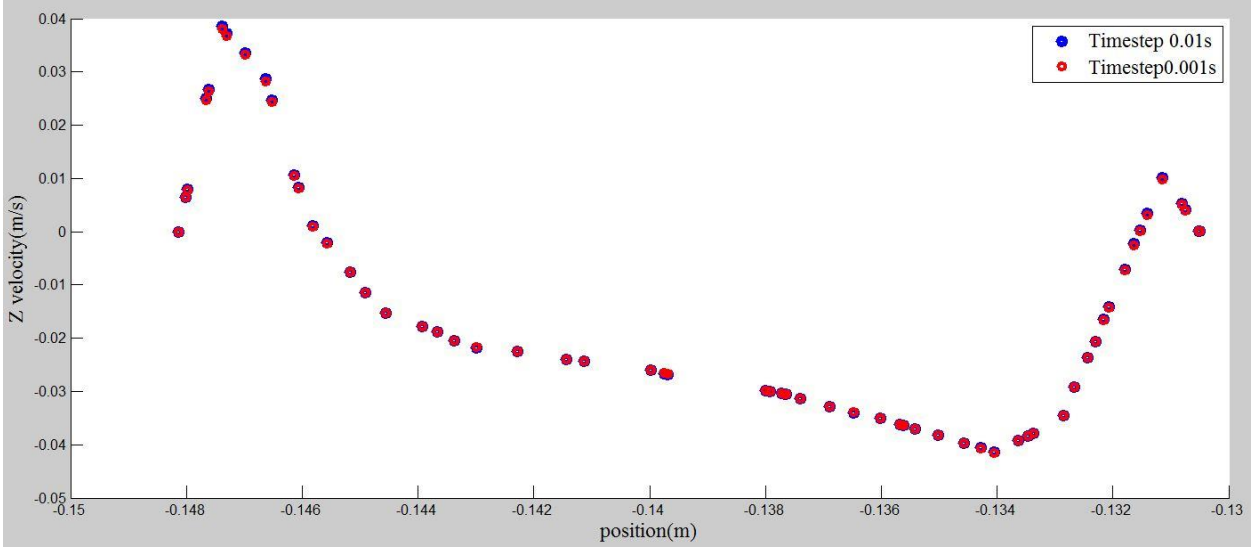

Figure 3-18. Time step sensitivity analysis. It is seen that both time steps 0.01 and 0.001 gave the same results so we can conclude that we achieved a good temporal resolution.

For mesh 0.7 the convergence of the governing equations was checked for each time step. Figure 3-19 shows that the continuity equation initializes from 1 and momentum from 0.01. According to Ansys criteria of checking convergence if each of the equations falls 3 orders of magnitude under their initial values they are converged and so this happened by setting convergence tolerance to 0.001 for each of the equations. For further confidence on convergence of equations, two more simulations were done for convergence tolerance of 0.0001 and 0.00001 for each equation and at point 1 in Figure 4-9 wall shear stress was monitored. Figure 3-20 shows that all three simulations gave the same results for WSS at point 1. Therefore we can conclude that equations have converged throughout the cycle.

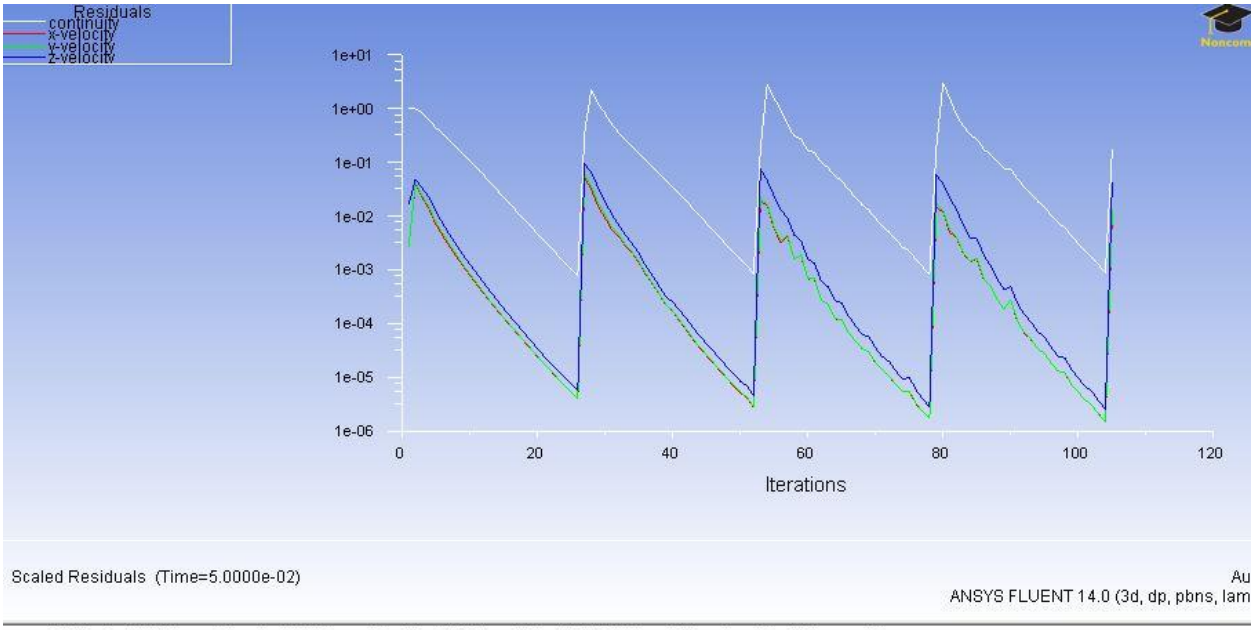


```
   102 1.7242e-03 3.0566e-06 3.0517e-06 5.5195e-06  0:03:22   66
   103 1.2335e-03 2.0633e-06 2.0611e-06 3.6559e-06  0:03:18   65
!  104 solution is converged
   104 8.9439e-04 1.5014e-06 1.4996e-06 2.5471e-06  0:03:15   64
Flow time = 0.04s, time step = 4
396 more time steps

Updating solution at time levels N and N-1.
 done.
  iter continuity x-velocity y-velocity z-velocity     time/iter
!  104 solution is converged
   104 8.9439e-04 1.5014e-06 1.4996e-06 2.5471e-06  0:04:34   90
   105 1.7018e-01 1.0280e-02 1.2391e-02 4.2608e-02  0:04:48   89
```

Figure 3-19. Convergence of the governing equations for each time step. It is seen that each of the equations fall three orders of magnitude under their initial value

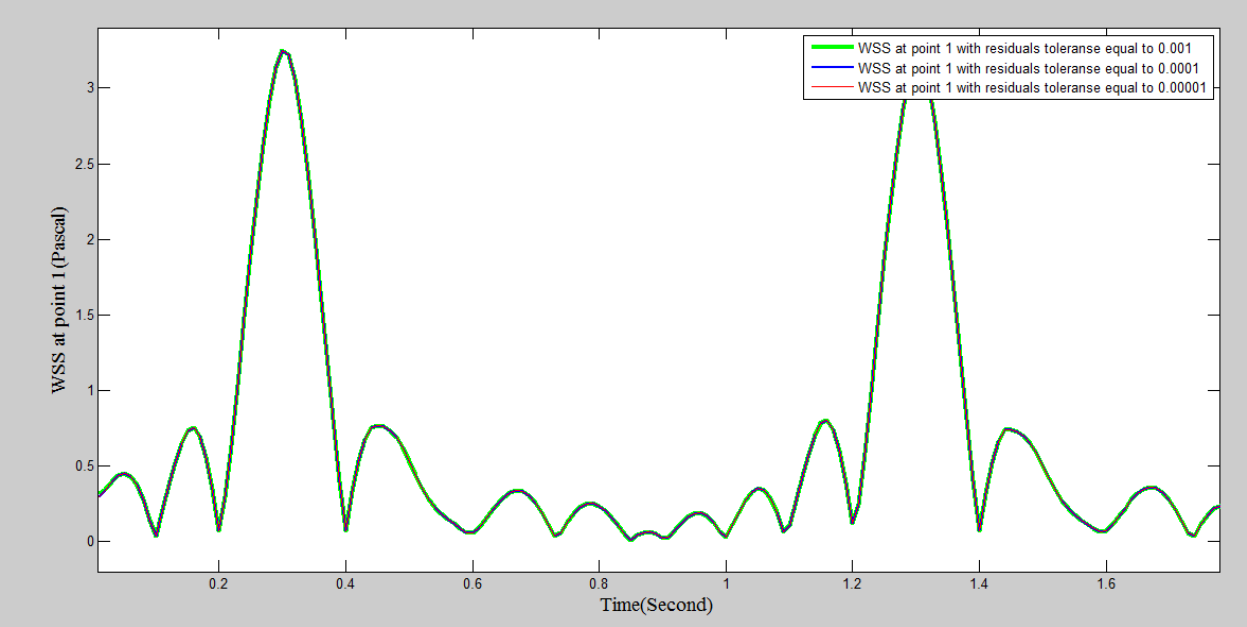

Figure 3-20. Residual sensitivity analysis. Green and blue graphs are monitored values of WSS at point 1 of Figure 4-9 on the Patient A model. Although the tolerance criteria was set to 0.001 and 0.0001 and 0.00001 simulation results didn't change, meaning that all 4 equations has been converged for each time step.

3.8.2 Validation of CFD results

In order to validate results from CFD a straight tube of 1.27 cm diameter and 150cm length was considered from[47]. At distance 100 cm from the inlet, a 30% blockage in diameter was applied; Figure 3-21 shows the cross section. Flow had Reynolds of 1250, Womersley number of 4.4, viscosity of 0.0038 Ns/m^2 and density of 1070 kg/m^3. A sinusoidal flow wave (Figure 3-22) was applied as inlet boundary condition and no-slip conditions were applied at the wall. The outlet had no constraints.

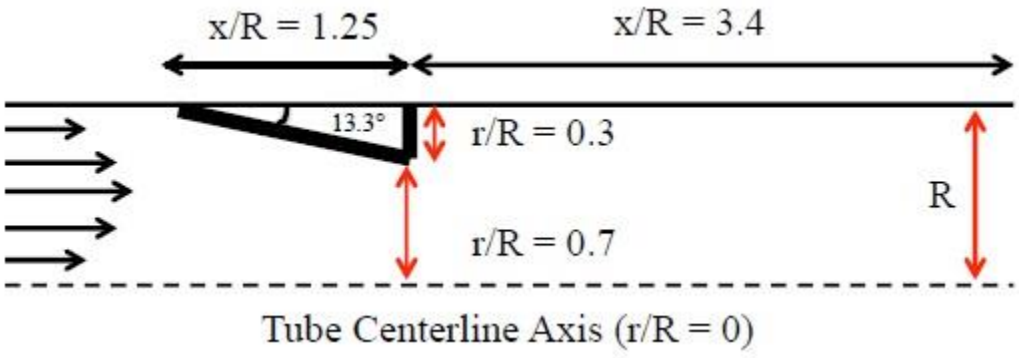

Figure 3-21. Schematic of a cross section of the tube, dashed line is the centerline and the triangle represents the blockage[47]

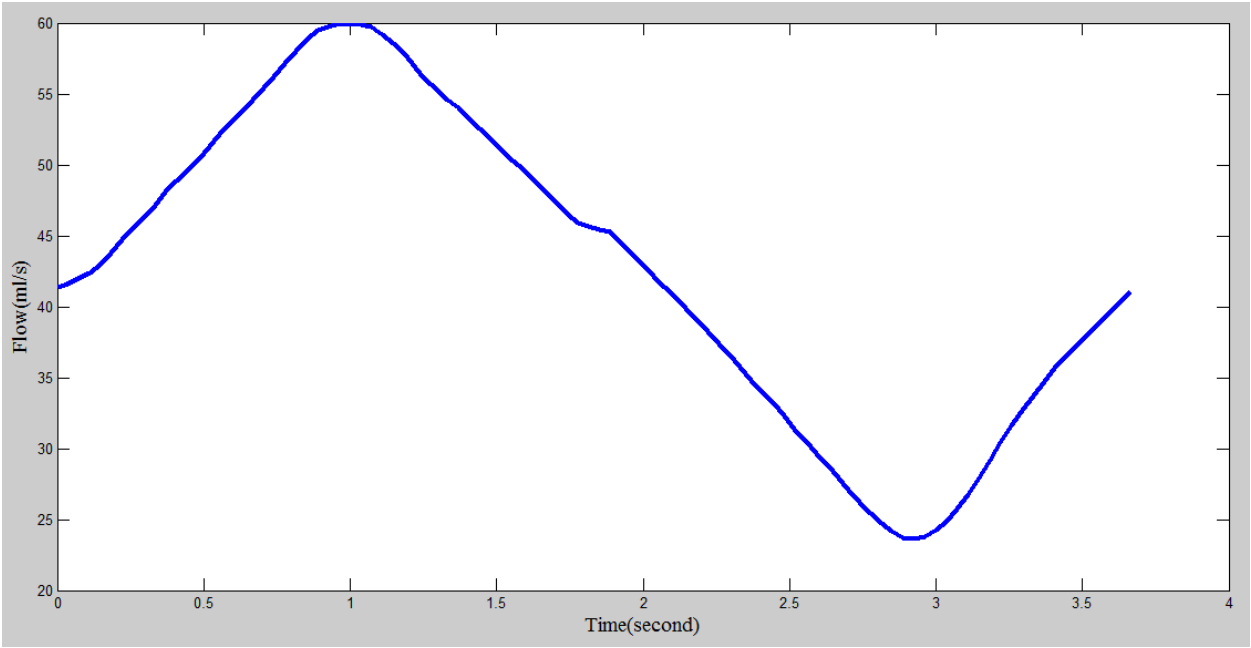

Figure 3-22. Flow at the inlet of rigid tube[47]

At two distances downstream of the blockage and at 3 instants throughout the cycle, velocities were plotted to be compared with experimental data.

1- At 0.19 cm and time 1.07 s

2- At1.9 cm and time 1.07s

3- At 0.19 cm and time 2.33 s

4- At 1.9 cm and time 2.33s

5- At 0.19 cm and time 3.55s

6- At 1.9 cm and time 3.55s

3.8.3 Results

Figure 3-23 shows the cross section of the tube at time instant 1.07 second: a recirculation region is seen downstream of the blockage.

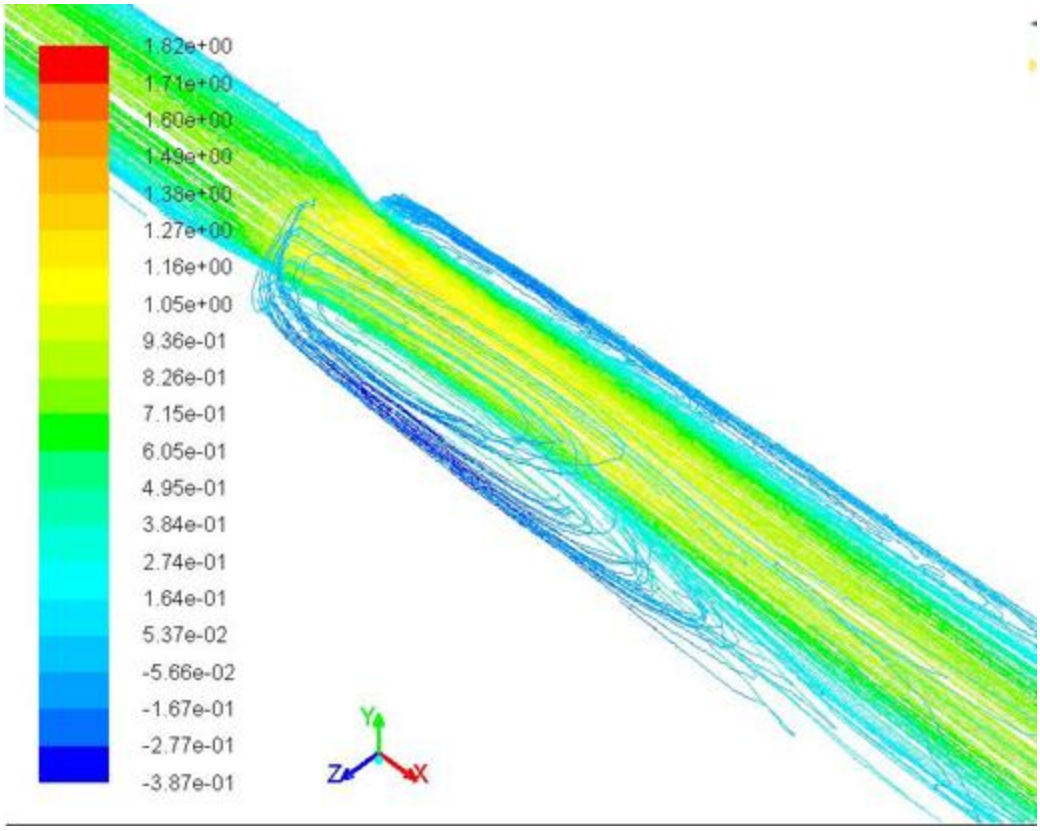

Figure 3-23. Velocity streamlines at time 1.07 s, downstream of the blockage a recirculation region is noticeable

In the following graphs Figure 3-24, Figure 3-25 it is seen that at 0.19 cm distance from the blockage both experiment and CFD show recirculation at the wall. The results show a correlation of 81 percent. This correlation coefficient means the two graphs behave similarly 81percent. The value gained from normalized covariance of the two curves. At distance 1.9 of the same time instance there is no recirculation detected by the experiment and CFD shows recirculation. The difference between experiment and CFD results can be explained by the following reasons: 1- flow could be transient at the stenotic site because of reduction in diameter and increase in velocity, while it was considered laminar in the CFD study; 2- The length of the tube is 1.5 m but the grid had to be kept relatively coarse due to cpu costs. 3- There could be small experimental errors that further increase the difference between the two results.

Despite these errors, the results show an acceptable correlation and they provide confidence with respect to the CFD simulations performed.

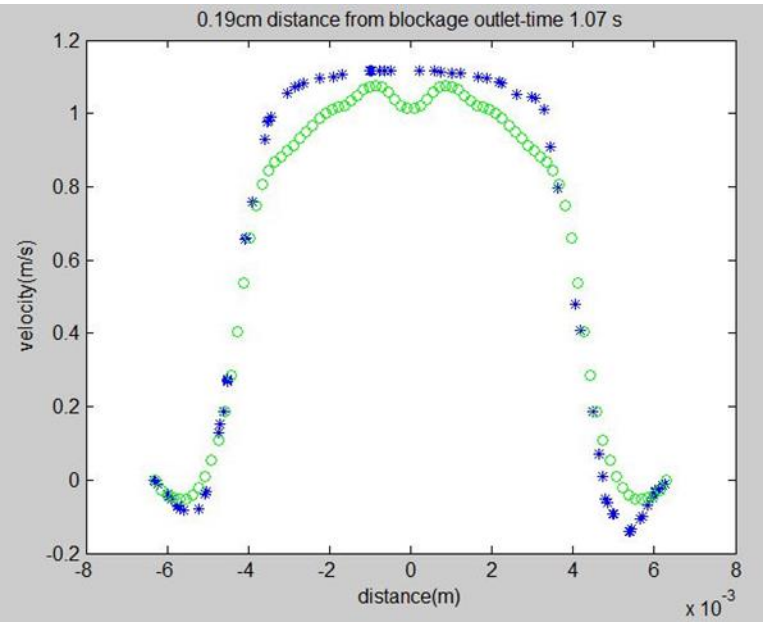

Figure 3-24. At distance 0.19cm from the blockage and time 1.07 s. Correlation coefficient=0.81 green curve is experiment and blue curve is CFD

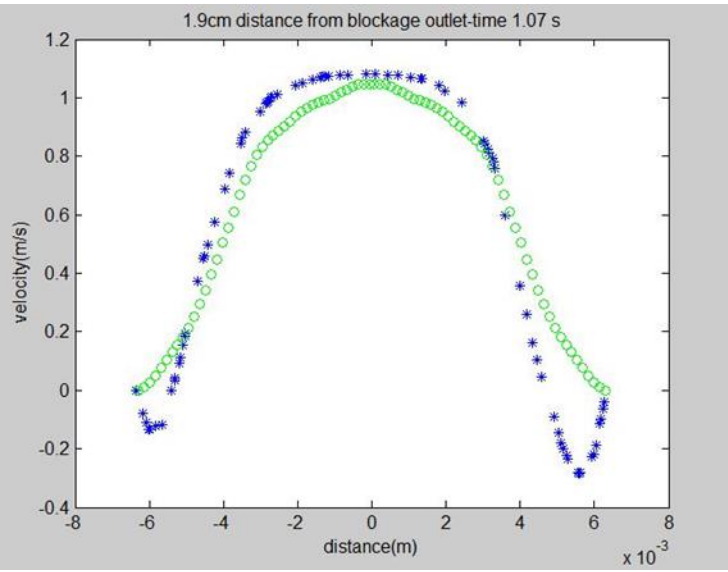

Figure 3-25. At distance is 1.9cm from the blockage and time 1.07 s. Correlation coefficient=0.9 green curve is experiment and blue curve is CFD

In the following graphs Figure 3-26, Figure 3-27 and Figure 3-28obtained at 0.19 cm and 1.9 cm distance from the blockage respectively, a recirculation is detected by the experiment and can be seen in the CFD results as well. The graphs show correlation coefficient of 0.83 and 0.93 respectively.

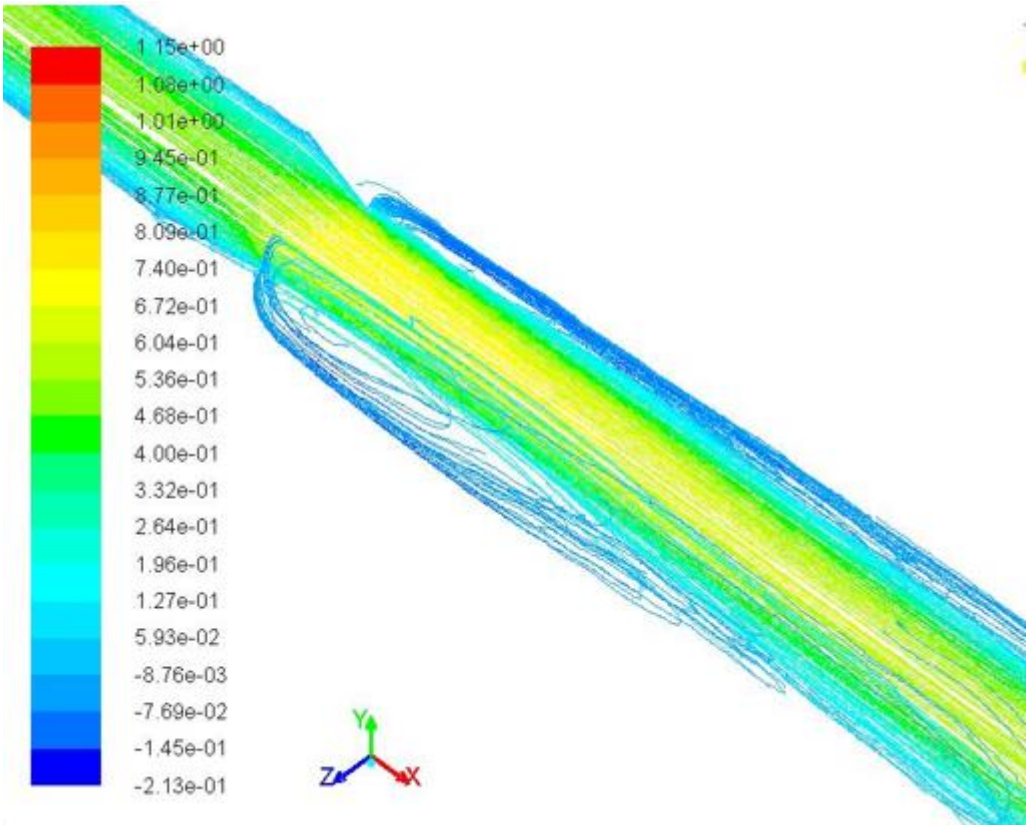

Figure 3-26. Velocity streamlines at time 2.33

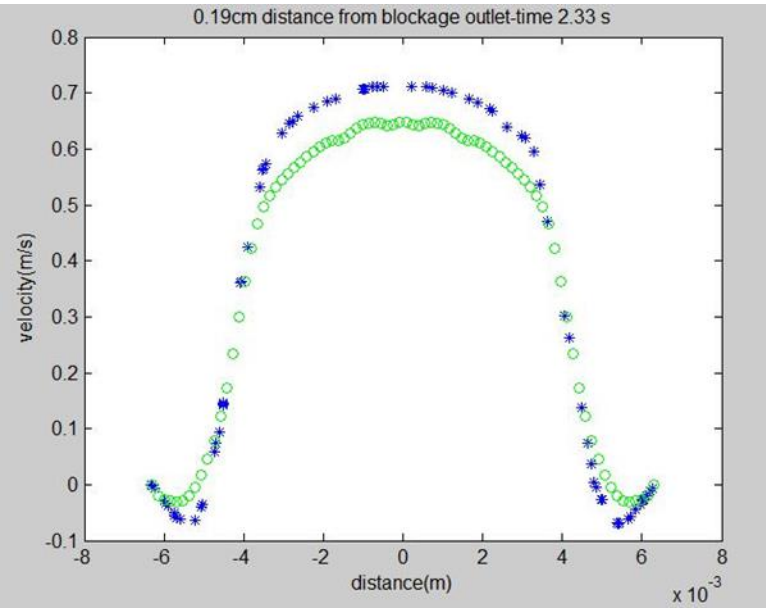

Figure 3-27. At distance 0.19cm from the blockage and time 2.33 s. Correlation coefficient=0.83

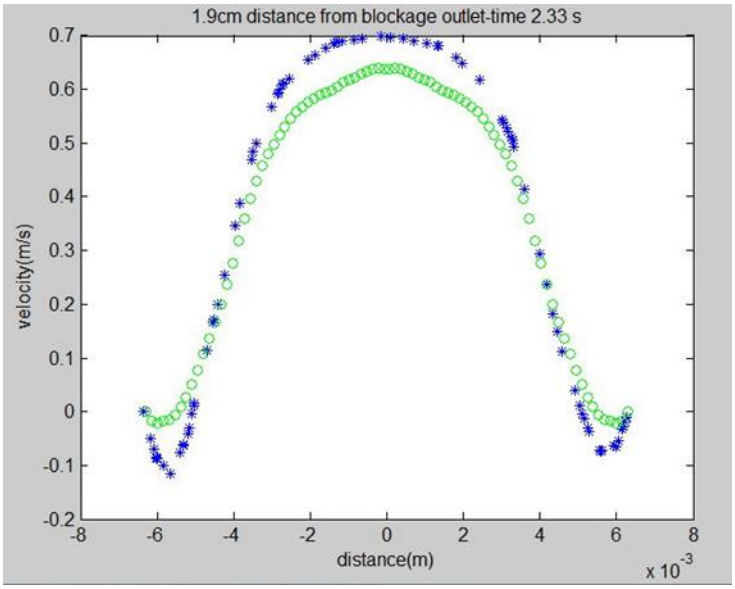

Figure 3-28. At distance 1.9cm from the blockage and time 2.35 s. Correlation coefficient=0.93

In the following graphs Figure 3-29, Figure 3-30 and Figure 3-31 at 0.19 cm and 1.9 cm distance from the blockage respectively, a recirculation is detected by the experiment and can be seen in CFD results as well. Results show correlation coefficient of 0.83 and 0.95 respectively.

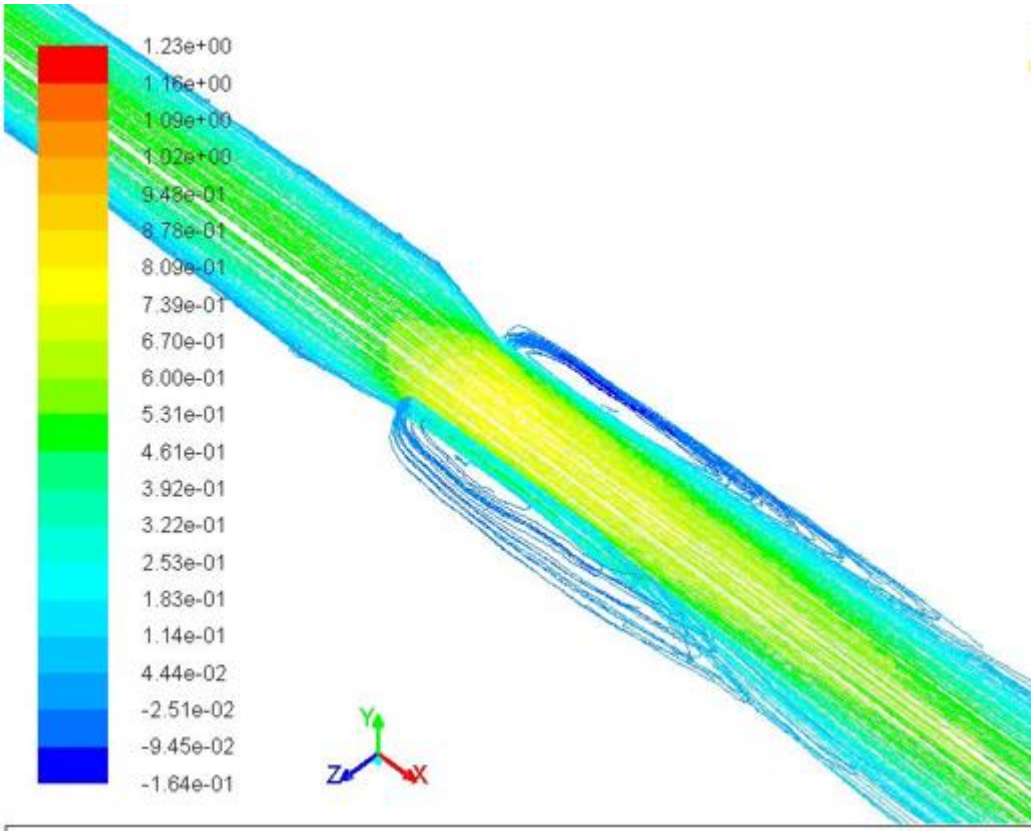

Figure 3-29. Velocity streamlines at time 3.55 s

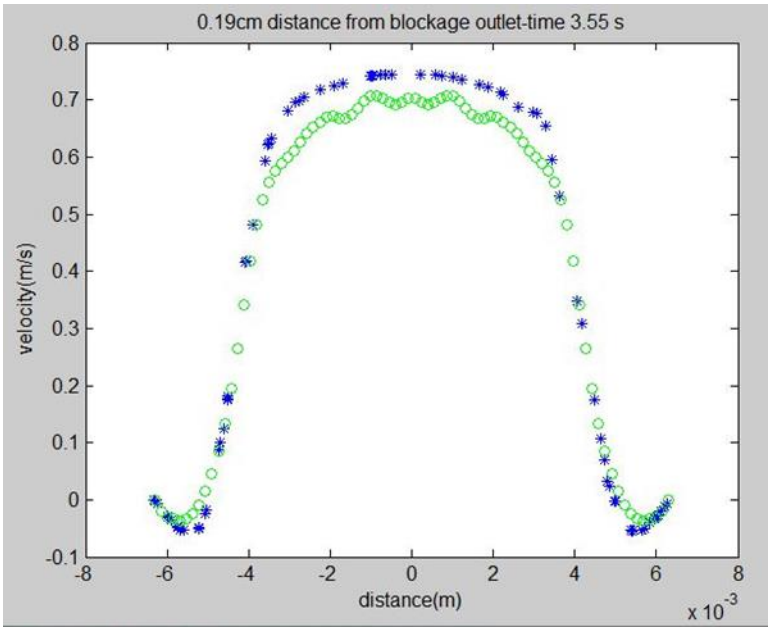

Figure 3-30. At distance 0.19 from the blockage and time 3.55 s. Correlation Coefficient =0.83

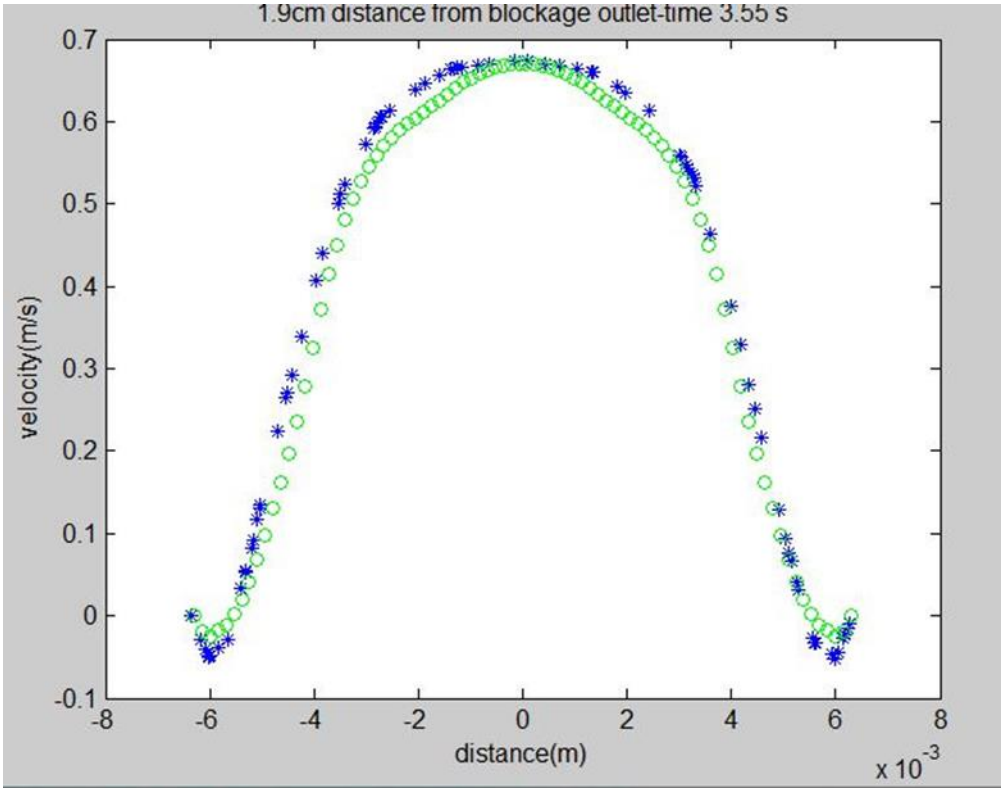

Figure 3-31. At distance 0.19cm from the blockage and time 3.55 s. Correlation coefficient=0.95

How to measure the accuracy of the CFD results for the AAA model?

1- The CFD set up is reliable as demonstrated by the experimental validation

2- The geometry is accurate and obtained from patient specific images using validated image analysis techniques.

3- The boundary conditions are realistic.

4- The simulation is not mesh or time step dependent.

5- The governing equations converged at each time step

The conclusion is that the AAA simulation results are accurate enough to describe some of the hemodynamic features of the disease.

3.9 EXPERIMENTAL METHODS

Surgical specimens were obtained from Patient A and tissue samples were analyzed as follows.

After completing the CFD analysis, a MATLAB code was produced to make a map of mean wall shear stresses on 24 regions of the aneurysmal area. On the same 24 regions mechanical stresses were computed by means of finite element static stress analysis, using wall properties from the literature[45] and a pressure load of 120 mmHg. Tissue samples of these regions were collected during open surgery of the patient.

Specimens were selected among the ones obtained to have a wide range of shear stress (low, mid, high). The experimental protocol includes:

- Histology: H&E Stains and Musto Pentachrome stains. The protocol is outside the scope of this Thesis. The histologies were performed by the Human Performance Laboratory at Foothills Hospital.
- Mechanical testing: Specimens were cut into square samples (with side 10–12mm in length) with two edges, one (axis 1-3) parallel to the circumferential direction in the aorta, and the other one perpendicular to it (axis 2-4). To retain their material properties, unused specimens were frozen, and then thawed before they were tested—after preconditioning—using the Bose Planar Biaxial system (Bose ElectroForce, Eden Prairie, Minnesota) with strain control and load control protocols reaching a maximum stretch of 40% on both axes. A frequency of 0.333 Hz and 10 cycle count was used for each experiment. Using the acquired data, an average modulus of elasticity (stiffness) was obtained by finding the average slope of the stress-strain curve between 10% and 20%, which represent physiological values of strain.

- Histochemical analysis: molecular profiling will be done on selected specimens to measure the presence of inflammatory markers. This portion of the study is under way and no results are available.

The maps produced by my portion of the research were instrumental in collecting pieces of the aneurysmal wall corresponding to high and low wall shear stresses. The results will allow the correlation of histological and hystochemical markers of inflammation and wall degeneration to the wall shear stresses (and wall stresses).

4 RESULTS OF COMPUTATIONAL ANALYSIS

4.1 THREE GEOMETRIES WERE ANALYZED AS DESCRIBED IN SECTION 0D MODEL

An idealized geometry (similar to ones that were used in many articles in the literature), Patient A and Patient B. First, results for the ideal geometry, then for Patient A and finally for Patient B will be discussed. The results of the CFD simulations were obtained at 4 instants of the cardiac cycle. These instants are shown in Figure 3-7. Velocity streamlines, wall shear stresses, pressure contours and mean wall shear stress for both real aneurysm models and idealized aneurysm model were

Results for the instantaneous wall shear stress as calculated by Equation 11 were imported in MATLAB software in order to calculate mean wall shear stress, which is the variable affecting VECs.

Equation 11

$$\tau_{ij} = \mu(\frac{\partial u_i}{\partial x_j} + \frac{\partial u_j}{\partial x_i})$$

μ is the viscosity, u_i, u_j are velocity in x and y direction and x_j and x_j are the position at y and x direction respectively and τ is the shear stress.

Ideal geometry model

Figure 4-1 shows the streamlines in ideal geometry model. In the early systole the first figure from left show that flow is recirculating at the bulge region. At this phase flow is accelerating but when flow enters to the bulge it decelerates and recirculates. The second figure shows the mid systole, where flow streamlines stay forward without recirculation emphasizing the effect of powerful flow

at this phase in preventing the blood particles from recirculating. The third figure is showing peak systole where flow is decelerating. And at the point of the bulge it decelerates and eventually stops and recirculates. The last image is at end systole, where flow is still decelerating and producing a very low velocity regimen both in upstream and the bulge area.

The pressure and instantaneous wall shear stress pattern of this model are shown in the appendix. Figure 4-20 shows the MWSS for this geometry which will be discussed later.

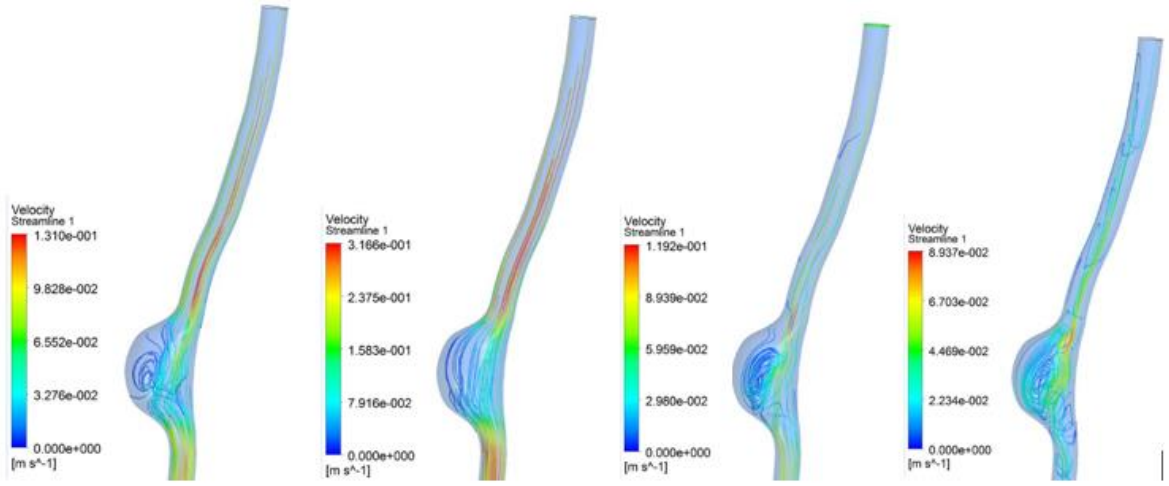

Figure 4-1. Velocity streamline for ideal geometry model of aneurysm

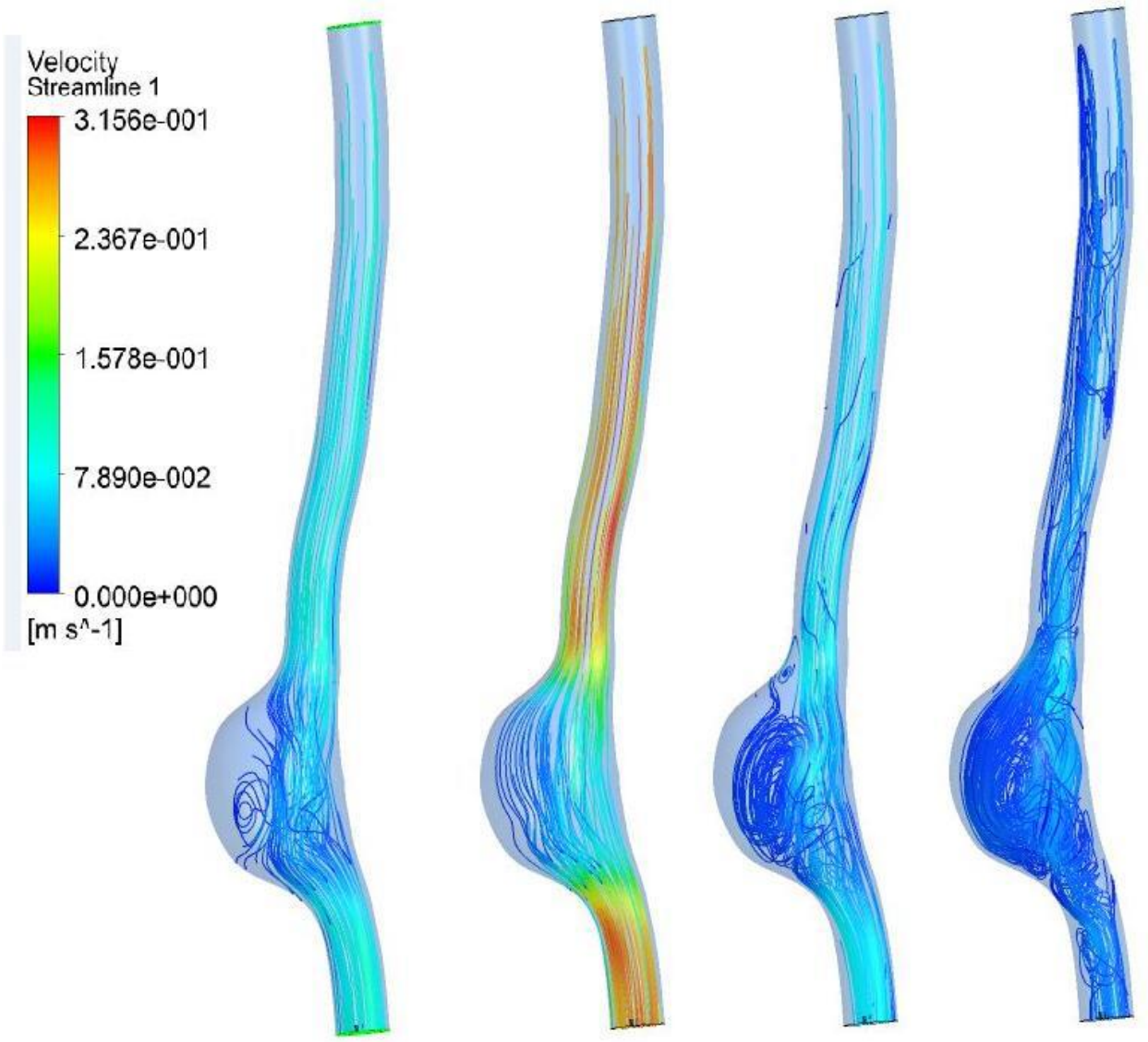

Figure 4-2. Velocity streamlines for ideal geometry model of aneurysm with the same legend

Patient A

Figure 4-3 shows velocity streamlines in patient A during 4 times of the cycle. From left to right: slightly before early systole, mid systole, peak systole and end systole. It is seen that during the cycle the velocity is higher at the inlet section and at the bifurcation comparing to the bulge area. What is noticeable is that the streamlines pattern changes at different phases. At early systole the

accelerating flow is not reversed and at mid systole, corresponding to peak flow velocity, the flow power prevents it from recirculating.Therefore streamlines stay forward with no disturbance. But in the two later phases of peak systole and end systole there is an area of recirculation, which could be due to decelerating flow that has more time to recirculate. In other words, flow has two deceleration components, 1- deceleration over time 2- deceleration because of developing into the bulge area. These two components produces a big positive pressure gradient which stops flow at the bulge and reverses it producing a recirculation region. Figure 4-4 also shows the pattern of streamlines during different phases of the cycle with the same legend.

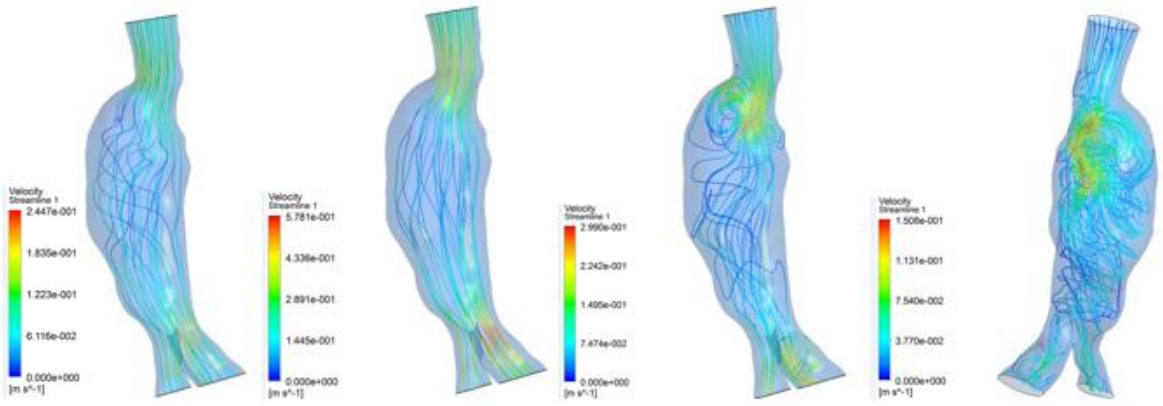

Figure 4-3. Velocity streamlines of Patient A aorta

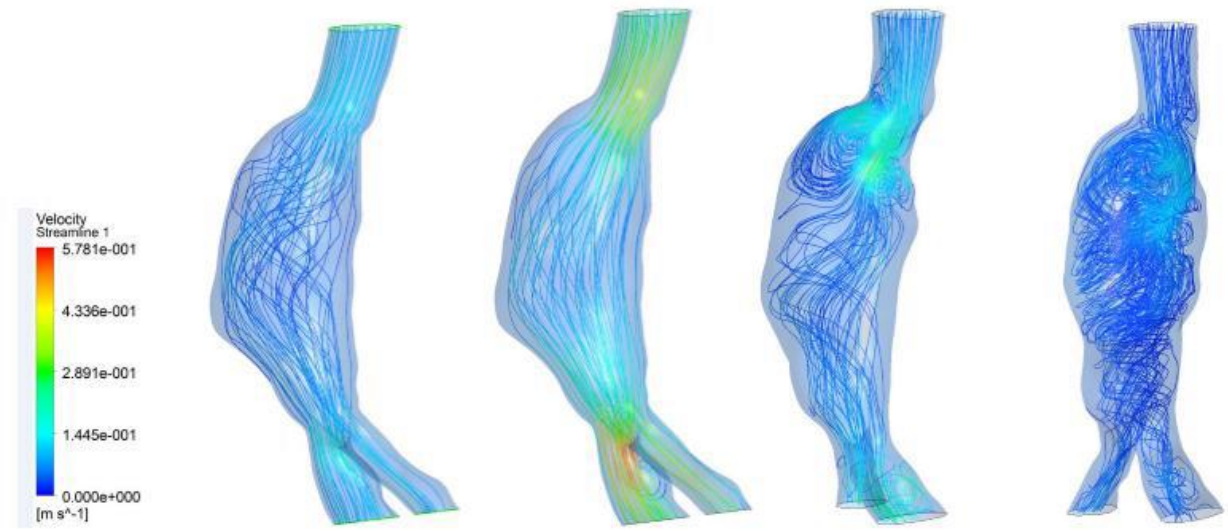

Figure 4-4. Velocity streamlines for Patient A with the same legend

Figure 4-5 shows the pattern of wall shear stress in a cycle. It is seen that the wall shear stress is close to zero on the aneurysmal section all over the cycle while on the upstream and downstream normal lumen of the model and on bifurcation the values of shear stress are noticeably higher. However the most critical phases of the cycle in terms of reduction in wall shear stress are peak systole and end systole, which are exposed to recirculating flow regions at the bulge. The second figure from the left shows highest values of shear stress at mid systole. This shows the importance of high speed flow in producing values of wall shear stress in the normal range. This can be achieved by exercising as mentioned by Dua [25]. Figure 4-6 also shows the pattern of wall shear stress during different phases of the cycle with the same legend.

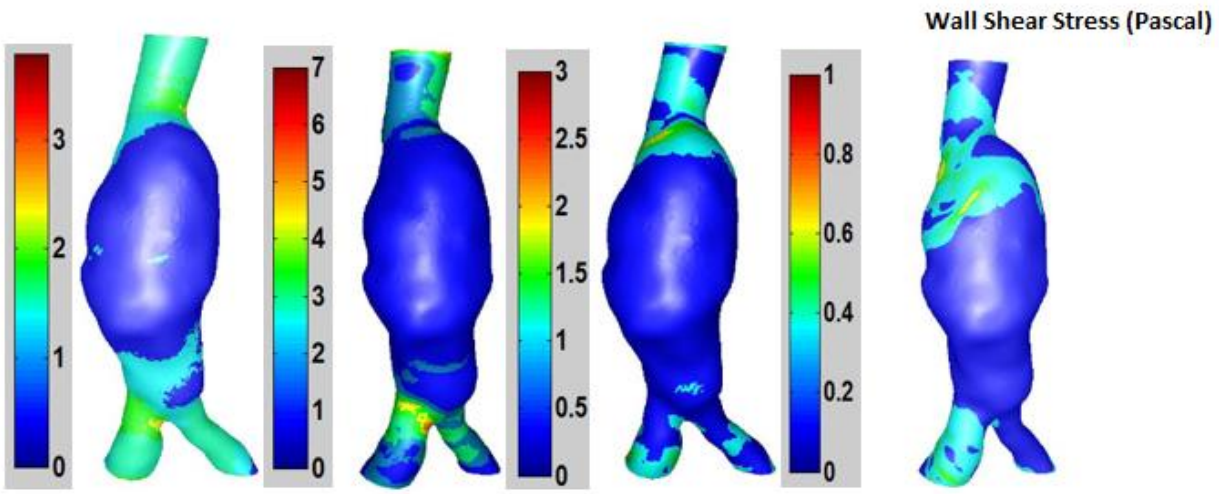

Figure 4-5. Wall shear stress contours at four times of the cardiac cycle. From left: early systole, mid systole, peak systole end systole

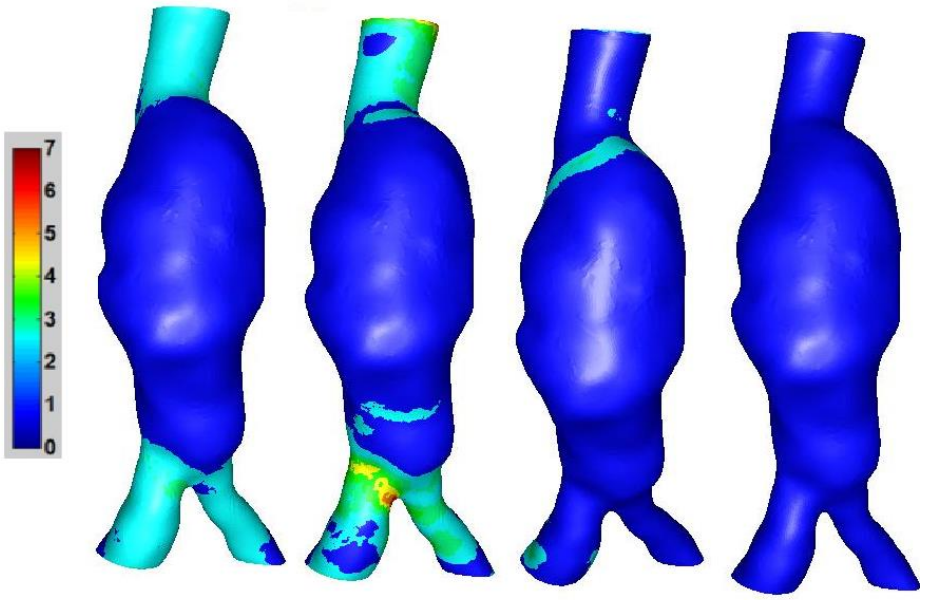

Figure 4-6. Wall shear stress (Pascal) contours at four times of the cardiac cycle. From left: early systole, mid systole, peak systole end systole

Figure 4-7 shows the pressure contours for one cycle. The pressure at end systole over the wall including the bulge is about 8500 Pascal, with slight differences across the aorta, and the pressure gradient is negative from inlet to outlets, but at mid systole the pressure is 13000 Pa with a uniform distribution. In the latter two phases of mid systole and peak systole the gradients become slightly positive resulting in recirculating flow. At peak systole the pressure is 16000 Pa or 120 mmHg and at end systole it is 13000 Pa. Pressures at end systole and mid systole are the same but flow is very different, and this is because of pulse wave effects causing the same pressure at the wall while having very different flow. It is capability of the current model capturing this effect. Figure 4-8 also shows the pattern of wall pressure during different phases of the cycle with the same legend.

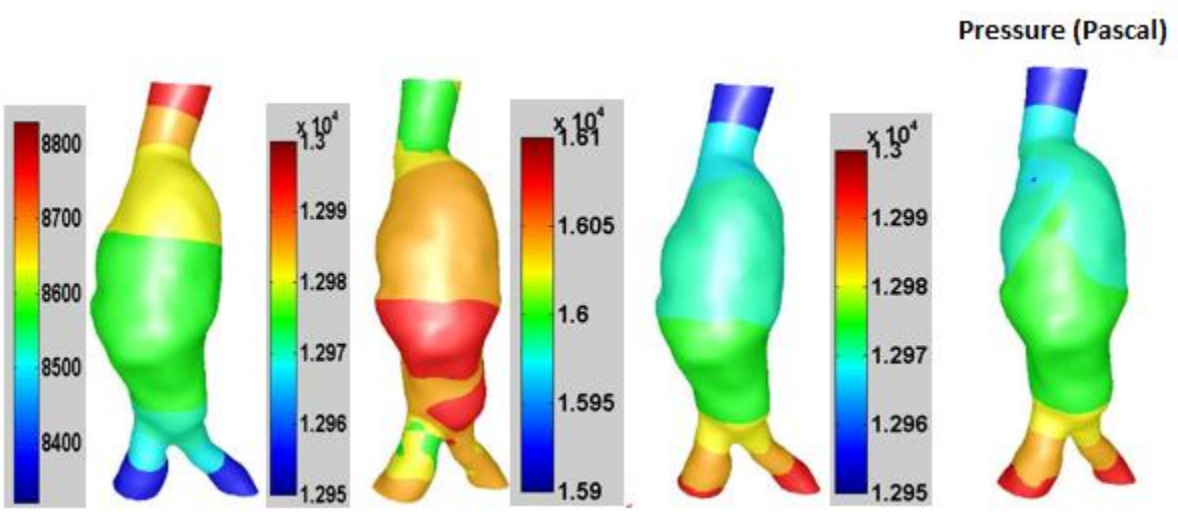

Figure 4-7. Wall pressure contours at four times of the cardiac cycle. From left: early systole, mid systole, peak systole end systole

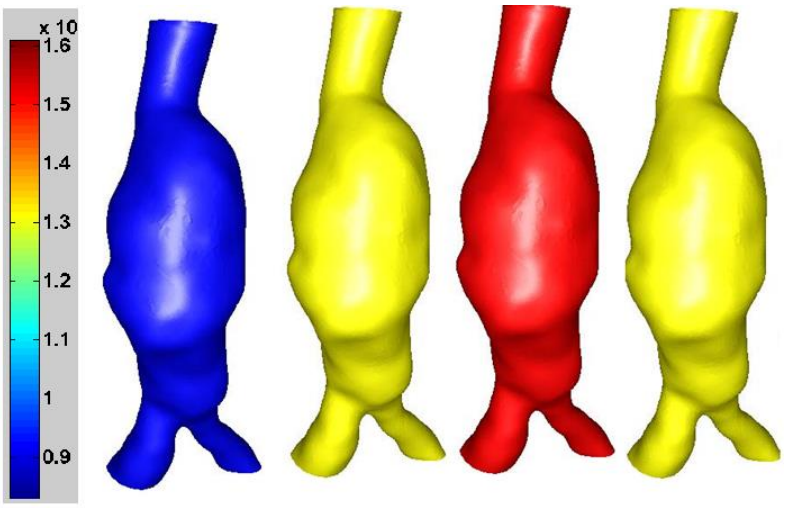

Figure 4-8. Wall pressure (Pascal) contours at four times of the cardiac cycle with the same legend. From left: early systole, mid systole, peak systole end systole

Figure 4-9 is the pressure- time curve at points 1, 2 and 3. As it can be observed, there is very little difference between the 3 curves and the shape of the curve is physiologically realistic, although physiologically the amplitude of pressure curve should slightly increases moving toward the iliac bifurcation. In this model the reduction is not appreciated due to the assumption of rigid walls.

Figure 4-10 shows the pressure curve at the same 3 points in the same model when the simulation is performed assuming zero pressure at the outlet. It is obvious that the pressure curves for this model are non-realistic both in terms of values and shape of the curve, indicating that having good boundary conditions is a must consideration in modeling the flow in AAA.

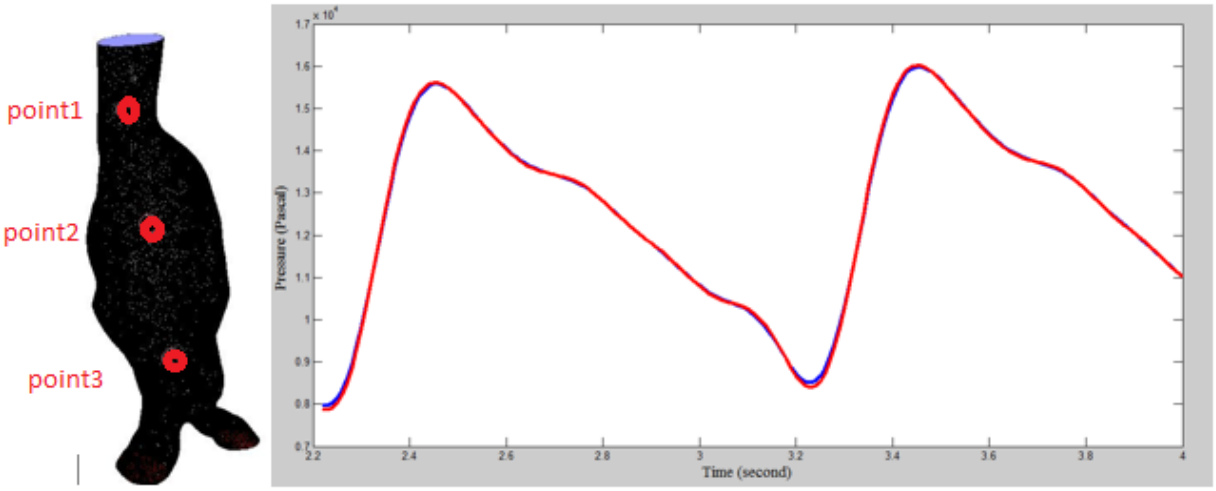

Figure 4-9. Pressure curve observed at points 1,2 and 3. Point 1 is green which is not seen because corresponds to red graph which is point 2 and blue graph is point1

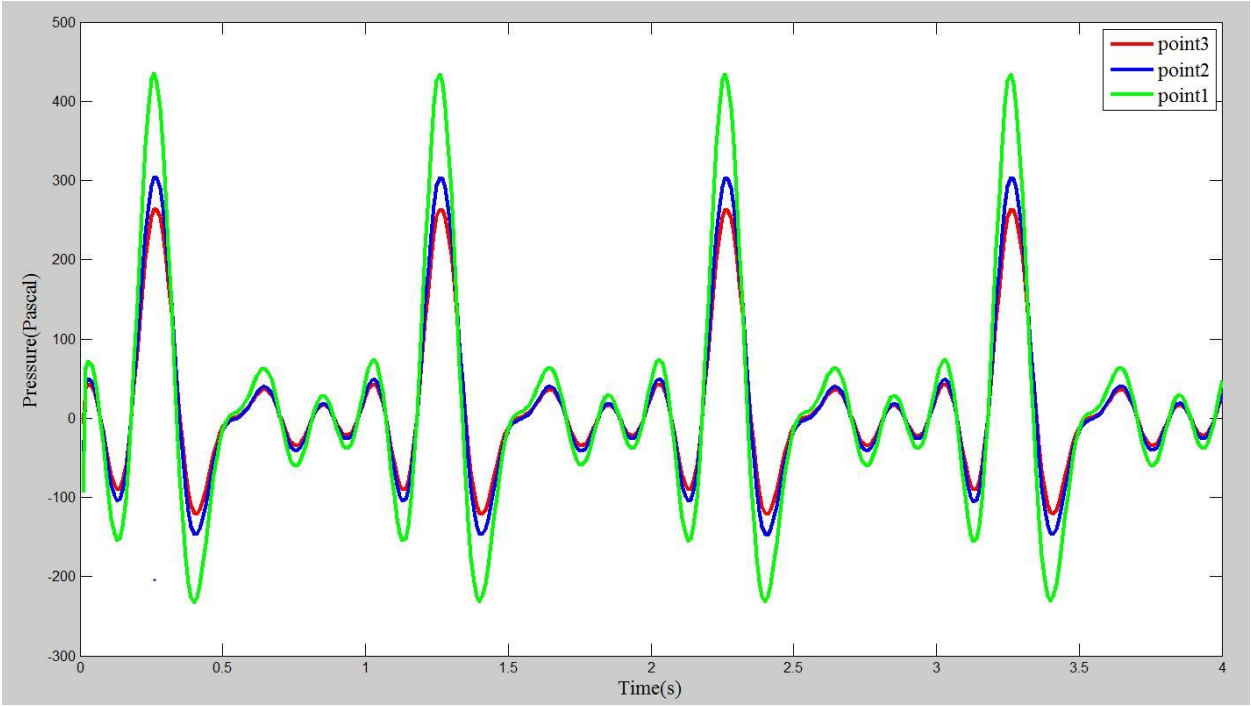

Figure 4-10. Pressure curve measured from point 1 and 2 and 3 of the Figure 5-4 in a model where the outlet pressure is set zero. It is seen that pressure curve is shrinking from point 1 to point 3, and it is close to the flow curve in contour

Patient B

Figure 4-11 and Figure 4-12 show velocity streamlines in patient B. It is seen that flow velocity in the narrowed region of the vessel above the aneurysm is higher than in the bulge itself and upstream areas. Because the velocity pattern is directly dependent to the vessel diameter we expect to see lower velocity in bigger diameter than in smaller diameters. In the real geometry of patient B the diameter of the lumen is slightly smaller than the normal upstream diameter of the vessel and there is a narrowed region above the aneurysm. So in the narrowed regions velocity is larger than at the upstream larger diameter and in the bulge area. Streamlines in the first two phases of the cycle stay forward, apparently because flow is accelerating transiently and is strong enough to wash away the accumulating platelets and red blood cells. While in the peak systole and end systole slowing down flow recirculates in the cavity and the increased residency time for blood cells may result in thrombus production. Figure 4-13 also shows the pattern of streamlines during different phases of the cycle with the same legend.

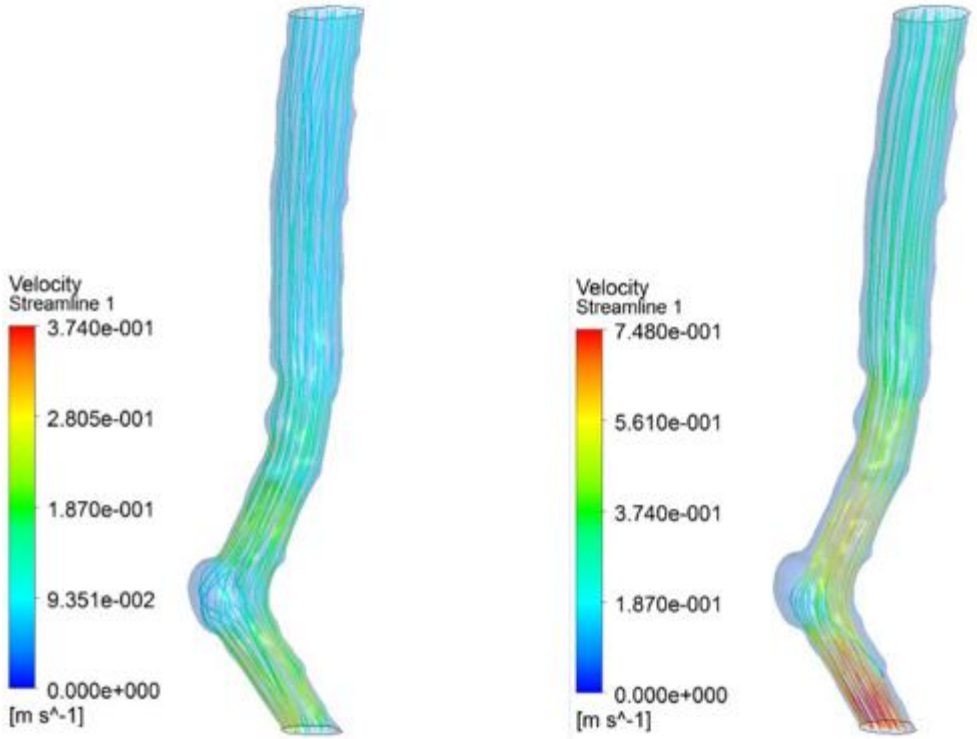

Figure 4-11. Velocity streamlines of Patient B aorta

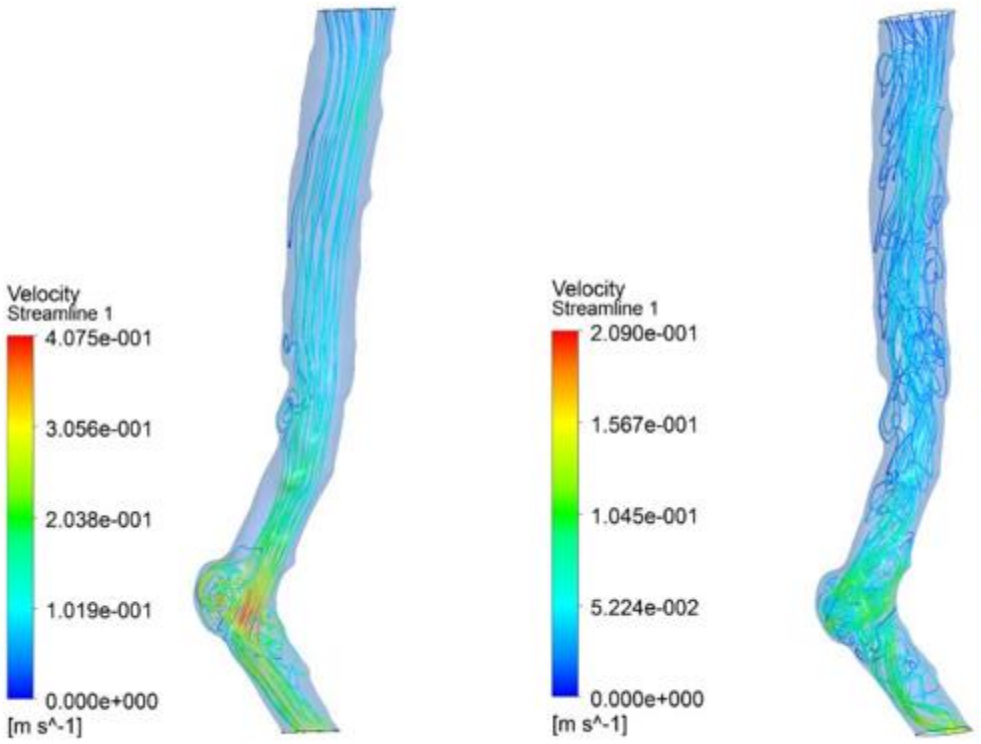

Figure 4-12. Velocity streamlines of Patient B aorta

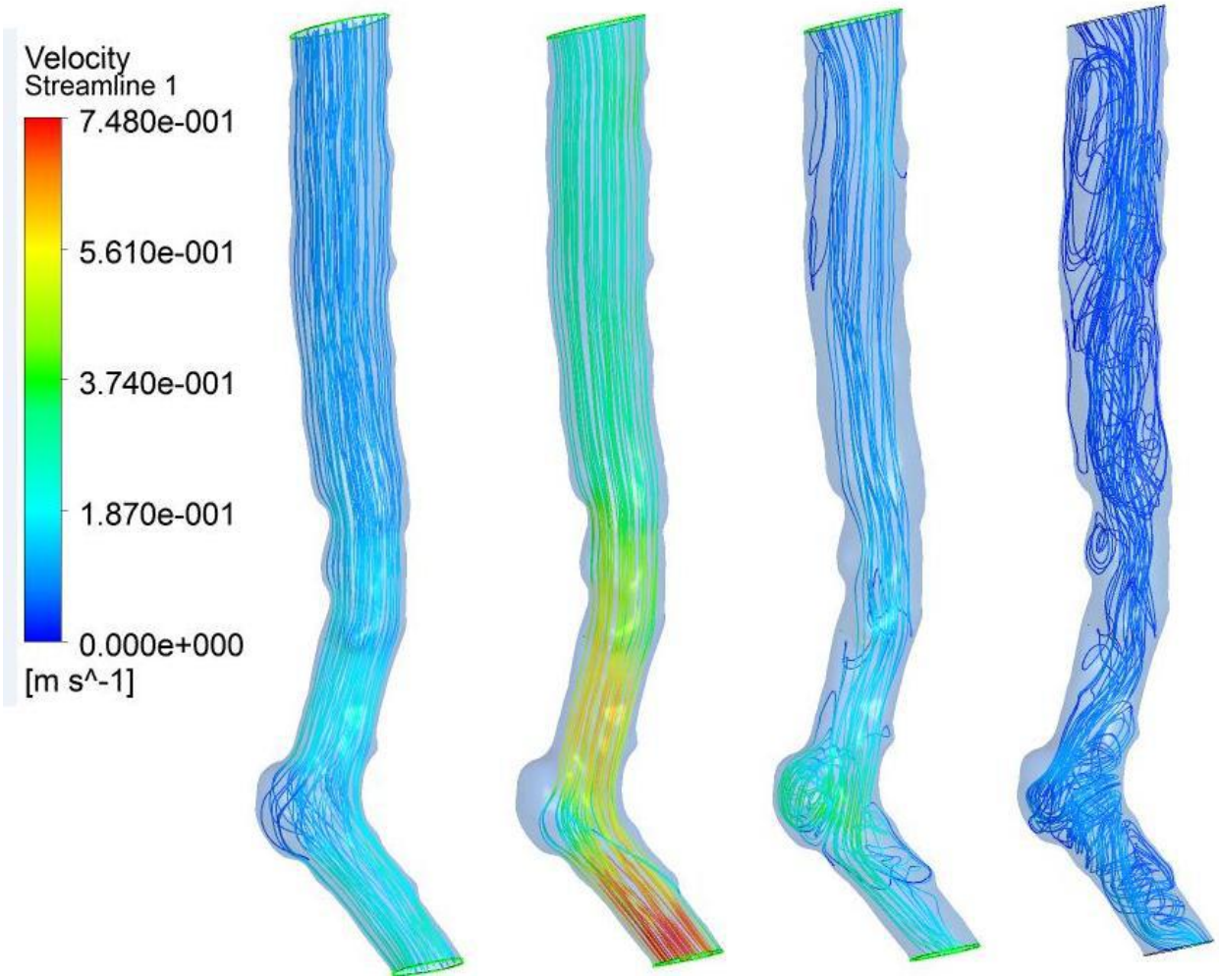

Figure 4-13. Velocity streamlines of Patient B aorta with the same legend

Figure 4-14 shows the wall shear stress pattern for patient B. At the early systolic phase it is seen that bulge shows a zero wall shear stress while at the upstream and downstream portions higher values of wall shear stress are noticed. When the flow is accelerated in mid systole (second figure from the left) wall shear stress increases and there is little difference between wall shear stress values between upstream segment and downstream segments. However in the later two phases of peak systole and end systole the shear stress values drops and also bulge is exposed to similar values compared to upstream regions. This results highlights the importance of patient specific

geometry in CFD simulations: in this case it appears that the lumen at the bulge has become small enough due to thrombus formation that there is no more low shear stress effect at this stage of the cycle, while in the Patient A the bulge still had the lowest values of the wall shear stress compared to the rest of the vessel. Furthermore, at end systole, patient B is exposed to low wall shear stress across the wall both in the bulge and corresponding to the normal regions of the aorta. This is due to low flow velocity at this phase. Figure 4-15 also shows the pattern of wall pressure during different phases of the cycle with the same legend.

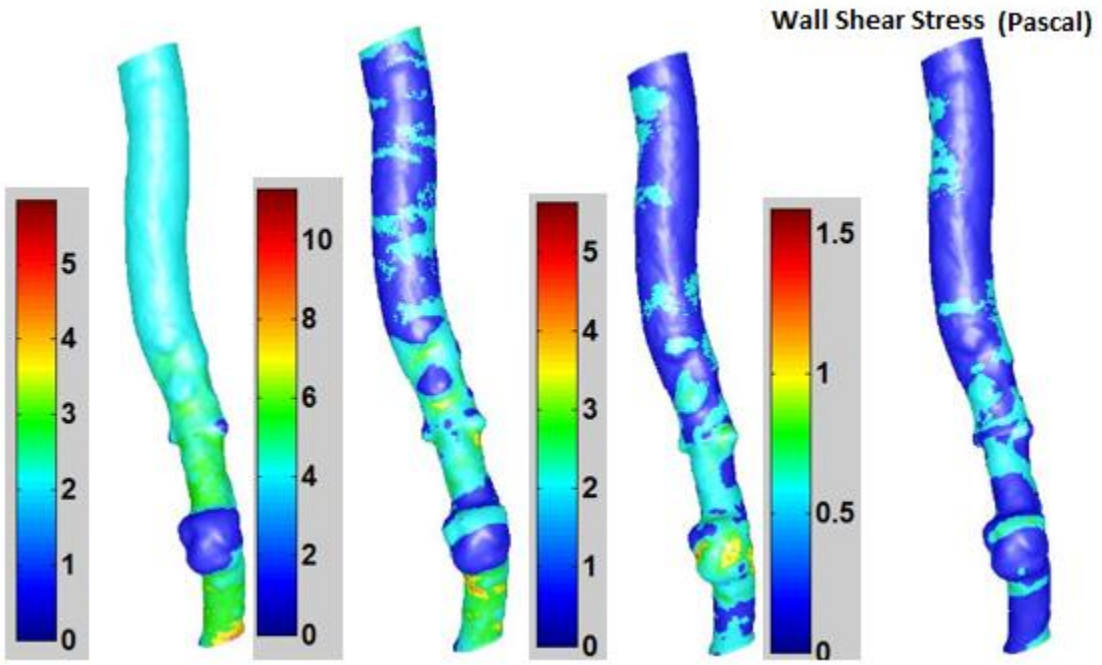

Figure 4-14. Wall shear stress contours of Patient B aorta. From left: early systole, mid systole, peak systole, end systole

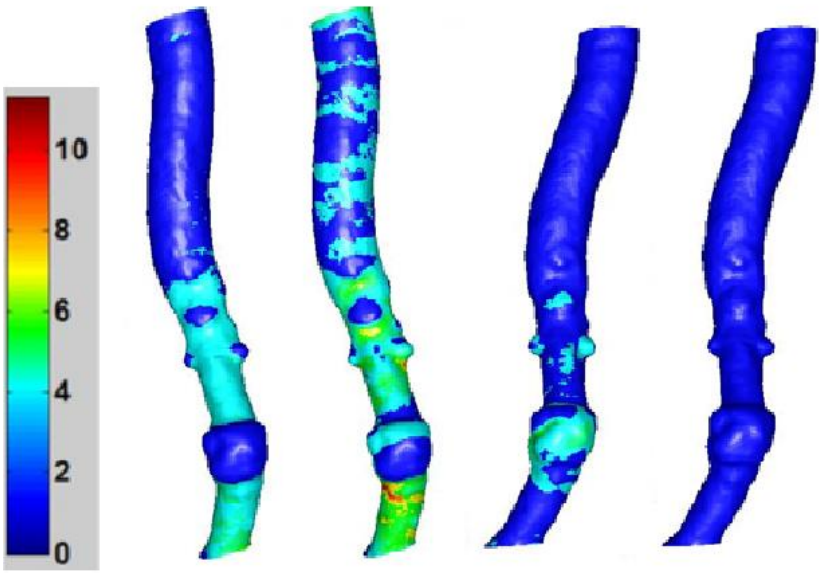

Figure 4-15. Wall shear stress (Pascal) contours of Patient B aorta with the same legend. From left: early systole, mid systole, peak systole and end systole

Figure 4-16 shows pressure contours at early systole ranging between 8300 and 9700 Pa with a negative gradient from inlet to outlet. In next phase, however, a very slight positive gradient is obtained due to convective deceleration, which in later phases becomes adverse causing flow to recirculate at the bulge region. Pressure at mid systole and end systole is about 13000 Pa and in peak systole it ranges between 15600 and 16100 Pa. Figure 4-17 also shows the pattern of wall pressure during different phases of the cycle with the same legend.

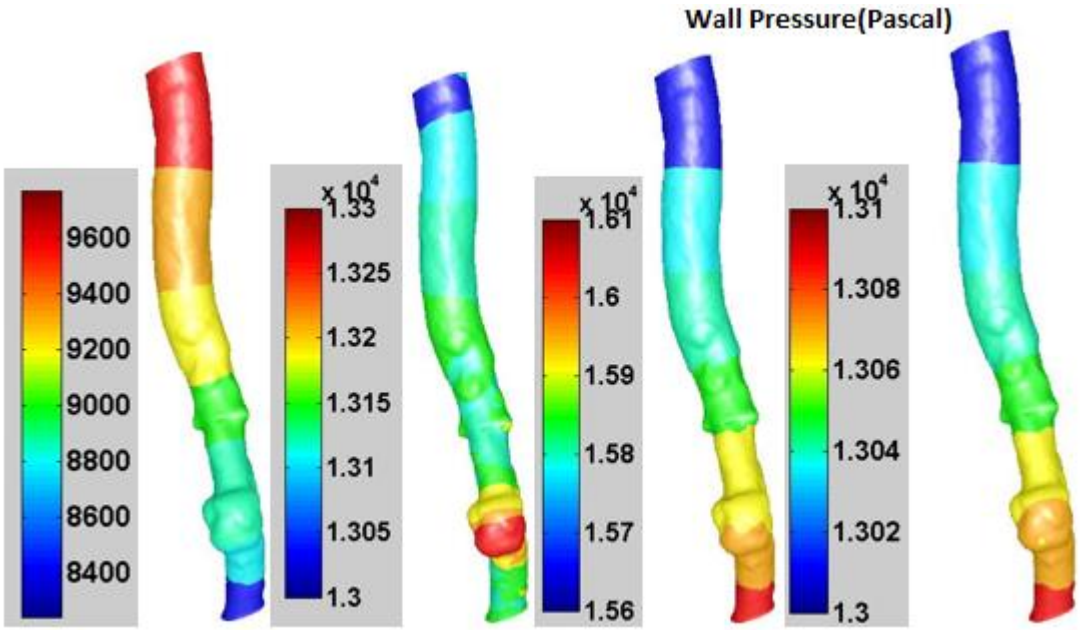

Figure 4-16. Wall pressure contours of Patient B aorta. From left early systole, mid systole, peak systole, end systole.

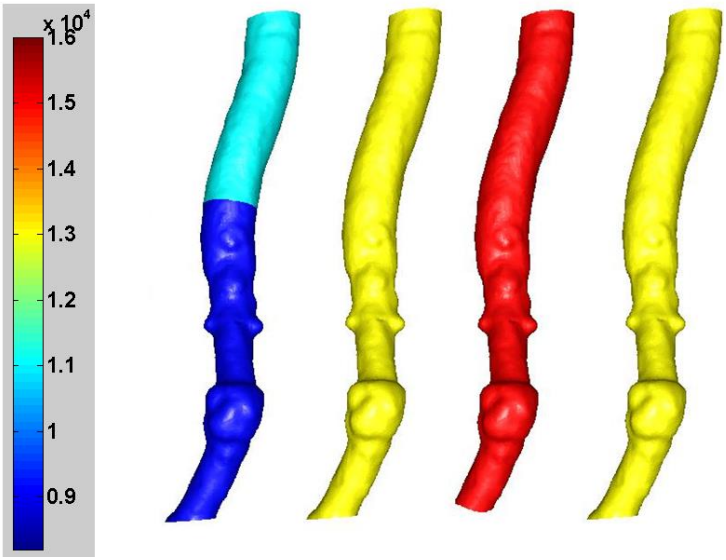

Figure 4-17. Wall pressure (Pascal) contours of Patient B aorta with the same legend. From left early systole, mid systole, peak systole and end systole.

Mean Wall Shear Stress

Figure 4-18, Figure 4-19 and Figure 4-20 show mean wall shear stress distributions over one cycle. It is important to calculate MWSS as it is the variable that VECs are sensitive to. Figure 4-18 shows MWSS for patient A, reporting low values at the bump and higher values at the normal regions and at the bifurcation.

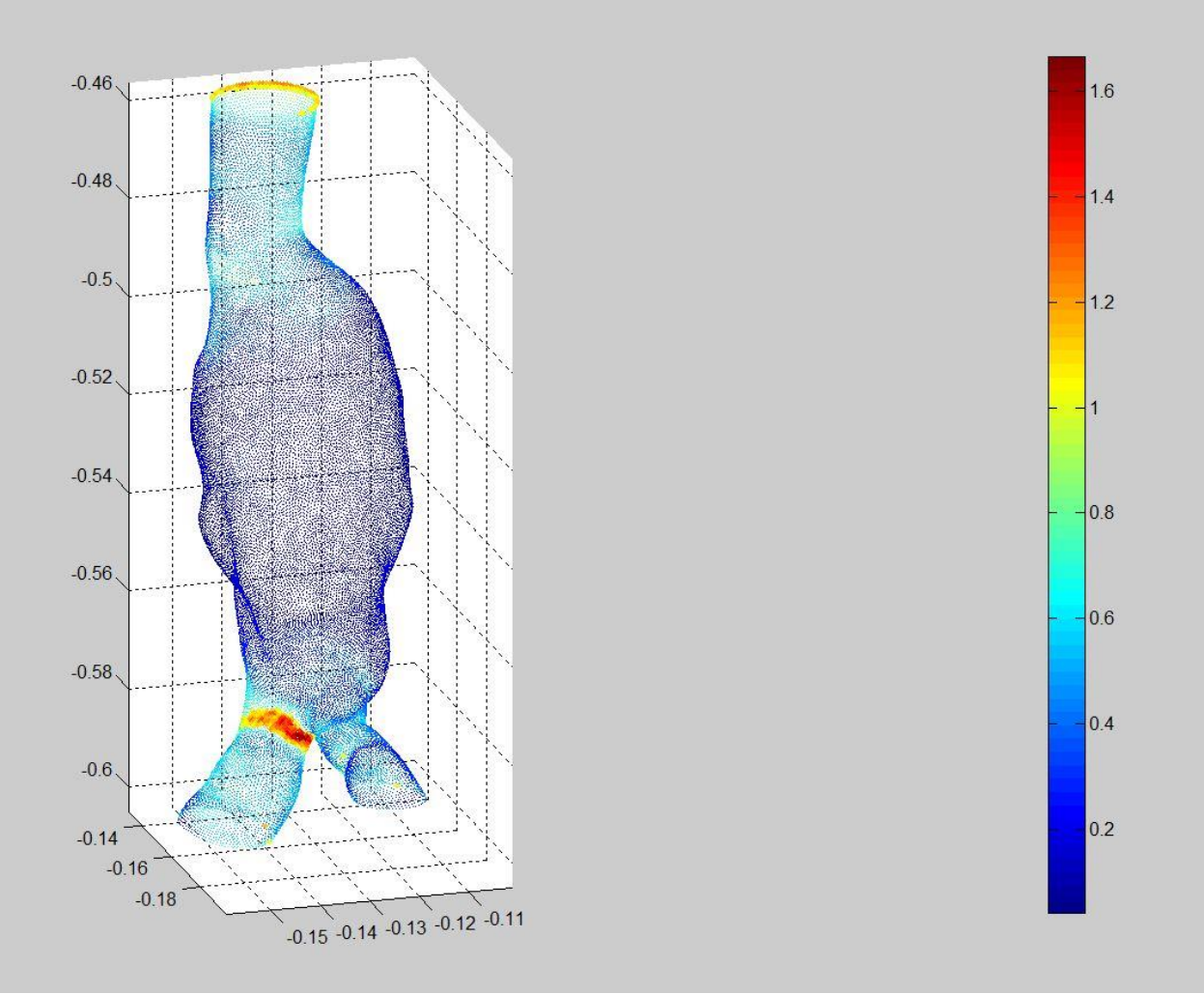

Figure 4-18. Mean wall shear stress values at patient A aorta

Figure 4-19 shows MWSS for patient B. The result is very different from the map of MWSS for patient A. At the bulge values are higher than at the upstream regions or downstream region. This is due to the geometry of the patent lumen. The wall of the aneurysm for Patient B has a much higher diameter than the lumen due to thrombus formation. Figure 4-20 shows the MWSS for an ideal geometry, which is similar to Patient A in pattern and opposite to Patient B emphasizing the

importance of patient specific geometry simulations. The results of the ideal geometry cannot be used for both patients A and B.

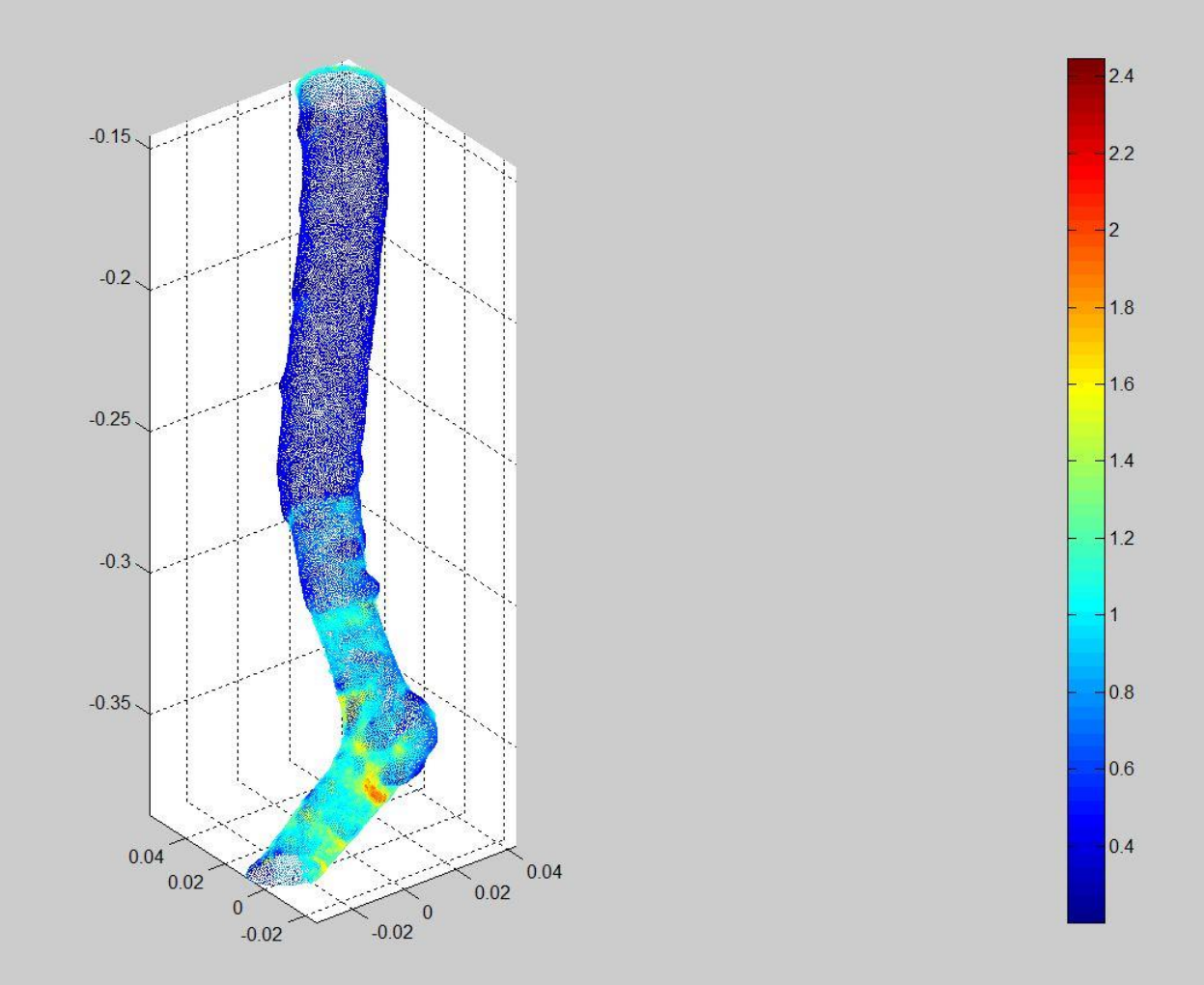

Figure 4-19. Mean wall shear stress values for Patient B aorta

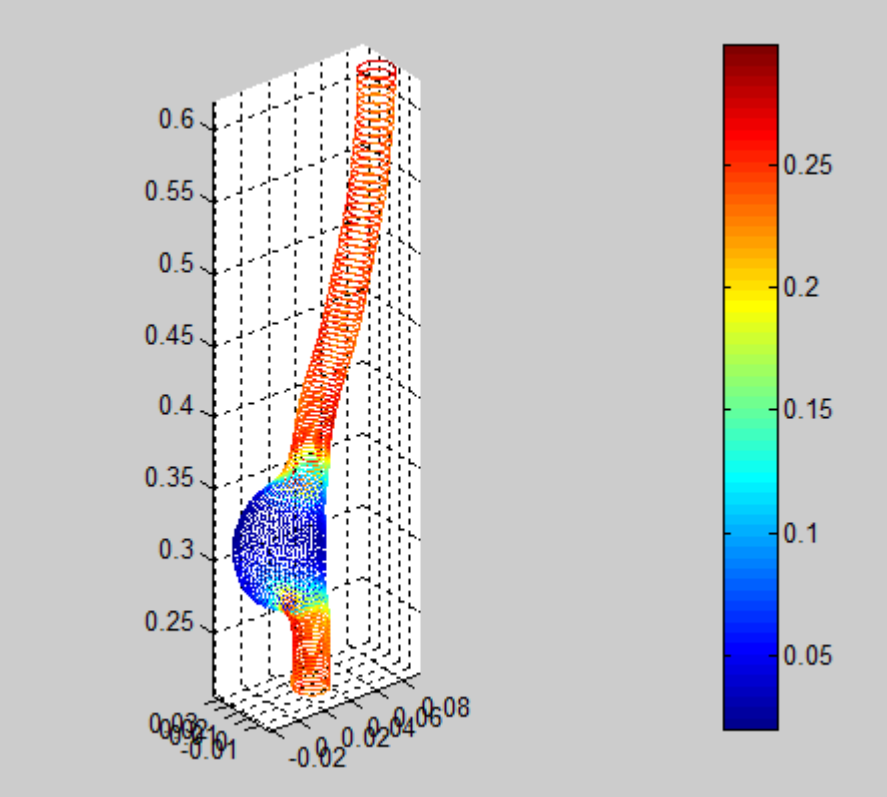

Figure 4-20. Mean wall shear stress values for the idealized aneurysm

5 EXPERIMENTAL RESULTS

After obtaining the instantaneous wall shear stress for patient A, the maps of time average wall shear stress for 12 Left lateral or lp and 12 right lateral or rp regions of the wall were made. These 24 regions served as a guide during surgery to collect specimens from Patient A's aorta.. Figure 5-1and Figure 5-2show these maps and regions with an average value of mean wall shear stress for each region.

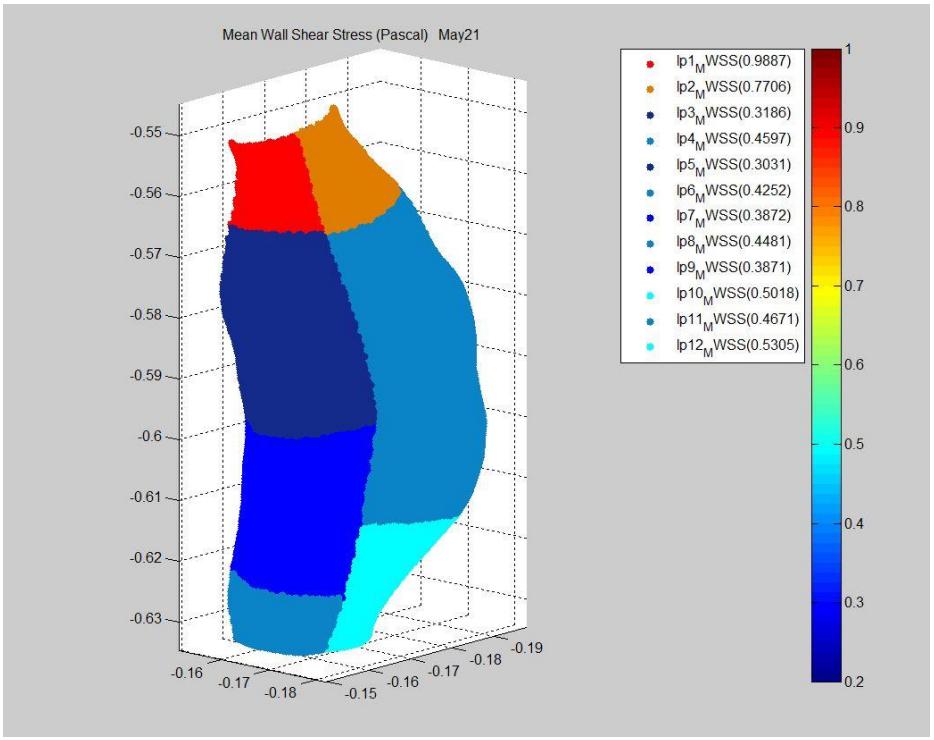

Figure 5-1. Mean wall shear stress map of lp regions

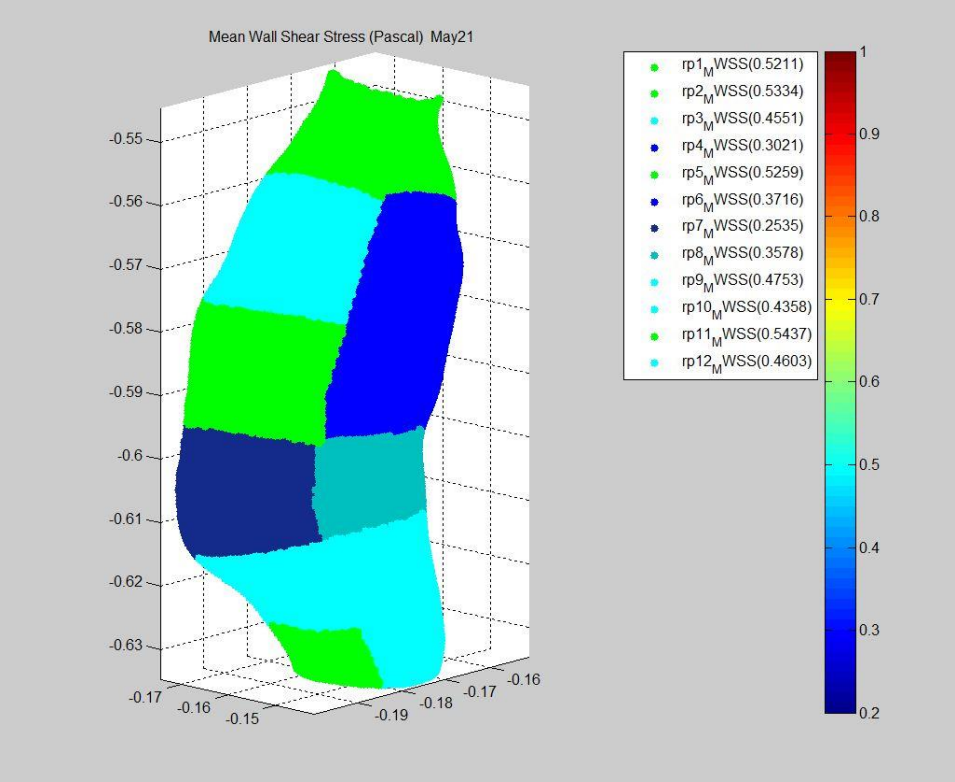

Figure 5-2. Mean wall shear stress map of rp regions

From H&E and Musto pentachrome histology stains, the thickness of the media, presence of elastic lamellae presence of collagen and SMCs, and degree of inflammation were recorded. H&E and Musto stains for two slices obtained for 5 specimens from Patient A aorta are shown in Figure 5-3. Mechanical stress values were also obtained on each of the region by using FEM (Finite Element Method).

The experimental completed so far included mechanical tests (biaxial tests, see Methods) and histologies. Only three specimens were large enough to perform tensile tests (biaxial). The gathered data were collected in Table 1.

Figure 5-3. Histology on 5 specimens and neck (upstream) of Patient A aneurysm. Musto result: Nuclei and elastic fibre is black. Collagen is yellow. Ground substance, mucin is blue. Fibrin is red and Muscle is red.

Table 1. Table of Computational and histological data on Patient A aneurysm tissue samples (see Figure 5-1 and 5-2 for a map of the specimens location)

Specimen ID	Thickness (mm)	Thrombus thickness (mm)	Wall shear stress (Pa)	Mechanical stress (KPa)	Stiffness (from tensile test)(KPa)	Inflammation (from histology)
LP2	0.66	0.9	0.77	104		
LP7	1.5	10.4	0.39	147		Little elastin fragmented, some collagen and some mucoid degeneration (inflammation)

LP10	0.2	11.3	0.5	112	609	No elastin, collagen +++, no inflammation
RP5	1.8	4.3	0.52	152		Fragmented elastin lots of mucoid degeneration (inflammation ++)
RP9	1.7	9.8	0.47	126.5		Inflammation +, some collagen
neck	2.1	0	N/A	N/A	191	Lots of elastin, smc, little inflammation, little collagen
RP7	N/A	4.7	0.25	151	20	
LP4	N/A	5.5	0.45	107.1	1085	

Results show that the thickness of the wall appears to be lower behind thicker thrombus (result not statistically significant, probably on account of the small number of specimens so far). The values of mechanical stress seem to follow the opposite trend with respect to the mean wall shear stress. Histology data shows that most of the specimens have some degree of inflammation except the neck, which has no thrombus and the LP10 region, which has a massive amount of thrombus protecting it from high mechanical stress. Moreover LP10 region is seen to have a strong collagen deposition, probably in response to the environment stimuli (high stress).

These results do not allow drawing conclusive statements. More subjects need to be enrolled in the study in order to verify if the observation have statistical significance. However, from the results obtained on one patient we can conclude that wall is very heterogeneous in terms of variable studied. Results from the immohystochemistry are not yet available. These results along with the inclusion of larger group of subjects will provide valuable data in showing the interplay between wall shear stresses, mechanical stresses and the response of VECs and other vascular cells; moreover, they will also provide data on the effect of thrombus, providing more information on its dual role, on one hand causing wall degradation, while on the other hand shielding it from mechanical and fluid dynamic stresses.

6 DISCUSSION

The hemodynamics in two aneurysmal subjects and one idealized model of aneurysm were analysed. The goal was to achieve a physiologic model of flow dynamics inside a patient specific aneurysm, so that results and intra-operative specimen selection could be individualized to the specific patient under study. Therefore patient specific geometries were considered and the boundary conditions inspired by the nature of wave production in the heart were simulated. Because the pressure produced by heart is the result of flow ejected from the heart added to the effect of pulse wave reflected from the downstream vasculature, it was decided to capture this effect by coupling a 3-element Windkessel model to the 3D model of the aorta. By doing this, the pressure produced at the outlet of 3D model was the result of flow coming from the inlet and of the reflection of pulse wave from the 3-element Windkessel model that represents the downstream impedance. An external subroutine to be coupled with the CFD code was developed so that these boundary conditions would be enforced automatically during the transient simulation of the blood.

The CFD simulation performed on the aneurysm models showed that during the cardiac cycle depending on whether the flow is decelerating or accelerating and whether it is in the bulge area or in the upstream healthy parts the flow pattern changes. It was noticeable that during the deceleration phases flow was separating from the wall at the point of the bulge and reattaching and recirculating, producing a region of stagnation for blood particles, which is thought to cause the formation of thrombus. Conversely, at the peak flow, which happened at mid systole, the flow was smooth all over the lumen. Although at the early systole flow was almost the same speed as in the

peak systole, the pattern was totally different. At peak systole, flow was recirculating while at early systole flow had no recirculation pattern in the bulge. This could be due to decelerating flow at peak systole while flow is accelerating at early systole, preventing the pressure field from having positive gradient. We also calculated the wall shear stress over the wall for all models. Over one cardiac cycle for both patient A and for the idealized model the values of wall shear stress were low at the bulge comparing to the upstream or downstream normal regions, although the values were dependent on time through the cycle. Interestingly, the pattern of wall shear stress for Patient B was very different from both Patient A and the idealized geometry. This may be due to the large amount of thrombus filling the lumen in the case of Patient B, making it small enough to prevent low wall shear stress patterns. This shows the importance of patient specific geometry. To understand the effect of the geometry even better one can look at the mean wall shear stress patterns for the three models. To compare the pressure pattern on the wall we also performed an additional simulation on patient A with a constant zero pressure at the outlet (and no Windkessel model). Comparing the results showed that the constant pressure simulation gave not only wrong contours of pressure over the wall but also very unrealistic values of pressure. In contrast to this, the simulation performed including the impedance boundary condition (Windkessel model) gave more accurate pressure values and shapes of the curve. Moreover the phase difference at the inlet area of the model was well captured by using the impedance model.

Lashers [48] states that immediately after peak systole a recirculation regime of flow in the bulge occurs, which gets slower in the center. This statement is based on digital PIV measurements of an idealized aneurysm model. Figure 6-1 shows the results. Both sides of the symmetry plane show a recirculation in the bulge and there are regions of low shear stress, which becomes higher at the center of the aneurysm. In our research it was noted that for both the idealized aneurysm ad for a

real aneurysmal geometry, the recirculation occurs at both peak systole and end systole, which is the phase of flow deceleration. However, in spite of the differences in geometry between our models and the one by Lashers, especially with regards to the symmetry, we found qualitatively similar results.

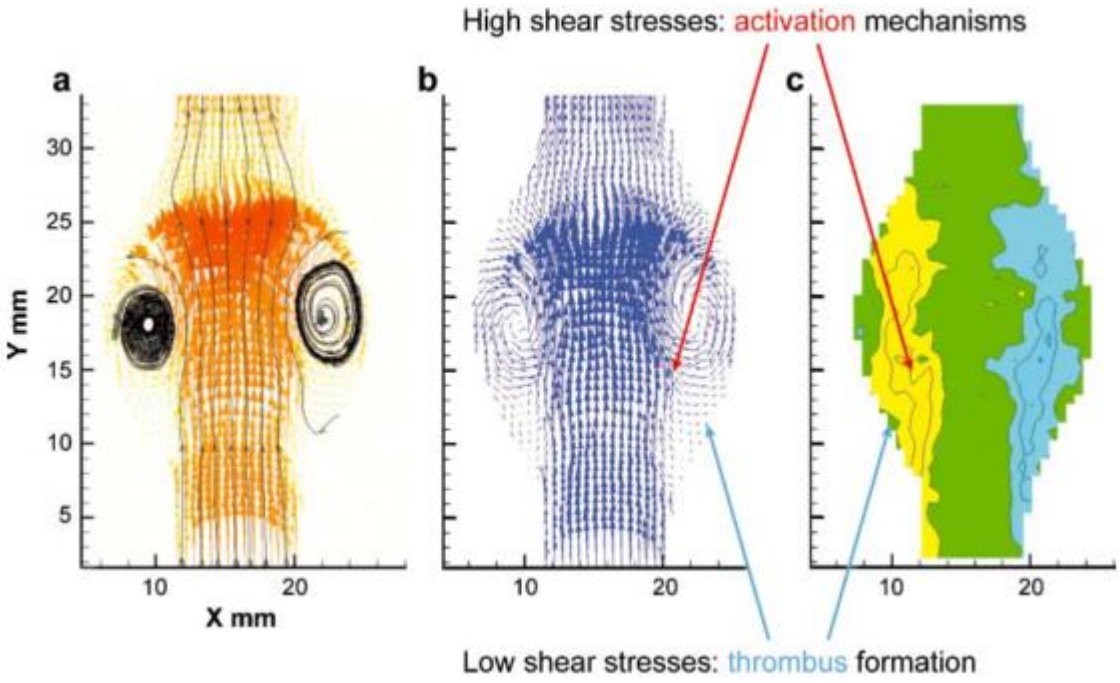

Figure 6-1. Digital Particle Image Velocimetry measurements, showing a: recirculation at the bulge b and c: thrombus formation[48]

The time averaged wall shear stress plots show that for the real geometry for Patient B we do not see lower values of wall shear stress at the bulge compared to the normal aortic regions; the only time we do see this is when the flow is accelerating in mid systole and right after the early systolic phase. At other times, we found close to normal values of wall shear stress in the bulge or even higher. This was contradictory to literature results [10][49] for the wall of aneurysms, which is expected to experience lower wall shear stress. The result may be due to the particular geometry

of Patient B and in particular to the ratio between lumen and thrombus. In this particular case, the intraluminal thrombus is arranged in a way that causes the diameter of the vessel in correspondence to the bulge to be lower than at higher sections.

If we look at the results for the idealized geometry, the results we found in terms of shear stress are consistent with the literature: they show low wall shear stress at the bulge at all 4 times plotted throughout the cycle. Similarly, when averaged in time, the bulge experiences low amounts of shear stress compared to normal regions. This observation brings about the idea that the ratio of bulge diameter to normal diameter plays a role in inducing higher or lower values of wall shear stresses. Comparing the upstream diameters with the bulge diameters we find 2 cm vs. 5 cm for the idealized geometry, while for Patient A the ratio is 2 cm vs. 3.7 cm and for Patient B the upstream diameter is still 2 cm but the bulge diameter is less than 2 cm. We could speculate that the lower shear was present at the time of the intraluminal thrombus formation for Patient B and that it has facilitated thrombus formation while at the same time recovering higher (more physiologic) shear stresses. This "positive" effect of the thrombus, however, is annulled with time by the degenerative effect that a thick layer of thrombus has on the characteristics of the "covered" wall behind the thrombus. These observations are confirmed by our preliminary histological observations on Patient A. The aorta adjacent to a thicker thrombus is thinner and appears to have the hallmark of an inflamed disorganized tissue. Our findings are confirmed by Lasheras et al [48] who state that the progression of aneurysm and the formation of thrombus could be simultaneous with larger aneurysms resulting in an improved wall shear stress (increased) due to decreasing lumen size on account of thrombus formation, while at the same time the thrombus puts the anterior tissue of the bulge at hypoxic risk. Lashers also states that thrombus formation activates release of inflammatory enzymes which can cause degradation of smooth muscle cells and interrupt their

healthy performance. Moreover tensional stresses on the wall can trigger more collagen to be produced by smooth muscle cells and fibroblasts, inducing stiffening of the wall, which in turn modifies the biomechanical environment of the wall and may trigger further wall degeneration. We did find the highest stiffness among the specimens tested for a specimen that was behind a thick thrombus and subjected to higher mechanical stresses. Overall, the preliminary results gathered from only one patient suggest that hemodynamics may not be the main reason for rupture, but that it may be more involved in the progression of the dilatation and formation of thrombus. Judging from our preliminary data on Patient B, it would appear that when the lumen diameter at the bulge becomes closer to normal size the hemodynamics effects are reduced and the continued expansion of the wall behind a thick thrombus and its eventual rupture may happen because of loss of integrity of the wall tissue due to high enzymatic activity co-localized with high mechanical stresses. These observations will need to be further confirmed by more simulations coupled with experimental tests, before any conclusive remarks can be made.

With respect to the fluid dynamics simulations performed, for all three models the timing of the cardiac cycle is well achieved. From a physiological point of view a phase lag between velocity and pressure curve exists where the maximal phase of velocity corresponds to the mid systolic phase of the pressure curve; this is well captured by the model. In contrast, in the literature, results obtained imposing zero pressure at the outlet give non-realistic pressure contours which are negative or very small in value while also wrongly assuming that peak flow is in phase with peak systolic pressure[49] (Figure 6-2). There is another report in the literature of a study performed applying the velocity of the heart at the inlet and the aortic pressure at the outlet; however, because there is no coupling between these two boundary conditions, the velocity and pressure waves work independently and the results phase lag between velocity and pressure contours is not captured[5].

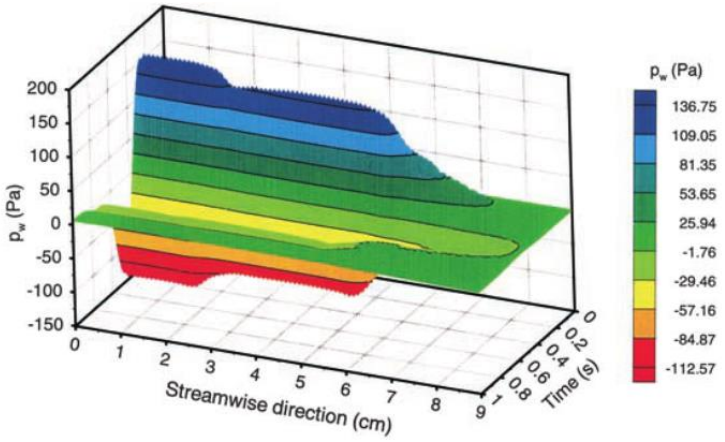

Figure 6-2. Pressure values at the wall of an aneurysm model for which the outlet pressure is set to zero[49]

Calculating the pressure without considering the effect of pulse wave can also result in a different pattern of wall shear stresses as well. Taylor [50] also showed in a stenotic iliac artery that constant boundary conditions result in incorrect levels of pressure and in an inaccurate shape of the pressure wave.

Although our model produces the same phase shift throughout the whole length of the aorta it is able to produce the correct phase lag at the inlet region along with accurate pressure values and contours all over the length of the vessel. An improvement to our model can be to couple the inlet with a lump model of the heart to capture the phase lag thought the whole length of the aorta.

7 CONCLUSION

From three models we conclude that 1- it is important to do a transient simulation of AAA because during the cardiac cycle the flow features differ. 2- It is important to have appropriate boundary conditions in order to produce realistic results and explain the natural features of the pulsating flow. 3- Using a patient specific geometry (as opposed to an idealized one) has a huge impact on the flow features and applying the results of the idealized aneurysm models to every patient may prevent one from understanding the specific condition of the disease related to a patient. This is important in the clinical management of AAA as lack of a correct understanding of the situation may result in a wrong diagnosis. The use of a Windkessel model to impose the boundary conditions produces better calculations of pressure at the wall of the aneurysm than a zero pressure boundary condition at the outlet. It captures the phase difference between flow and pressure correctly, produces realistic values of pressure and considers the effect of the pulse wave.

The objective of the research presented in this Thesis was to provide correct haemodynamic simulations in patient-specific models of aneurysms so that intra-operative specimens can be obtained at locations of known wall shear stress values. The simulations performed proved to be appropriate to produce pre-operative maps of wall shear stress. Biomechanical and histological analyses were performed on the surgical pieces obtained from Patient A according to the wall shear stress maps. The results confirm the role of the thrombus as a "factory" of enzymatic activity that results in a weaker, more inflamed wall. More experiments will need to be performed on other aneurysmal patients to confirm the findings; however, we succeeded in developing a protocol for

hemodynamic simulations from patient specific data that provide accurate results and can be used to inform the obtainment of surgical specimens.

7.1 LIMITATIONS AND FUTURE WORK

One of the limitations of the model is that because the inlet is at the level of descending aorta for Patient B and at the level of diaphragm for patient A the velocity profile is neither uniform nor fully developed. To alleviate this effect the model should include the geometry of the aortic arch and the uniform velocity should be applied at the aortic root. Or a Womersley profile had to be considered.

The present simulation neglects the effect of the wall compliance. Although AAAs occur mostly in the elderly and for this category of patients the aortic wall is stiffer than in the young, nonetheless, considering a rigid wall overestimates the effect of the pulse wave in augmenting the static pressure.

The model simulates the hemodynamics in the patent lumen. The effect of intraluminal thrombus (ILT) is, however, important, especially its role as a barrier preventing VEC from receiving hemodynamics stimuli and oxygen and nutrients from reaching the wall of the aneurysm. A transport model could be implemented to study these effects.

While the current model is a rigid one, if the effect of fluid-structure interaction were to be considered, then the effect of the spinal column in limiting the posterior movement of the wall would also have to be considered along with effect of the abdominal cavity organs in reducing anterior movement of the aneurysm wall.

For a much more accurate results flow should to be considered non-Newtonian.

Finally, it was mentioned in the results section that the pressure curve is the same at 3 points within the bulk of the model. This could be compensated by coupling a lump model of the heart at the inlet of the model, so that this additional lump model would be responsible of producing the pulse wave.

8 REFERENCES

[1] J. Golledge, J. Muller, A. Daugherty, and P. Norman, "Abdominal aortic aneurysm: pathogenesis and implications for management.," *Arteriosclerosis, thrombosis, and vascular biology*, vol. 26, no. 12, pp. 2605–13, Dec. 2006.

[2] J. C. Lasheras, "The Biomechanics of Arterial Aneurysms," *Annual Review of Fluid Mechanics*, vol. 39, no. 1, pp. 293–319, Jan. 2007.

[3] E. a. Finol and C. H. Amon, "Blood Flow in Abdominal Aortic Aneurysms: Pulsatile Flow Hemodynamics," *Journal of Biomechanical Engineering*, vol. 123, no. 5, p. 474, 2001.

[4] P. Rissland, Y. Alemu, S. Einav, J. Ricotta, and D. Bluestein, "Abdominal aortic aneurysm risk of rupture: patient-specific FSI simulations using anisotropic model.," *Journal of biomechanical engineering*, vol. 131, no. 3, p. 031001, Mar. 2009.

[5] a Sheidaei, S. C. Hunley, S. Zeinali-Davarani, L. G. Raguin, and S. Baek, "Simulation of abdominal aortic aneurysm growth with updating hemodynamic loads using a realistic geometry.," *Medical engineering & physics*, vol. 33, no. 1, pp. 80–8, Jan. 2011.

[6] C. M. Scotti, J. Jimenez, S. C. Muluk, and E. a Finol, "Wall stress and flow dynamics in abdominal aortic aneurysms: finite element analysis vs. fluid-structure interaction.," *Computer methods in biomechanics and biomedical engineering*, vol. 11, no. 3, pp. 301–22, Jun. 2008.

[7] S. Oivind, "PULSATILE PRESSURE AND FLOW IN AN ARTERIAL," *Biomedical engineering online*, vol. 3, pp. 153–158, 1981.

[8] E. a Finol and C. H. Amon, "Flow-induced wall shear stress in abdominal aortic aneurysms: Part II--pulsatile flow hemodynamics.," *Computer methods in biomechanics and biomedical engineering*, vol. 5, no. 4, pp. 319–28, Aug. 2002.

[9] S. Kelly and M. O'Rourke, "Fluid, solid and fluid-structure interaction simulations on patient-based abdominal aortic aneurysm models," *Proceedings of the Institution of Mechanical Engineers, Part H: Journal of Engineering in Medicine*, vol. 226, no. 4, pp. 288–304, Feb. 2012.

[10] E. a Finol and C. H. Amon, “Flow-induced wall shear stress in abdominal aortic aneurysms: Part I--steady flow hemodynamics.,” *Computer methods in biomechanics and biomedical engineering*, vol. 5, no. 4, pp. 309–18, Aug. 2002.

[11] R. D. Shepherd, S. M. Kos, K. D. Rinker, and A. Canada, “Flow-dependent Smad2 phosphorylation and TGIF nuclear localization in human aortic endothelial cells,” vol. 1, no. 21, pp. 98–107, 2011.

[12] N. Sakalihasan, R. Limet, and O. D. Defawe, “Abdominal aortic aneurysm.,” *Lancet*, vol. 365, no. 9470, pp. 1577–89, 2005.

[13] J. D. H. C. Bellini1, J. Ferruzzi1, S. Roccabianca1, E.S. DiMartino2, “A Microstructurally Motivated Model of Arterial Wall Mechanics with Mechanobiological Implications,” *Annals of biomedical engineering*, no. October, 2013.

[14] E. S. Di Martino, G. Guadagni, A. Fumero, G. Ballerini, R. Spirito, P. Biglioli, and A. Redaelli, “Fluid-structure interaction within realistic three-dimensional models of the aneurysmatic aorta as a guidance to assess the risk of rupture of the aneurysm.,” *Medical engineering & physics*, vol. 23, no. 9, pp. 647–55, Nov. 2001.

[15] a.-V. Salsac, S. R. Sparks, J.-M. Chomaz, and J. C. Lasheras, *Evolution of the wall shear stresses during the progressive enlargement of symmetric abdominal aortic aneurysms*, vol. 560. 2006, p. 19.

[16] C. Reeps, M. Gee, A. Maier, M. Gurdan, H.-H. Eckstein, and W. a Wall, “The impact of model assumptions on results of computational mechanics in abdominal aortic aneurysm.,” *Journal of vascular surgery : official publication, the Society for Vascular Surgery [and] International Society for Cardiovascular Surgery, North American Chapter*, vol. 51, no. 3, pp. 679–88, Mar. 2010.

[17] M. D. Gasbarro, K. Shimada, and E. S. Di Martino, “Explicit finite element method for in-vivo mechanics of abdominal aortic aneurysm,” *Revue européenne de mécanique numérique*, vol. 16, no. 3–4, pp. 337–363, Jun. 2007.

[18] D. a Vorp and J. P. Vande Geest, “Biomechanical determinants of abdominal aortic aneurysm rupture.,” *Arteriosclerosis, thrombosis, and vascular biology*, vol. 25, no. 8, pp. 1558–66, Aug. 2005.

[19] E. Georgakarakos, C. V Ioannou, Y. Papaharilaou, T. Kostas, and A. N. Katsamouris, “Computational evaluation of aortic aneurysm rupture risk: what have we learned so far?,” *Journal of endovascular therapy : an official journal of the International Society of Endovascular Specialists*, vol. 18, no. 2, pp. 214–25, Apr. 2011.

[20] J. Shum, G. Martufi, E. Di Martino, C. B. Washington, J. Grisafi, S. C. Muluk, and E. a Finol, “Quantitative assessment of abdominal aortic aneurysm geometry.,” *Annals of biomedical engineering*, vol. 39, no. 1, pp. 277–86, Jan. 2011.

[21] G. Martufi, M. Auer, J. Roy, J. Swedenborg, N. Sakalihasan, G. Panuccio, and T. C. Gasser, “Multidimensional growth measurements of abdominal aortic aneurysms.,” *Journal of vascular surgery*, vol. 58, no. 3, pp. 748–55, Sep. 2013.

[22] T. M. McGloughlin and B. J. Doyle, “New approaches to abdominal aortic aneurysm rupture risk assessment: engineering insights with clinical gain.,” *Arteriosclerosis, thrombosis, and vascular biology*, vol. 30, no. 9, pp. 1687–94, Sep. 2010.

[23] J. D. Humphrey and G. a Holzapfel, “Mechanics, mechanobiology, and modeling of human abdominal aorta and aneurysms.,” *Journal of biomechanics*, vol. 45, no. 5, pp. 805–14, Mar. 2012.

[24] R. L. Dalman, M. M. Tedesco, J. Myers, and C. a Taylor, “AAA disease: mechanism, stratification, and treatment.,” *Annals of the New York Academy of Sciences*, vol. 1085, pp. 92–109, Nov. 2006.

[25] M. M. Dua and R. L. Dalman, “Hemodynamic influences on abdominal aortic aneurysm disease: Application of biomechanics to aneurysm pathophysiology.,” *Vascular pharmacology*, vol. 53, no. 1–2, pp. 11–21, 2010.

[26] Z.-D. Shi and J. M. Tarbell, “Fluid flow mechanotransduction in vascular smooth muscle cells and fibroblasts.,” *Annals of biomedical engineering*, vol. 39, no. 6, pp. 1608–19, Jun. 2011.

[27] J. S. Matsumura, D. C. Brewster, M. S. Makaroun, and D. C. Naftel, “A multicenter controlled clinical trial of open versus endovascular treatment of abdominal aortic aneurysm.,” *Journal of vascular surgery*, vol. 37, no. 2, pp. 262–71, Feb. 2003.

[28] J.-J. Wang, N. G. Shrive, K. H. Parker, A. D. Hughes, and J. V Tyberg, “Wave propagation and reflection in the canine aorta: analysis using a reservoir-wave approach.,” *The Canadian journal of cardiology*, vol. 27, no. 3, pp. 389.e1–10, 2011.

[29] J.-J. Wang, A. B. O’Brien, N. G. Shrive, K. H. Parker, and J. V Tyberg, “Time-domain representation of ventricular-arterial coupling as a windkessel and wave system.,” *American journal of physiology. Heart and circulatory physiology*, vol. 284, no. 4, pp. H1358–68, Apr. 2003.

[30] N. Westerhof, J.-W. Lankhaar, and B. E. Westerhof, “The arterial Windkessel.,” *Medical & biological engineering & computing*, vol. 47, no. 2, pp. 131–41, Feb. 2009.

[31] A. Noordergraaf, *Blood in Motion ,Chapter 5 Transmission of Arterial Signals, Venous Nonlinearity, and Body Movement*. New York, NY: Springer New York, 2011.

[32] H. J. Kim, I. E. Vignon-Clementel, C. a Figueroa, J. F. LaDisa, K. E. Jansen, J. a Feinstein, and C. a Taylor, “On coupling a lumped parameter heart model and a three-dimensional finite element aorta model.,” *Annals of biomedical engineering*, vol. 37, no. 11, pp. 2153–69, Nov. 2009.

[33] M. L. Raghavan, M. W. Webster, and D. a Vorp, “Ex vivo biomechanical behavior of abdominal aortic aneurysm: assessment using a new mathematical model.,” *Annals of biomedical engineering*, vol. 24, no. 5, pp. 573–82, 1996.

[34] D. A. Vorp, “Biomechanics of abdominal aortic aneurysm.,” *Journal of biomechanics*, vol. 40, no. 9, pp. 1887–902, Jan. 2007.

[35] J. P. Vande Geest, E. S. Di Martino, A. Bohra, M. S. Makaroun, and D. a Vorp, “A biomechanics-based rupture potential index for abdominal aortic aneurysm risk assessment: demonstrative application.,” *Annals of the New York Academy of Sciences*, vol. 1085, pp. 11–21, Nov. 2006.

[36] J. P. Vande Geest, D. H. J. Wang, S. R. Wisniewski, M. S. Makaroun, and D. a Vorp, “Towards a noninvasive method for determination of patient-specific wall strength distribution in abdominal aortic aneurysms.,” *Annals of biomedical engineering*, vol. 34, no. 7, pp. 1098–106, Jul. 2006.

[37] R. Bhaskaran, L. Collins, “Introduction to CFD Basics,”, pp. 1–17.

[38] B.-K. Lee, “Computational fluid dynamics in cardiovascular disease.,” *Korean circulation journal*, vol. 41, no. 8, pp. 423–30, Aug. 2011.

[39] R. Eymard and P. G. Ciarlet, “Finite Volume Methods,” vol. M, no. October, 2006.

[40] J. Peir, “FINITE DIFFERENCE , FINITE ELEMENT AND FINITE VOLUME METHODS FOR PARTIAL DIFFERENTIAL,” *Differential Equations*, vol. M, pp. 1–32, 2005.

[41] I. ANSYS, “ANSYS Meshing User ’ s Guide,” vol. 15317, no. November, pp. 724–746, 2010.

[42] L. a. Freitag and C. Ollivier-Gooch, “A comparison of tetrahedral mesh improvement techniques,” Dec. 1996.

[43] D. Whitley, “A genetic algorithm tutorial,” *Statistics and Computing*, vol. 4, no. 2, Jun. 1994.

[44] M. S. Sacks, D. a Vorp, M. L. Raghavan, M. P. Federle, and M. W. Webster, “In vivo three-dimensional surface geometry of abdominal aortic aneurysms.,” *Annals of biomedical engineering*, vol. 27, no. 4, pp. 469–79, 1999.

[45] M. L. Raghavan, D. a Vorp, M. P. Federle, M. S. Makaroun, and M. W. Webster, “Wall stress distribution on three-dimensionally reconstructed models of human abdominal aortic aneurysm.,” *Journal of vascular surgery : official publication, the Society for Vascular Surgery [and] International Society for Cardiovascular Surgery, North American Chapter*, vol. 31, no. 4, pp. 760–9, Apr. 2000.

[46] F. N. van de Vosse and N. Stergiopulos, “Pulse Wave Propagation in the Arterial Tree,” *Annual Review of Fluid Mechanics*, vol. 43, no. 1, pp. 467–499, Jan. 2011.

[47] A. M. Walker, C. R. Johnston, and D. E. Rival, “On the Characterization of a Non-Newtonian Blood Analog and Its Response to Pulsatile Flow Downstream of a Simplified Stenosis.,” *Annals of biomedical engineering*, pp. 1–37, Aug. 2013.

[48] J. C. Lasheras, “The Biomechanics of Arterial Aneurysms,” *Annual Review of Fluid Mechanics*, vol. 39, no. 1, pp. 293–319, Jan. 2007.

[49] E. a Finol and C. H. Amon, “Flow-induced wall shear stress in abdominal aortic aneurysms: Part II--pulsatile flow hemodynamics.,” *Computer methods in biomechanics and biomedical engineering*, vol. 5, no. 4, pp. 319–28, Aug. 2002.

[50] I. E. Vignon-Clementel, C. Alberto Figueroa, K. E. Jansen, and C. a. Taylor, “Outflow boundary conditions for three-dimensional finite element modeling of blood flow and pressure in arteries,” *Computer Methods in Applied Mechanics and Engineering*, vol. 195, no. 29–32, pp. 3776–3796, Jun. 2006.

9 APPENDIX (EXTRA FIGURES)

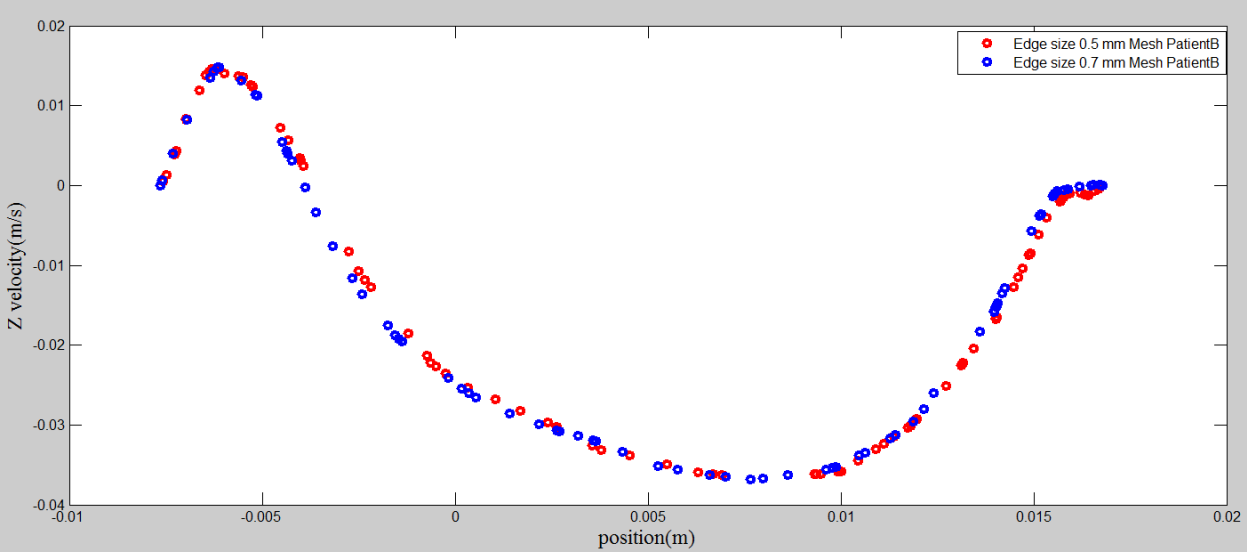

Figure 9-1. Mesh sensitivity analysis of patient B model, it is seen that mesh edge size 0.7 and 0.5 show almost the same velocity profile

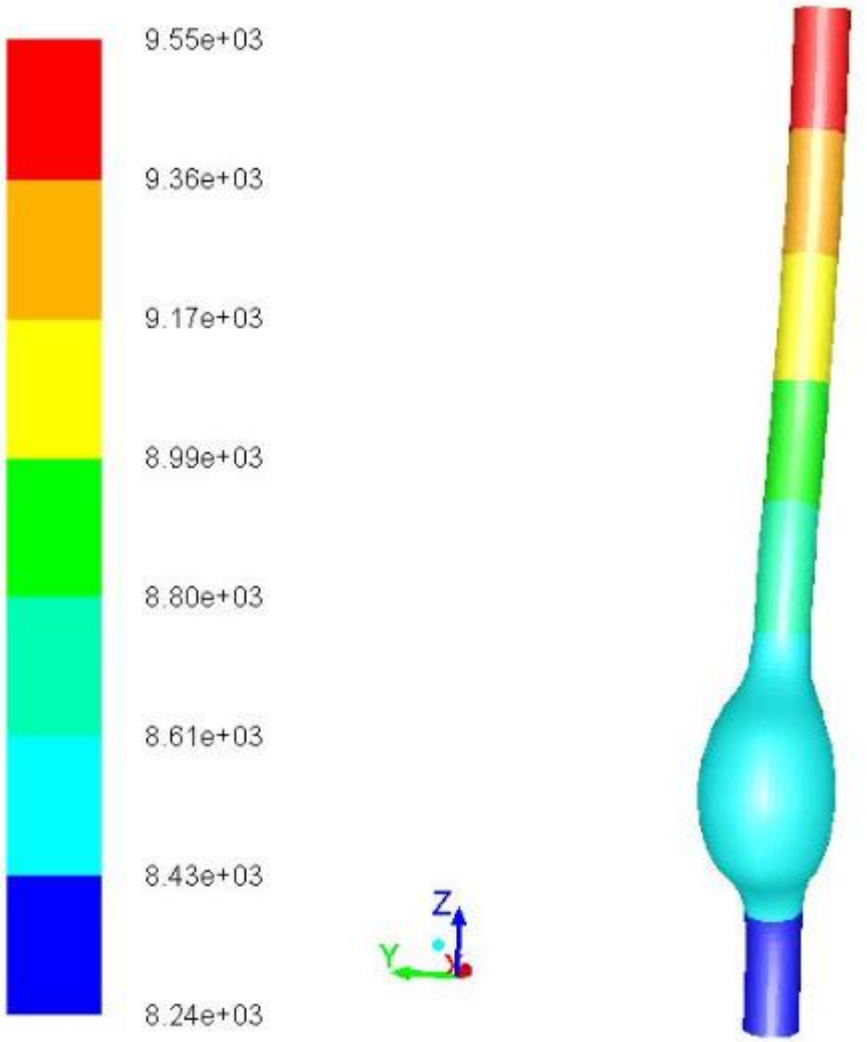

Figure 9-2. Wall pressure contours of the ideal geometry model at early systolic phase

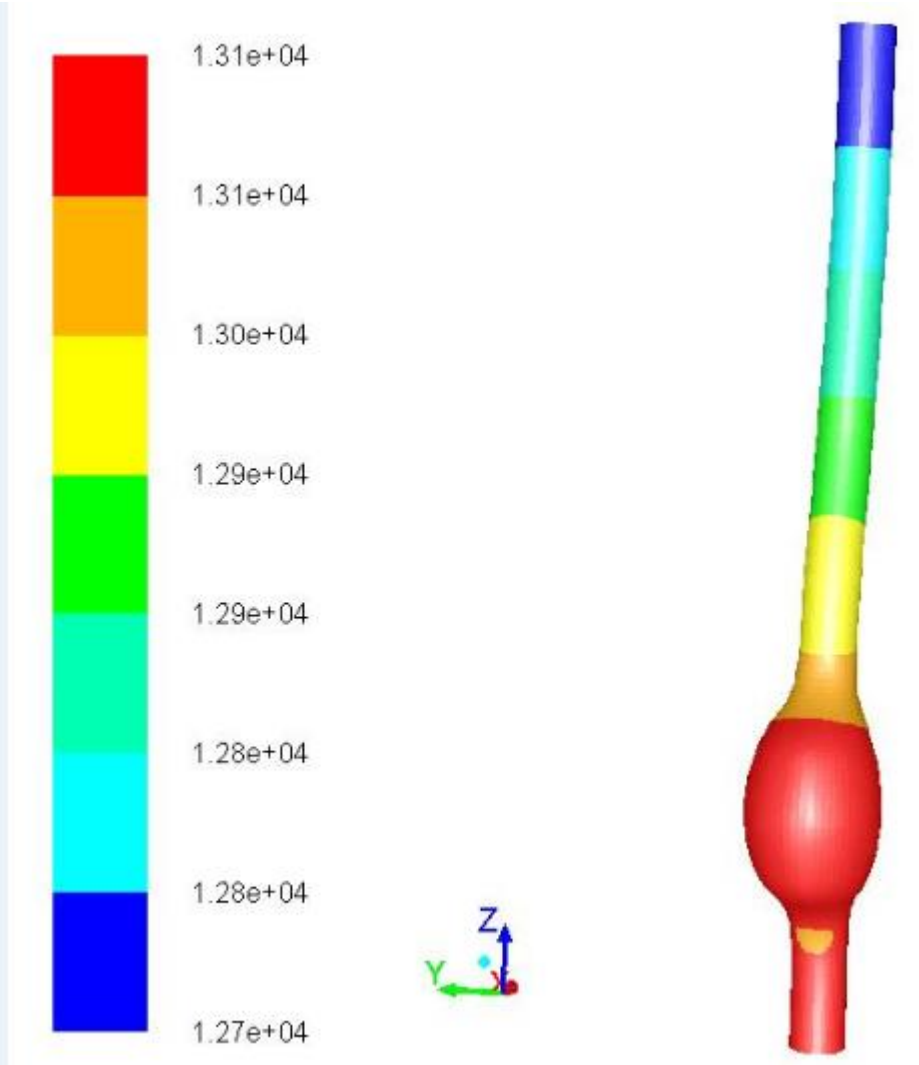

Figure 9-3. Pressure contours of the ideal geometry model at mid systole phase

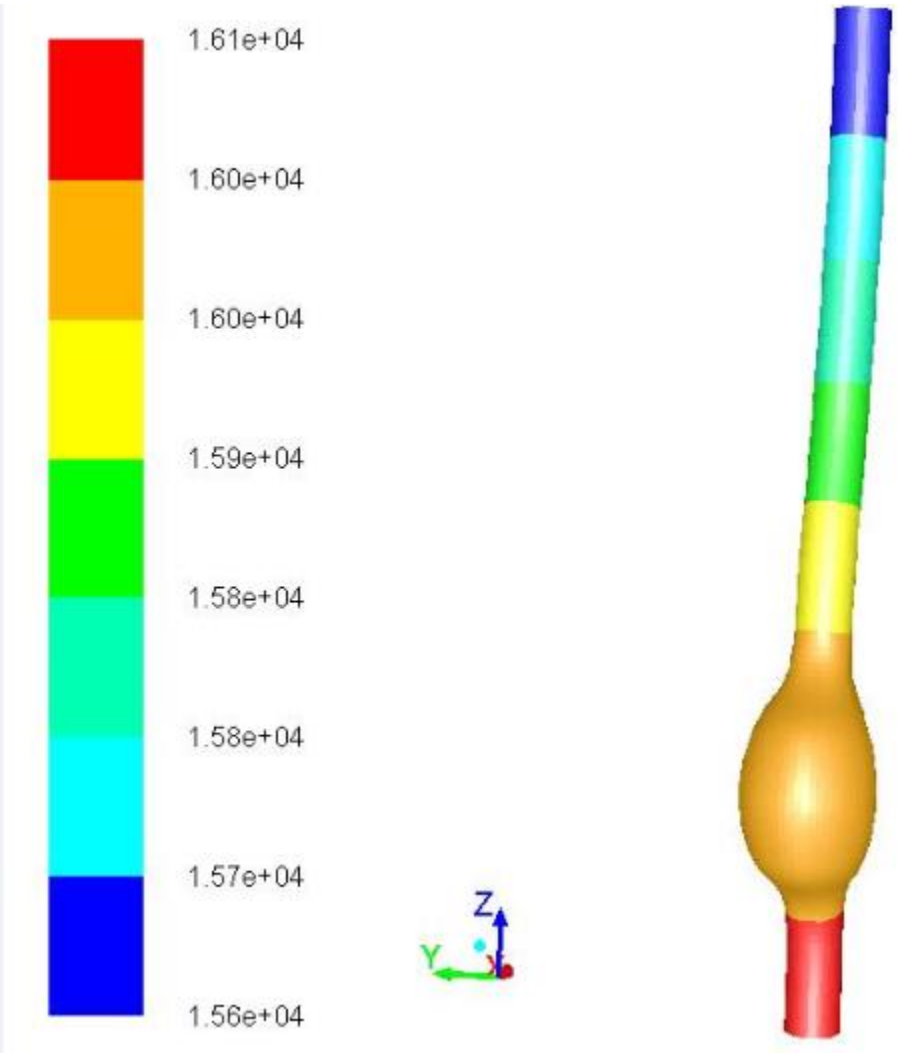

Figure 9-4. Pressure contours of the ideal geometry model at peak systole phase

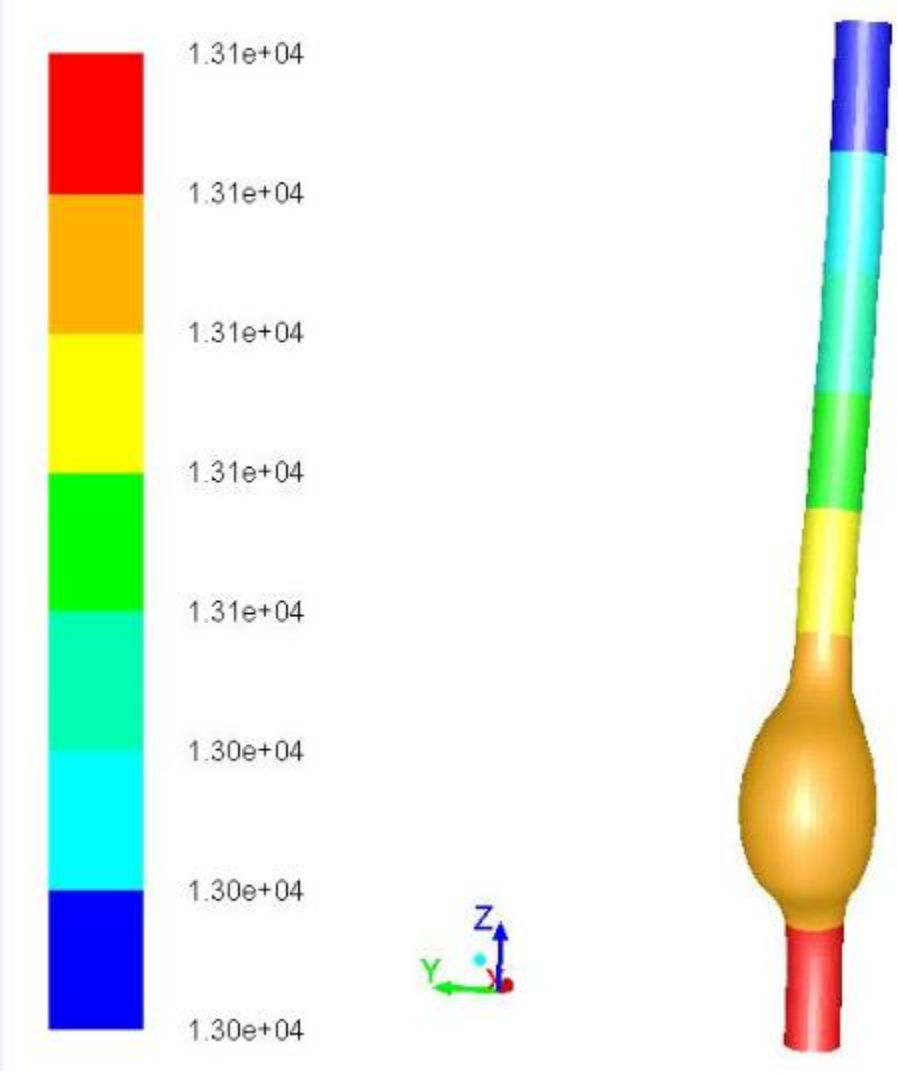

Figure 9-5. Pressure contours of the ideal geometry model at end systole phase

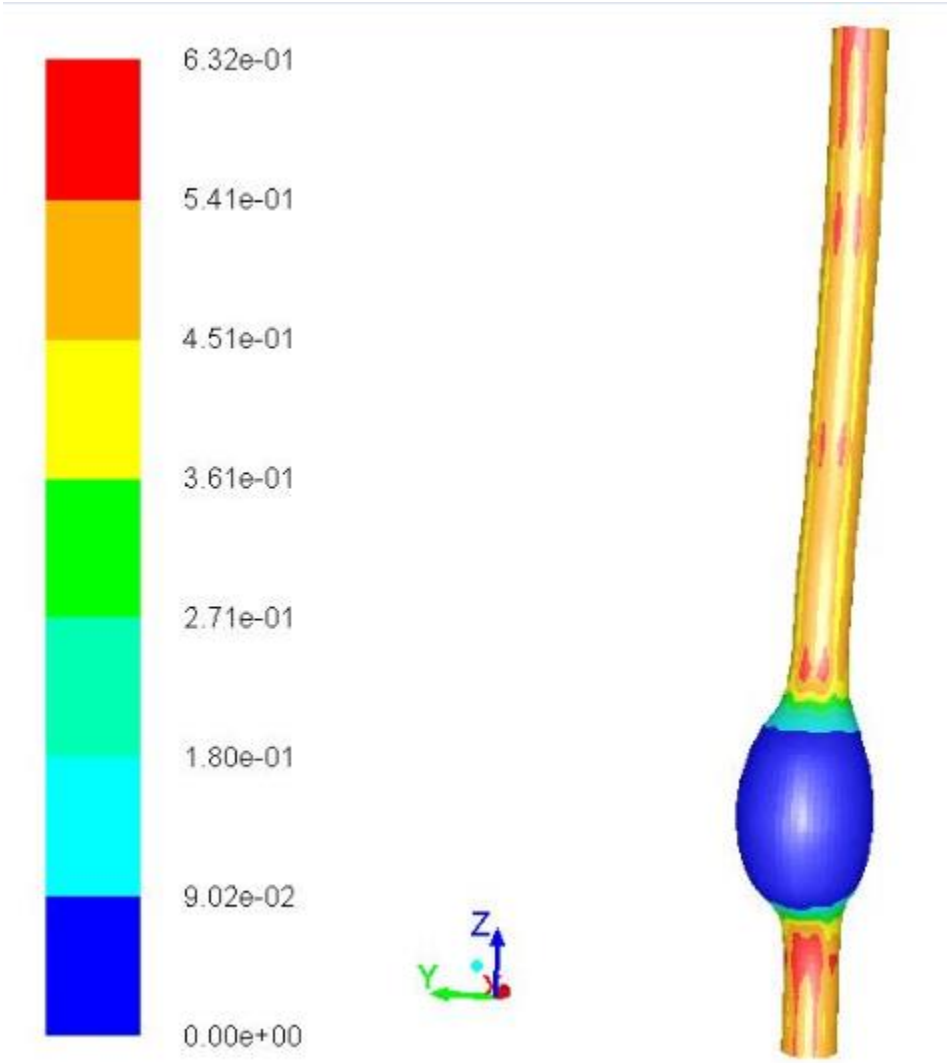

Figure 9-6. Wall shear stress of ideal geometry at early systole phase

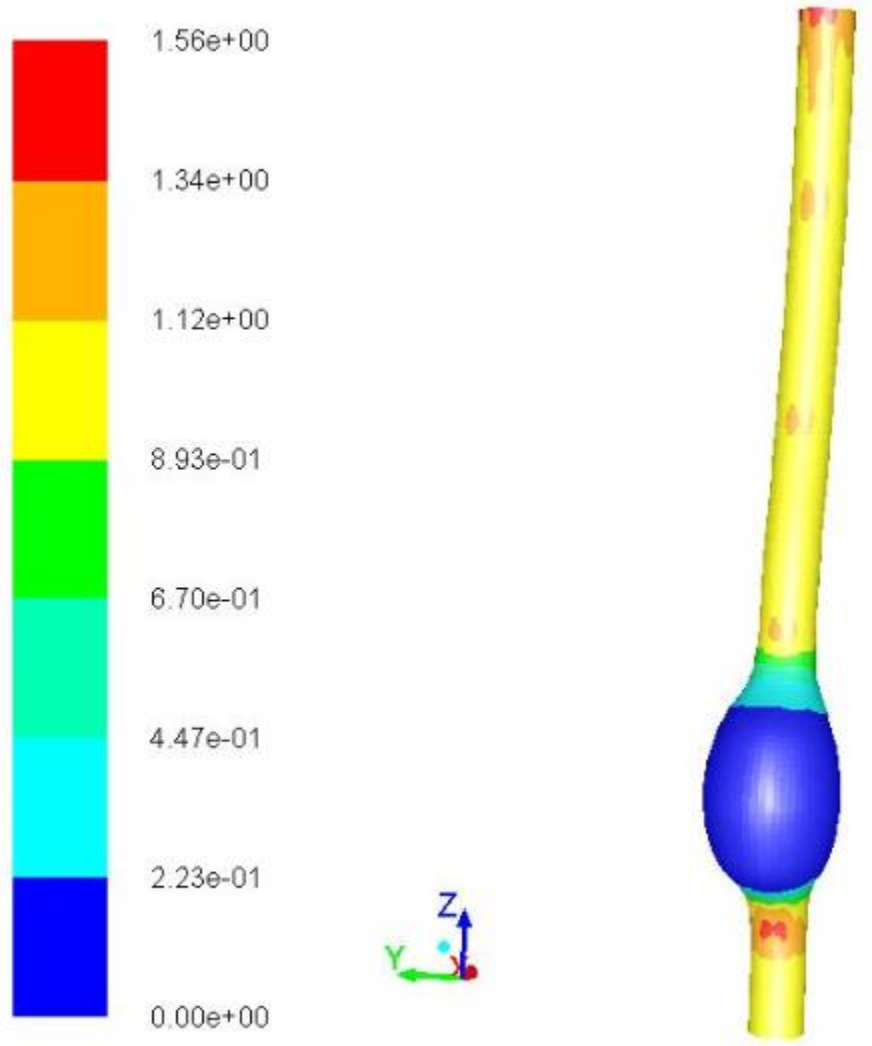

Figure 9-7. Wall shear stress of ideal geometry at mid systole phase

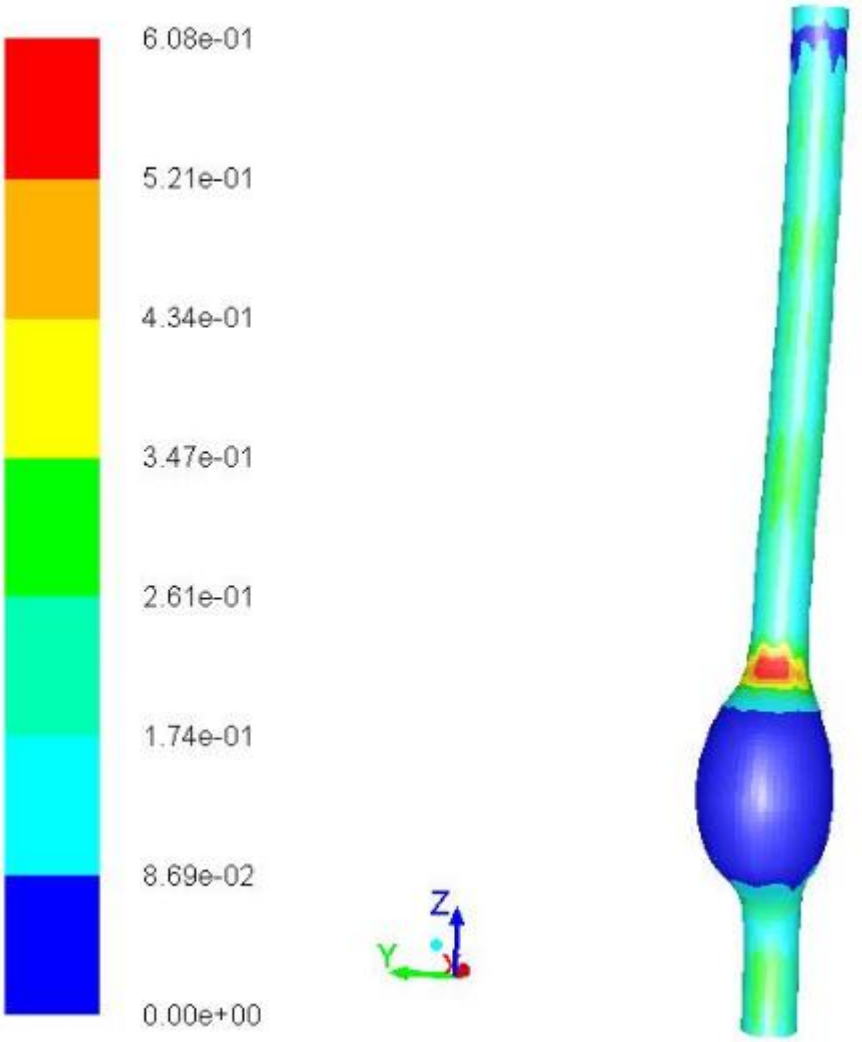

Figure 9-8. Wall shear stress of ideal geometry at peak systole phase

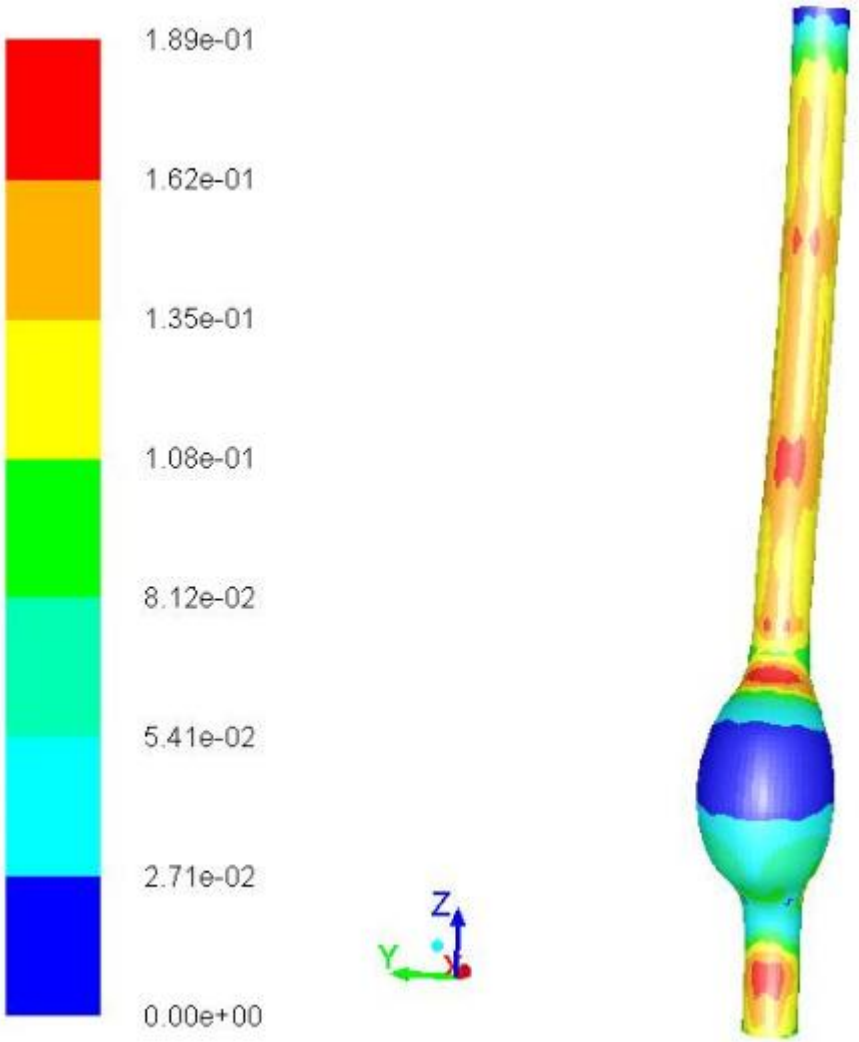

Figure 9-9. Wall shear stress of ideal geometry at end systole phase